The Dissertation Committee for Kyeon Hur
certifies that this is the approved version of the following dissertation:

Methodology for Characterizing Electric Power System Response and Locating the Energized Capacitor Banks using Conventional Power Quality Data

Committee:

Surya Santoso, Supervisor

W. Mack Grady

Edward J. Powers

Mircea D. Driga

Carlos H. Caldas

Methodology for Characterizing Electric Power System Response and Locating the Energized Capacitor Banks using Conventional Power Quality Data

by

Kyeon Hur, B.S., M.S.

DISSERTATION

Presented to the Faculty of the Graduate School of

The University of Texas at Austin

in Partial Fulfillment

of the Requirements

for the Degree of

DOCTOR OF PHILOSOPHY

THE UNIVERSITY OF TEXAS AT AUSTIN

May 2007

Dedicated to my wife Younjung Choi; parents, Don Hur and Hyangsik Kim.

To the memory of my grandfather, Jae Hwan Kim.

Acknowledgments

I would like to extend my deepest appreciation to my dissertation advisor, Professor Surya Santoso. My graduate study and research under the supervision of Professor Santoso have been a great gift from God. His encouragement, commitment and enthusiasm inspired me to successfully complete doctoral study at The University of Texas at Austin.

I would also like to thank the distinguished members of my dissertation committee: Professors W. M. Grady, E. J. Powers, and M. D. Driga in the Department of Electrical and Computer Engineering, and Professor C. H. Caldas in the Department of Civil Engineering. Their interest and encouragement of my research have provided the guidance leading to the successful completion of this dissertation.

I would like to appreciate Professor B. F. Womack for his kind support and guidance while I worked as a TA for Senior Design Lab (EE464). I had a valuable chance to collaborate with Professor I. Y. H. Gu in the Department of Signals and Systems, Chalmers University of Technology, Sweden while developing the damping estimation method. I appreciate her insightful comments and advice on signal processing applications on power quality problems. I would also like to express my appreciation for the support and guidance from faculty members, especially Professors. Kwang Bang Woo, Jin Bae Park and

Hagbae Kim at Yonsei University, Seoul, Korea during my undergraduate and graduate programs. I am also pleased to acknowledge those brilliant engineers at Samsung Electronics where I could understand why they used to say that engineering should be differentiated from science. I am grateful to Korea Science Engineering Federation (KOSEF) and Electric Power Research Institute (EPRI) for kindly granting study abroad scholarship and funding my graduate research projects.

I cannot forget the friendship with graduate students who shared office space in the Department of Electrical and Computer Engineering and many Korean students in Austin, especially Soon Hyeok Choi and many other Yonsei alumni who kindly helped me settle in Austin and Yeo Joon Kim who has always willingly given his time and effort when I needed help or advice at the various stages of life in the United States.

Let me also say *Thank You* to my uncle Tae Ki Kim, who first introduced electrical engineering to me and has been my both technical and spiritual mentor for more than 30 years.

Of course, I am especially indebted to my parents, younger sister Jin Kyung, grandmother and late grandfather for their sustained love, encouragement and prayers. Without my parents' credit in me and persistent support, none of my dissertation research would have been possible. This writing opportunity seems like a good time to tell them that I feel so happy for them and most pleased to have them all. I am equally indebted to my parents-in-law for their sincere support. Especially, I deeply thank my mother-in-law for her love,

support and sacrifice during her stay in Austin for three months. Without her help, I don't believe I could pass my Ph.D qualifying exam. I just can't tell how much all of them mean to me. I love you all so much.

Eun and In, my precious little boys surely have deprived me of my good-night sleep for the last three years. However, their adorable smiles have energized me more than a 12-hour-sleep could do and encouraged me to continue my work. I love you so much: you're my reason for living.

Last but not least, I am deeply grateful for the love and understanding of my wife Younjung through all of my graduate studies at The University of Texas at Austin. Every figure and sentence in this dissertation are composed by her sacrifice, patience, and commitment. You're the only one I'd ever want to share my life. I love you so much.

I certify that this dissertation, and the research to which it refers, are the product of my own work, and that any ideas or quotations from the work of other people, published or otherwise, are fully acknowledged in accordance with the standard referencing practices of the discipline.

Kyeon Hur

The University of Texas at Austin

April 2007

Methodology for Characterizing Electric Power System Response and Locating the Energized Capacitor Banks using Conventional Power Quality Data

Publication No. _____

Kyeon Hur, Ph.D.
The University of Texas at Austin, 2007

Supervisor: Surya Santoso

A relatively small harmonic current with frequencies near or at the power system parallel resonant frequencies could excite the power system into a resonance condition. While a capacitor bank is not the root cause of the condition, it facilitates and helps cause the problem. This is because when the capacitor bank is energized, the system resonant frequency could shift closer to existing harmonic frequencies produced by nonlinear loads. Therefore, the objective of this dissertation is to quantify the power system characteristics corresponding to the parallel resonant frequencies and system damping. Additionally, since a capacitor bank actively facilitates the resonance condition, the relative or exact location of the involved bank must be determined.

This dissertation first presents a practical and accurate methodology to estimate system parallel resonant frequencies by performing spectral analysis

of the voltage and current transient data immediately after the capacitor bank switching. The proposed method is also robust in that the accuracy of the resulting estimates is not affected by prevalent harmonics in the system.

This dissertation provides two efficient algorithms for estimating the system damping parameters using the Hilbert and analytic wavelet transforms. These algorithms take advantage of the principle of an asymptotic or weakly-modulated signal, for which the signal phase varies much more rapidly than the amplitude. The zero-input voltage response or free response of the capacitor bank energizing can be categorized into these asymptotic signals, and one can assign a unique time-varying amplitude with the system damping information and phase pair by building analytic signals. System model reduction theory also allows us to interpret or quantify this damping as an effective X/R ratio.

This dissertation defines two fundamental signatures of shunt capacitor bank energizing. It demonstrates that these two signatures can be utilized to accurately determine the relative location of an energized capacitor bank whether it is upstream or downstream from the monitoring location. This dissertation also presents an efficient and accurate methodology for finding the exact location of an energized capacitor bank. Once a PQ monitor is found to be upstream from the capacitor bank by the relative location finding algorithm, the proposed algorithm can further determine the exact location of the switched capacitor bank by estimating the distance between the PQ monitor and the energized capacitor bank. Thus, one can pinpoint the energized capacitor bank causing the resonance.

Table of Contents

xiv

List of Tables

List of Figures

xix

Chapter 1

Introduction

1.1 Electric Power Distribution System

Electric power systems are generally comprised of four major components: generation, transmission, sub-transmission, and distribution systems [1]. Some smaller power systems may only have either a transmission or sub-transmission system due to a smaller service territory. In such cases, distribution systems are fed directly from one or more high-voltage transmission or sub-transmission lines. Figure 1.1 illustrates the major components of a typical electric power system. Among these components, the distribution system has traditionally been perceived as less important than the transmission and generation system. New technologies continue to emerge in the generation sector, as evidenced by larger and more efficient power plants – whether they are conventional fossil fuel or renewable generation plants. Various state and federal incentives have been implemented to encourage the development of new energy conversion and generation technologies. Similarly, the transmission sector continues to receive regulatory and public scrutiny since it is considered to be part of the nation's critical infrastructure[1]. In addition, electric power transmission

---

[1] Since 1990, the construction of new transmission infrastructures actually decreased by about thirty percent [3].
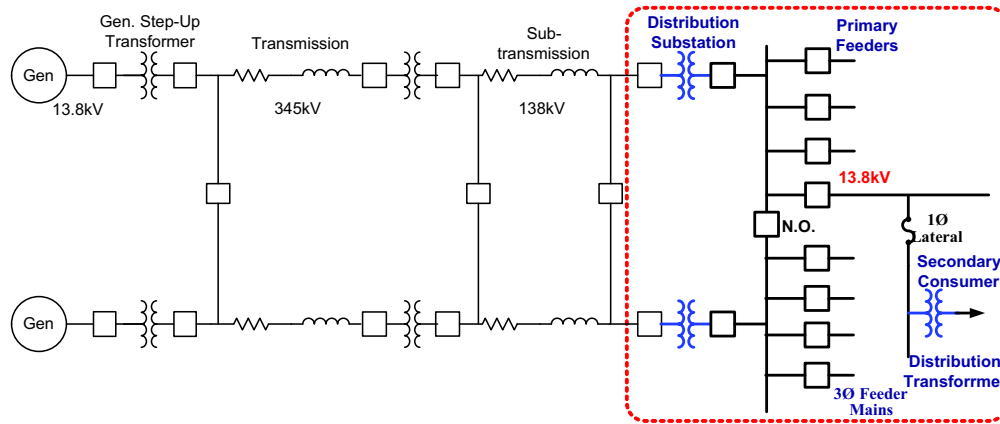
Figure 1.1: Typical electric supply system: The enclosed area represents the distribution system.

technologies have advanced rapidly in recent years. These advances have been spurred by a lack of new transmission system infrastructures, such as competing land uses, opposition to transmission system infrastructure (especially in urban areas), and uncertain government regulations. Flexible alternating current transmission systems (FACTS) controllers are primary examples of power transmission technologies. FACTS technologies include thyristor-controlled series capacitor (TCSC), static compensator (STATCOM), unified power flow controller (UPFC), dynamic voltage restorer (DVR), static VAR compensator (SVC) and high-voltage direct-current (HVDC) link [4]. These technologies have been successful in deferring transmission system infrastructure and in relieving transmission congestion problems.

Distribution systems are the last major component in the electric power service chain, as shown in Figure 1.1. Unfortunately, they have received much less attention compared to that of bulk transmission systems. This is per-

2

haps due to lack of market drives, coupled with the uncertainty of the electric deregulation process, as well as the perceived notion that because the distribution systems operate at lower voltage levels, they are not as critical as the bulk transmission systems. Despite this situation, end-users in all market sectors (residential, industrial, and commercial) are more demanding than ever regarding the quality of electric service and reliability. Ironically, anecdotal evidence shows that distribution utilities appear to receive most of the blame for electrical power problems, irrespective of the actual source of the problems.

Although the service area of a distribution system is much less than that of a transmission system, the analysis of distribution systems is no less complex. As a matter of fact, it can be far more complicated since the per-phase analysis approach does not typically apply [5]. Distribution systems are inherently unbalanced, due to, most notably, single- and two-phase lateral taps and various single- and three-phase loads along distribution feeders. In addition, distribution overhead lines are un-transposed and their loads may be linear, non-linear, or a combination thereof. Figure 1.2 represents a typical primary distribution feeder with its various equipment: circuit switchers, feeders, distribution transformers, capacitor banks, end-user loads, and protective devices, such as fuses, substation breakers, and reclosers.
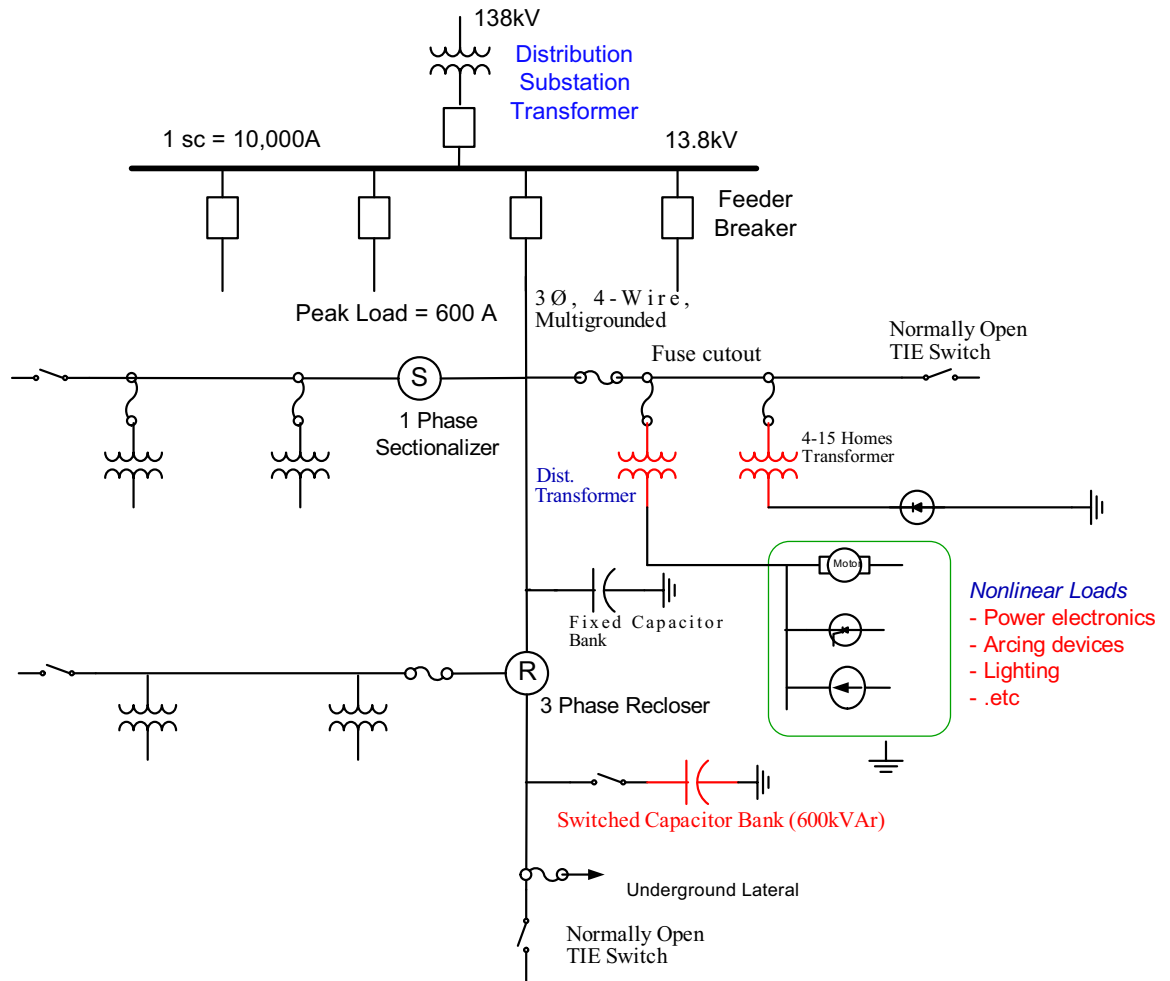
Figure 1.2: Primary distribution feeder [1].

1.2 Power Quality Problems in Power Distribution Systems

Due to reasons described above, distribution system operations can be challenging, especially in voltage regulation, protective device coordination, and maintaining adequate power quality (PQ) levels [6]. Most of these difficulties stem from three fundamental distribution system characteristics:

- Most distribution systems - especially rural systems - are operated in a radial configuration. That is, there is one source and the feeders extend radially from the source as shown in Figure 1.2. In a radial system, fault clearing requires the opening of only one device since only one source contributes current to the fault. In contrast, meshed transmission systems require breakers at both ends of a faulted line to open.

- Loads are served at the distribution system, and they can adversely impact the quality of electric power by injecting harmonic currents back into the distribution system while consuming the fundamental current at the power frequency.

- Switching operation of distribution system equipment, such as capacitor and transformer banks, and nonlinear loads can interact adversely, causing harmonic resonance and dynamic overvoltage phenomena.

Therefore, it should not be surprising that more power quality problems arise in the utility distribution system than in the transmission system. PQ prob-

lems may originate in the distribution system (such as equipment energizing/switching and circuit breaker clearing operations), or the customer's own facility or other customer facilities (where equipment can produce electrical emissions, i.e. harmonic currents). They can also arise from the interaction between customer loads or between customer loads and the utility system. In principle, there are three important groups of power quality disturbances frequently encountered in distribution systems [2]:

- Momentary outages and voltage sag disturbances due to breaker operations to clear faults on the same or parallel feeders or due to poor voltage regulation.

- Transient overvoltages due to the energizing and switching of distribution system equipment or due to lightning strikes entering the distribution system.

- Harmonic distortion problems due to end-user nonlinear loads and their adverse interaction with the distribution system equipment (shunt capacitor banks), i.e. power system harmonic resonance[2].

As stated above, power system harmonic resonance is a major source of power quality disturbances. Energizing shunt capacitor banks changes the

---

[2]The interaction of shunt capacitor banks with a source impedance always results in a parallel resonance characterized by a large impedance peak. Note that this dissertation focuses on this parallel resonance phenomenon and thus resonance or power system harmonic resonance refers to parallel resonance hereafter, if not specified.

system resonant frequencies. Even small harmonic currents can excite the system if one of the harmonic frequencies is close to one of these resonant frequencies. The resonance becomes salient when the system has low short-circuit capacity and damping. The impact of power system resonance includes increased power losses, as well as overheating and overloading of capacitors, transformers, and motors, which can cause catastrophic failures if they are not detected and mitigated. It can also cause interference with telecommunication lines and errors in power metering.

1.3   Motivation and Significance of This Research

The basic options for mitigating power system resonance are to reduce the harmonic currents, to add filters to siphon the harmonic currents off the system, or to modify the system impedance by either adding a shunt filter and reactor or changing the capacitor bank size. However, in cases where PQ monitoring is not available, it is not uncommon to see a blown fuse of the capacitor bank as a result of harmonic resonance. The simple reason for this equipment failure is that there are no practical techniques for:

1. identifying the system characteristics in order to perform these mitigation measures,

2. assessing the system operating conditions and detecting any symptoms of resonance before they cause serious power quality problems, and

3. correlating the resonance with operation of a specific capacitor bank.

Successful development and implementation of these techniques would bring enormous economic and technical benefits to power industries. Utilities could reduce considerable operating and maintenance cost and gather knowledge about the system operating conditions as well. The benefit of all these techniques would be improved power quality.

Therefore, this dissertation describes efficient and accurate techniques for identifying essential system characteristics (system resonant frequencies and damping) and determining the locations of the switched capacitor banks, specifically in radial power distribution systems. It should be also noted that many utilities have already implemented extensive power quality monitoring systems. In order to maximize economic as well as practical benefits, this dissertation takes full advantage of conventional PQ data, in particular that of capacitor bank switching transients. Thus, the proposed methodology can be easily implemented to work with the state-of-the-art PQ monitoring systems.

1.4 Objectives and Scope of This Research

This dissertation aims to address three primary entities that determine utility power distribution system characteristics: system parallel resonant frequencies, system damping, and capacitor banks. It then develops a series of five efficient algorithms to estimate, quantify, and locate these three elements, respectively, using only conventional PQ measurement data. Specifically, the dissertation aims are as follows:

- Developing an algorithm to empirically estimate power system parallel resonant frequencies,

- Developing algorithms to quantify overall damping and specific modal damping[3] of the power system in terms of X/R ratios, and

- Developing algorithms to correlate power disturbances with specific switched capacitor banks, i.e. to determine relative and exact location of the energized capacitor banks.

Figure 1.3 below illustrates the basic layout of the functionality of the developed algorithms. The input data used by the algorithms is capacitor switching transient data that is either real-time or stored in databases. Once symptoms for harmonic resonance are detected[4], the algorithms can be applied to provide valuable system information, specifically a profile of power system resonant frequencies, system damping (X/R ratio), and relative and exact locations of the switched capacitor banks.

---

[3]Note that damping in this dissertation should be differentiated from the damping in power system stability studies, which arises from the relationship between turbine-generator torque and speed characteristics, excitation system operation (PSS) and speed governing [7]. This will be discussed more in Chapter 2.

[4]A resonance current typically has one dominant harmonic riding on top of the fundamental sine wave, and one can observe salient increases in THD (Total Harmonic Distortion) values even after the typical transient time of capacitor switching has elapsed. These two signatures can be utilized to automatically detect harmonic resonance [8, 9]
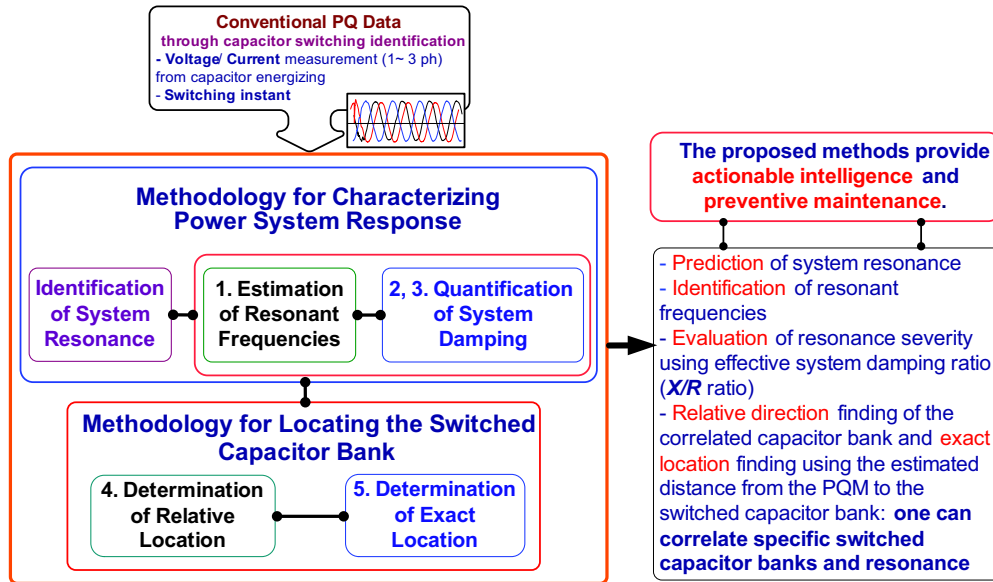
Figure 1.3: Research Objectives.

1.5 Contributions

In order to address some of the major issues with utility power distribution systems, this dissertation develops five practical algorithms for evaluating critical power system modal parameters[5] and locating the system equipment that causes the power systems to be vulnerable to resonance phenomena. This section discusses the academic and practical contributions of this dissertation.

---

[5]System resonant (natural) frequencies and their damping parameters are commonly called system modal parameters in mechanical and civil engineering. This dissertation uses the term mode to refer to resonance (oscillation) at specific natural frequencies and uses modal parameters to refer to resonant frequencies and associated damping ratios.

1.5.1 Methodology for Estimating Power System Parallel Resonant Frequencies

This dissertation presents a practical algorithm to estimate system parallel resonant frequencies accurately using conventional power quality data only [10]. Spectral analysis of the voltage and current transient waveforms immediately after capacitor bank switching is shown to provide accurate estimates of the system resonant frequencies. The rationale for this method is that the oscillatory transient frequencies embed valuable information about new resonant frequencies introduced into the power system. This methodology provides a fundamentally sound option for monitoring the existence of harmful resonance conditions using existing measurement data and power quality monitoring devices. Unlike the impedance scan method [11], this empirical method does not require any system short-circuit data. A profile of system parallel resonant frequencies is obtained by applying the proposed method to a series of capacitor switching transient events captured during a given monitoring period. The parallel resonant frequency profile provides a more useful tool than a single snapshot of frequency estimates obtainable from the conventional impedance scan.

1.5.2 Methodologies for Quantifying Power System Damping

This dissertation proposes two efficient algorithms to estimate system damping quantified in terms of X/R ratio. Combined with the estimated resonant frequencies from the first algorithm, the system damping provides all

essential knowledge concerning system response. These algorithms take advantage of the notion of an asymptotic or exponentially-damped sinusoidal, for which the signal phase varies much more rapidly than the amplitude. The zero-input (free) response of the capacitor bank transient voltage waveforms can be categorized into these asymptotic signals, and one can assign a unique time varying amplitude and phase pair through building analytic signals. This time varying amplitude includes the system damping information and the phase includes the system resonant frequency information, respectively. Two different techniques have been developed under this research objective. The first technique is based on the Hilbert transform [12], and the second is based on the wavelet transform [13]. System model reduction theory also allows one to interpret this damping as an effective X/R ratio.

1.5.3 Methodology for Determining the Relative Location of the Energizing Capacitor Banks

This dissertation provides a practical and accurate algorithm for determining the relative location of an energized capacitor bank, whether it is upstream or downstream from the monitoring location [14]. Mathematical analysis of capacitor bank energizing proves that: (1) the energized capacitor bank affects only the upstream reactive power flow and (2) at the energizing instant, the gradients of voltage and current waveforms measured upstream from the capacitor location will have opposite signs. Alternatively, the gradients of voltage and current waveforms measured downstream from the same capacitor location will have equal signs at the energizing instant. Thus, one

can precisely determine the relative location of switched capacitor banks by evaluating power factor changes and the signs of voltage and current waveform gradients at the switching instant. The developed method is very practical in that one can determine the relative location of switched capacitor banks by simply observing conventional capacitor switching data. It is also academically important in that the method is built solely upon the physics of capacitor bank energizing.

1.5.4 Methodology for Determining the Exact Location of the Energizing Capacitor Banks

Finally, this dissertation presents an efficient and accurate methodology for estimating the exact distance of an energized capacitor bank from a monitoring location [15]. This is the first analytical study of the initial voltage change due to a capacitor bank switching associated with locating an energized capacitor bank. The accuracy of the proposed method depends on the sampling rate of the waveform. In general, the higher the sampling rate, the more accurate the results of the algorithm. However, the proposed method can be applied to existing power quality monitors with a sampling rate of 256 samples/cycle to produce accurate results. On-going advances in power quality monitoring technology with improved data acquisition capability will allow very precise distance estimation.

13

1.6 Organization of the Dissertation

This dissertation is organized as follows. Chapter 2 provides detailed descriptions on the three key elements of power system response with particular reference to power system resonance phenomena. These key elements that define power system response are system resonant frequencies, system damping, and the interactions between nonlinear loads and capacitor bank energizing. The subsequent three chapters provide algorithms to empirically estimate the system impedance. Specifically, Chapter 3 details a methodology to estimate the system parallel resonant frequencies using only the capacitor bank switching transient data. Chapters 4 and 5 describe methodologies to estimate system damping. Chapters 6 and 7 are devoted to methodologies to correlate capacitor bank energizing disturbances with specific capacitor banks by determining both the relative and exact locations of the capacitor banks. Chapter 8 summarizes dissertation research problems and discusses future research opportunities based on the current research objectives and outcomes.

Chapter 2

Characteristics of Power Systems Response

The main objective of this chapter is to introduce fundamental characteristics of power distribution systems response in terms of system impedance, harmonic currents, and interactions between them, i.e. resonance phenomena and thus provide background of this dissertation research. Fundamentals of physics underlying system resonance phenomena are described and extended to resonance[1] in electric power distribution systems. Resonance (oscillation) issues in transmission level are briefly addressed and compared with those in distribution systems. Significant role of system damping on these power system oscillatory transient disturbances is also discussed. Related previous work in literature is summarized as well.

2.1 System Resonance

The term resonance came from acoustics where the audible resonances of musical instruments have been known for a long time. In physics, we define resonance as the increase in amplitude of oscillation of an electric or mechan-

---

[1]It should be noted that this dissertation focuses on parallel resonance phenomena in power distribution systems.
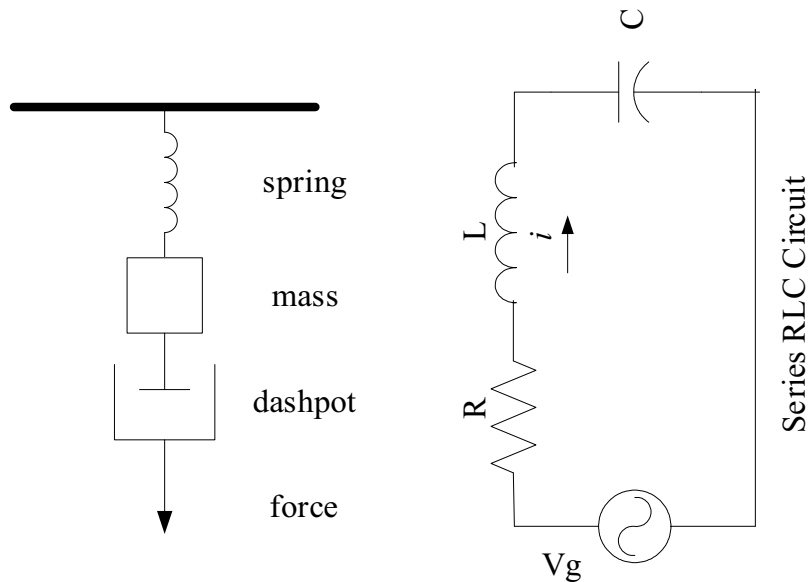
Figure 2.1: Mechanical spring and a series RLC circuit.

ical system exposed to a periodic force whose frequency is equal or very close to the natural undamped frequency of the system [16]. This system's natural frequency is also known as the system's natural frequency of vibration, resonant frequency, eigenfrequency or normal mode. As an example, a soprano may break a crystal goblet with her voice alone by properly producing a note at precisely the right frequency. Also, a bridge may be severely wobbled if it is subjected to a periodic force with the same frequency as one of its natural frequencies[2]. A simple example of resonant systems is shown in Figure 2.1. We

---

[2]On its opening day in June 2000, the Millennium footbridge over the river Thames in London started to wobble surprisingly under the weight of thousands of people and the bridge was closed two days later. It has been perceived that the pedestrians walked along, they became more synchronized with each other and the bridge started to wobble even more. In this case, pedestrian-induced movements were the external forces on the Millennium Bridge. [17]

Table 2.1: Mechanical spring and a series RLC circuit analogy.

Inductance L	$\leftrightarrow$	Mass m
Resistance R	$\leftrightarrow$	Damping constant c
$1/$(capacitance C)	$\leftrightarrow$	Spring constant k

choose a mechanical spring and a series RLC circuit because there is such a beautiful analogy between them in that the two different physical systems correspond to the same mathematical model. The natural modes and frequencies of a system are the solution of an eigenvalue problem that is quadratic [18]. These two physical systems can be described using similar differential equations: a series RLC circuit is described by Eq. (2.1) and a mechanical spring is described by Eq. (2.2).

$$LI(t)'' + RI(t)' + \frac{1}{C}I(t) = V\omega\cos\omega t \qquad (2.1)$$

$$my(t)'' + cy(t)' + ky(t) = r(t) \qquad (2.2)$$

where $V_g = V\omega\cos\omega t$, $i = I(t)$, $y(t) =$ the displacement of the body from the static equilibrium position $(y = 0)$, with the positive direction downward and $r(t)$ is an external force on the body. Table 2.1 presents the mechanical spring and a series RLC circuit analogy in terms of system parameters.

In both systems, we have a forcing term $r(t)$ and $V\omega\cos\omega t$, and what it forces is oscillation at the driving frequency, ω. Our goal is to solve equation for current or the displacement of a spring with the driving force. It is well

17

known that the solution[3] of any linear differential equation is the sum of a homogeneous solution or natural response, and a particular solution or forced response [19]. We first find the natural response of the given second order electrical system, which provides the resonant frequency of the system and then describe the resonant phenomena from the perspective of forced response in the following section. We can easily explain the behavior of a mechanical spring in an analogous fashion.

Note that the resonant systems illustrated here are called lumped-parameter resonators, since two forms of energy (potential vs. kinetic or magnetic vs. electrical) are stored in well-defined system components (capacitor or spring). Many resonators do not allow for a clear separation of different forms of energy, and such systems are called distributed-parameter resonators. An electric transmission or distribution line or a violin can support the distributed-parameter resonances, exhibiting multiple resonances.

2.1.1   Natural Response

We analyze the electric circuit by finding current $I(t)$ for $t > 0$ without V_g in Figure 2.1. Then, we can describe the circuit by the following differential

---

[3]The solution for the natural (free) response represents the transient solution and the forced response tends to the steady-state solution.

equations and obtain the characteristic equations,

$$LI'' + RI' + \frac{1}{C}I = 0 \tag{2.3}$$

$$s^2 + \frac{R}{L}s + \frac{1}{LC} = 0 \tag{2.4}$$

The natural response frequencies are as follows:

$$s_{1,2} = -\frac{R}{2L} \pm \sqrt{\left(\frac{R}{2L}\right)^2 - \frac{1}{LC}} \tag{2.5}$$

There are three types of response, depending on the nature of the discriminant, $R^2 - 4L/C$ and $c^2 - 4mk$ for a mechanical system. We shall now briefly explain these three cases.

2.1.1.1   Overdamped Case

If the discriminant is positive, i.e., $R^2 - 4L/C > 0$, then the natural frequencies are real and distinct negative numbers. This is an overdamped case and here,

$$I = A_1 e^{s_1 t} + A_2 e^{s_2 t} \tag{2.6}$$

The reason for the term overdamped may be seen from the absence of oscillation (fluctuation in sign). The element values are such as to damp out any oscillatory tendencies. An example of an overdamped case is shown in Figure 2.2(a), where $I(t) = 5e^{-t} - 3e^{-3t}$.

2.1.1.2   Underdamped Case

If the discriminant is negative, i.e., $R^2 - 4L/C < 0$, then we have the underdamped case. The natural frequencies are complex, and contains sine

19
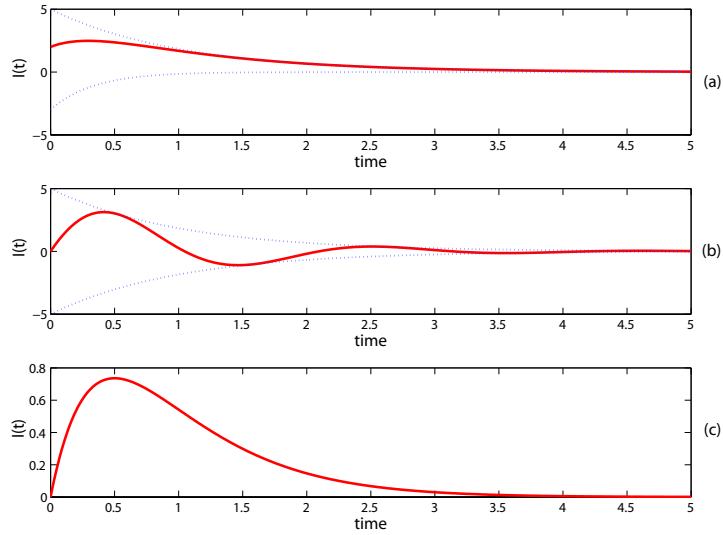
Figure 2.2: Sketch of an (a) overdamped, (b) underdamped and (c) critically damped response.

and cosine functions, which of course are oscillatory-type functions. In this case, it is convenient to define a resonant frequency[4],

$$\omega_0 = \frac{1}{\sqrt{LC}} \tag{2.7}$$

with a damping coefficient,

$$\alpha = \frac{L}{2R} \tag{2.8}$$

and a damped frequency,

$$\omega_d = \sqrt{\omega_0^2 - \alpha^2}. \tag{2.9}$$

---

[4]This is the frequency of free oscillation when there is no resistance, i.e. no damping. Note that this dissertation is interested in this underdamped case due to its practical importance.

Using these definitions, the natural frequencies are $s_{1,2} = -\alpha \pm j\omega_d$, and therefore the response is $I(t) = e^{-\alpha t}(A_1 \cos \omega_d t + A_2 \sin \omega_d t)$, which is oscillatory in nature. An example of an underdamped case is shown in Figure 2.2(b), where $I(t) = 5e^{-t} \sin 3t$ chosen arbitrarily.

2.1.1.3 Critically Damped Case

When the discriminant is zero, we have a critically damped case, for which $L = R^2 C/4$. In this case, the natural frequencies are real and equal, given by $s_{1,2} = -\alpha, -\alpha$, where $\alpha = L/2R$. The response is then $I(t) = (A_1 + A_2 t)e^{-\alpha t}$. An example of a critically damped case is shown in Figure 2.2(c), where $I(t) = 4te^{-2t}$.

2.1.2 Forced Response

As it was previously discussed, for a sinusoidally excited network to be in resonance, the amplitude of the network function must attain a prominent maximum or minimum value. The frequency at which this occurs is called the resonant frequency. The forced response to the input of $V_g(t) = V \sin \omega t$ will have the following form:

$$I(t) = a \cos \omega t + b \sin \omega t \tag{2.10}$$

Coefficients, a and b are as follows:

$$a = \frac{LV\omega(\omega_0^2 - \omega^2)}{L^2(\omega_0^2 - \omega^2)^2 + \omega^2 R^2}, \quad b = \frac{V\omega^2 R}{L^2(\omega_0^2 - \omega^2)^2 + \omega^2 R^2}$$

When the resistance, R is zero or the damping constant c is zero in the mechanical spring system, we can find the undamped forced response[5].

$$I(t) = a \cos \omega t = \frac{V\omega}{L(\omega_0^2 - \omega^2)} \cos \omega t \tag{2.11}$$

From the formula, we can see the main point: As ω approaches ω_0, resonance results. The denominator in this solution becomes small and the amplitude goes to infinity. In fact, the solution breaks down completely at $\omega = \omega_0$. If the initial conditions are $I(0) = 0$ and $I'(0) = 0$, the complete solution of the given linear differential equation is obtained: $I(t) = a(\cos \omega t - \cos \omega_0 t)$. This is the sum of a particular solution and a homogeneous solution. The output represents a superposition of two harmonic oscillations; the frequencies are the natural frequency $(\omega_0/2\pi)$ and the frequency $(\omega/2\pi)$ of the input. The maximum value becomes the following at much later times when two cosines are out of phase by 180 degrees:

$$I_{\text{max}} = 2a = \frac{2V\omega}{L(\omega_0^2 - \omega^2)} \tag{2.12}$$

An interesting and highly important type of oscillation occurs when ω is close to ω_0. The amplitude of $I(t)$ does not go to infinity but it goes far beyond the amplitude $2V\omega/L$ of the driving force[6]. In a radio signal, the large oscillations are heard as beats. The difference of cosines can be written as follows:

$$I(t) = 2a \sin \frac{\omega_0 + \omega}{2} t \sin \frac{\omega_0 - \omega}{2} t \tag{2.13}$$

---

[5]This case is called undamped forced oscillation

[6]It is like pushing a swing or a rocking chair at almost the right frequency but not quite.
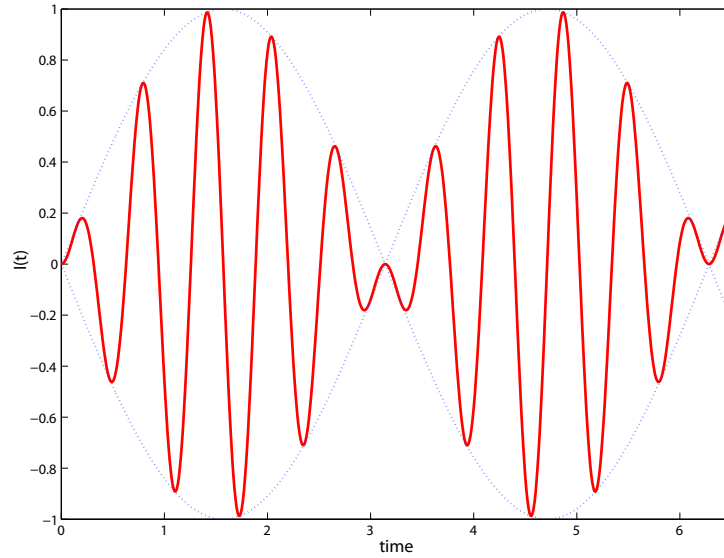
Figure 2.3: Forced undamped oscillation when the difference of the input and resonant frequency is small.

This equation contains two frequencies; the fast frequency $(\omega_0 + \omega)/2$ inside the envelope, and the slow frequency $(\omega_0 - \omega)/2$ of the envelope itself. Here, we select $\omega = 9$ near $\omega_0 = 11$.

In the case of the following pure resonance $(\omega_0 = \omega)$, we can find that the forced response becomes as follows:

$$I(t) = \frac{V}{2L\omega_0} t \sin \omega_0 t \tag{2.14}$$

As illustrated in Figure 2.4, $I(t)$ keeps growing but oscillates at the only one frequency (ω_0). In practice, this means that the systems with very little damping may undergo large vibrations that can destroy the system.

23
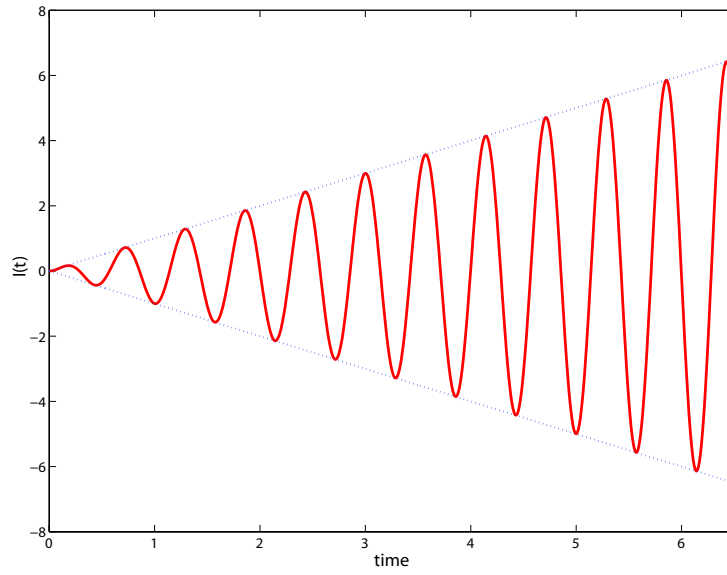
Figure 2.4: Forced response in the case of resonance.

While in the undamped case the amplitude of the forced response approaches infinity as ω approaches ω_0, this will not happen in the damped case $R \neq 0$ or $c \neq 0$. In this case the amplitude will always be finite, but may have a maximum for some ω's, depending on R or c. This may be called practical resonance. It is of great importance because it shows that some input may excite oscillations with such a large amplitude that the system can be destroyed. In addition to an electric power system of our interest, machines, cars, ships, airplanes and bridges are vibrating mechanical systems, and it is sometimes rather difficult to find constructions which are completely free of undesired resonance effects. To study the amplitude of $I(t)$ as a function of ω, we write
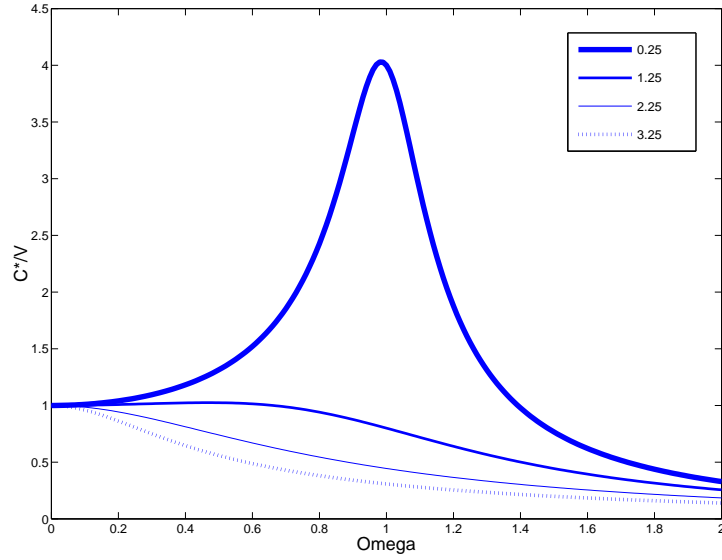
Figure 2.5: Amplification C^*/V as a function of ω for various values of R or damping constant c.

the $I(t)$ as follows:

$$I(t) = C^*(\omega) \cos(\omega t - \eta) \tag{2.15}$$

where $C^*(\omega) = \sqrt{a^2 + b^2} = \frac{V}{\sqrt{L^2(\omega_0^2 - \omega^2)^2 + \omega^2 R^2}}$ and $\eta = \tan^{-1}(b/a)$.

The maximum of C^* is determined by $dC^*/d\omega = 0$, which leads to the following relation: $R^2 = 2L^2(\omega_0^2 - \omega^2)$. As illustrated in Figure 2.5, C^* decreases in a monotone way as ω increases for sufficiently large damping ($R^2 > 2L^2\omega_0^2$) and C^* increases as R decreases and approaches ω_0 as R approaches zero for $R^2 \leq 2L^2\omega_0^2$.

In this Section 2.1, we provide a clear mathematical and conceptual description of the resonance phenomena in linear systems. When the system

25

does not have damping terms, the response is periodic. When the system includes damping terms, the system response loses energy and dies out, although the system response is totally different, depending on the damping and resonant frequencies. However, it might be very challenging to describe the resonance phenomena clearly in a time-varying nonlinear system such as a power distribution system of our interest. But, the enormous impact of the successful research on the power system operation is self-evident and this is our motivation for power system harmonic study. In the following sections, we detail resonance phenomena in an electric system.

2.2 Resonance in Electric Circuits

All electric circuits containing both capacitances and inductances also have one or more natural frequencies [20]. When one of those frequencies lines up with a frequency that is being produced by nonlinear loads, a resonance may develop in which the voltage and current at that frequency continue to persist at very high values. Since the exciting current is harmonic current, this type of resonance is called harmonic resonance. This harmonic resonance can be broken down into two groups, which are discussed in the following sections.

2.2.1 Parallel Resonance

Parallel resonance occurs in a parallel RLC circuit with equal inductive reactance ($X_L = 2\pi f L$) and capacitive reactance ($X_C = \frac{1}{2\pi f C}$), where f is the system frequency. Thus, the impedance seen by the load becomes very

(a) Parallel RLC Circuit   (b) Series RLC Circuit
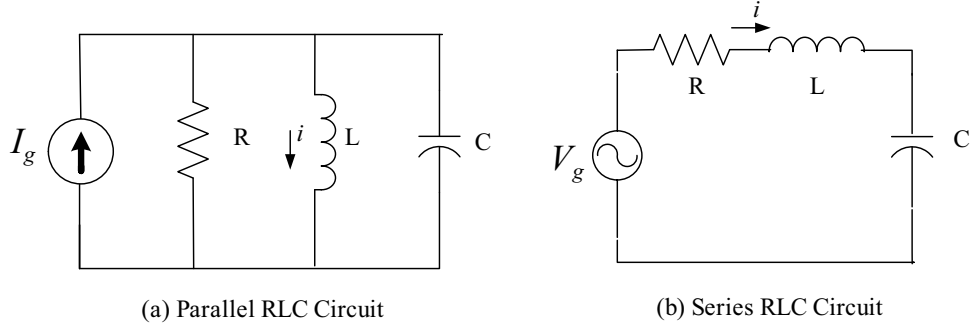
Figure 2.6: Parallel and series RLC circuit.

large and the effect of this is a large voltage distortion even for moderate current distortion. For the parallel RLC circuit of Figure 2.6(a), the equivalent impedance at the system frequency, Z_1 is as follows:

$$Z_1 = \frac{-jRX_LX_C}{R(X_L - X_C) - jX_LX_C}$$

For any harmonic h, $X_L(h) = hX_L$ and $X_C(h) = X_C/h$. Thus, $X_L(h)X_C(h) = X_LX_C$. Such that, the impedance at any harmonic, Z_h is:

$$Z_h = \frac{-jRX_LX_C}{R(hX_L - X_C/h) - jX_LX_C} \tag{2.16}$$

and its magnitude becomes:

$$|Z_h| = \frac{RX_LX_C}{\sqrt{[R(hX_L - X_C/h)]^2 + [X_LX_C]^2}} \tag{2.17}$$

For resonance at $h = h_r$, we have $h_rX_L = X_C/h_r = X_r$, which implies that $h_r = \sqrt{X_C/X_L}$ and $X_r = \sqrt{L/C}$. Thus, the circuit's impedance at resonance is purely resistive and is equal to R, i.e. $Z_{h_r} = R$. Note that the effect of the storage elements exactly cancels at resonance and the source sees only resistance.

27

2.2.2 Series Resonance

Analogous to parallel resonance, series resonance occurs in a series RLC circuits having equal inductive and capacitive reactance. The circuit impedance is very low and consequently a small exciting voltage results in a huge current. For a series RLC circuit as depicted in Figure 2.6(b), the equivalent impedance at the fundamental system frequency is $Z_1 = R + j(X_L - X_C)$. For any harmonic h, $Z_h = R + j(hX_L - \frac{X_C}{h})$. Thus,

$$|Z_h| = \sqrt{R^2 + \left(hX_L - \frac{X_C}{h}\right)^2}$$

For resonance at $h = h_r$, we have

$$h_r X_L = \frac{X_C}{h_r} = X_r$$

which implies that $h_r = \sqrt{\frac{X_C}{X_L}}$ and $X_r = \sqrt{\frac{L}{C}}$.

2.3 Power Systems Resonance

In addition to the nominal system frequency (50 or 60 Hz), all electrical and electromechanical power systems involve a wide range of resonant oscillatory modes[7] which are excited during disturbances and switching events. Most of these oscillations are considered harmless and die out owing to positive system damping that will be detailed in the following Section 2.4. However,

---

[7]In power system stability studies, power system mode refers to an eigenvalue of the linearized system and its associated eigenvector [21]. This corresponds to our previous definition of mode in Chapter 1, since the eigenvalue and eigenvector determine natural frequencies and mode shapes.

under some circumstances, a specific oscillation may have unacceptably high magnitude, sustain for a long period and lead to damage due to insulation, mechanical aging or breakdown, or system instability.

Given the inherent parameters of lines and equipment, power system oscillations that are contributed by mostly passive electrical components, their resonant frequencies are generally much higher than the system frequency. These resonance phenomena are generally described in the same way as aforementioned resonances in electric circuits and commonly observed in power distribution systems. However, when the oscillations involve both the electrical and rotating mechanical equipment coupled through the magnetic flux, one may observe frequencies much lower than the system frequency[8], which are mostly observed in power transmission systems. This section describes these resonance phenomena in both distribution and transmission levels and significant roles of the system damping associated with these oscillatory disturbances.

2.3.1 Resonance in Power Distribution Systems

Power systems are primarily inductive at the fundamental frequency and charging capacitive components of the lines are frequently neglected in studying utility distribution systems. In general, the impedance from the equivalent voltage source to the point of a capacitor bank is called a short-

---

[8]These frequencies are further categorized into low frequency oscillations (0.1 to 2.0 Hz) and subsynchronous resonance (10 to 50 Hz)

29

circuit impedance including resistance of the lines:

$$Z_{SC} = R_{SC} + jX_{SC} = \frac{kV^2}{MVA_{SC}} = \frac{kV \times 1000}{\sqrt{3}\,I_{SC}}$$

where Z_{SC} = short-circuit impedance, R_{SC} = short-circuit resistance, X_{SC} = short-circuit reactance, kV = phase-to-phase voltage (kV), MVA_{SC} = three-phase short-circuit (MVA) and I_{SC} = short-circuit current (Amps). Note that conventional harmonic studies suggest using the impedance of the transformer for assessing system resonance problem as a rule of thumb, if correct value of X_{SC} is not available. However, it is noteworthy that line impedance and damping from the load can change the system modal parameters significantly. Thus, careless adoption of this convention should be avoided. This will be discussed further in Chapter 4.

Note also that the system impedance changes significantly when shunt capacitor banks, either at the customer location for power factor correction, or on the distribution system for voltage control, are present, since the capacitive reactance together with the inductive reactance forms a new system impedance [2]. Figure 2.7(a) illustrates a simple distribution system with a capacitor bank installed at its substation. Suppose that a nonlinear load is located at the customer facility. The equivalent voltage source is assumed distortion-free, i.e., it has a fundamental voltage component only. From the perspective of the harmonic source, i.e., nonlinear load, the shunt capacitor bank, the shunt capacitor bank (X_C) is in parallel with the equivalent voltage source (X_{SC}) and the transformer leakage reactance at harmonic frequencies as depicted

(a)Simplified distribution circuit

(b)Parallel resonant circuit as seen from
the harmonic source
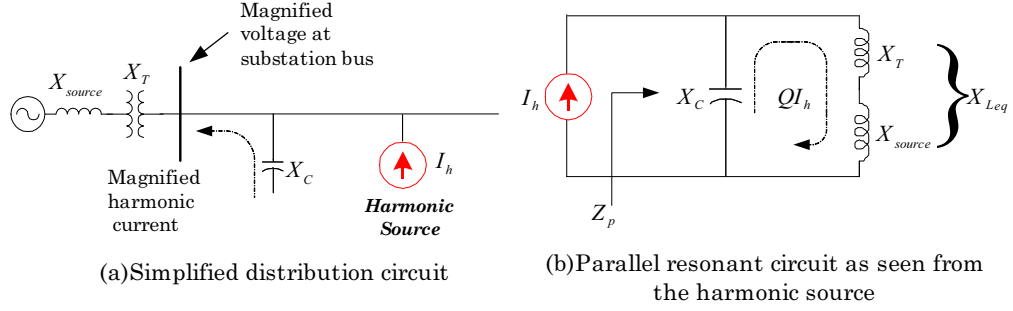
Figure 2.7: (a) A simple distribution system with a capacitor bank (b) A parallel resonant circuit as seen from the harmonic sources.

in Figure 2.7(b). The system voltage source appears short-circuited because the system source is distortion-free and thus there are no harmonic voltage sources. The apparent system impedance seen from the nonlinear load would be as follows:

$$
\begin{aligned}
Z_p(\omega) &= \frac{X_C\left(X_{Leq} + R\right)}{X_C + X_{Leq} + R} = \frac{X_C\left(X_{Leq} + R\right)}{R} \\
&= \frac{R + j\omega L_{eq}}{1 - \omega^2 L_{eq}C + j\omega RC}
\end{aligned}
\tag{2.18}
$$

where R (not shown in Figure 2.7), X_{Leq} or L_{eq} and C are the resistance and inductance of the combined equivalent source and transformer, and the capacitance of the capacitor bank, respectively.

As discussed in the previous section, parallel resonance occurs when the impedance seen from the harmonic source $Z_p(\omega)$ is at its maximum, i.e., when the denominator of $Z_p(\omega)$ is at its minimum. For any practical power system where the combined resistance R is very small, the apparent impedance X_C is maximized when the reactance X_c and that of the distribution system cancel

31

each other out. This condition occurs at the following frequency:

$$f_p = \frac{1}{2\pi} \sqrt{\frac{1}{L_{eq}C} - \frac{R^2}{4L_{eq}^2}} \approx \frac{1}{2\pi} \sqrt{\frac{1}{L_{eq}C}} \qquad (2.19)$$

The frequency f_p is the resonant frequency for the circuit shown in Figure 2.7. The system impedance at this frequency is as follows:

$$Z_p(\omega_p) = \frac{X_C\left(X_{Leq} + R\right)}{X_C + X_{Leq} + R} = \frac{X_C\left(X_{Leq} + R\right)}{R}$$

$$\approx \frac{X_{Leq}^2}{RC} = \frac{X_C^2}{R} = QX_{Leq} = QX_C \qquad (2.20)$$

where $Q = X_L/R = X_C/R$ and $R \ll X_{Leq}$. Note that all reactances are computed at the resonant frequency f_p. Q is known as the quality factor of a resonant circuit that indicates the severity of parallel resonances [2]. Q varies considerably by location on the power system. It might be less than 5 on a distribution feeder and more than 30 on the secondary bus of a large step-down transformer. From Eq. (2.20), it is clear that during parallel resonance, a small harmonic current can cause a large voltage drop across the apparent impedance, i.e., $V_p = QX_{Leq}I_h$. Since Q and X_{Leq} are large, the voltage V_p can be very large even when the harmonic current is very small. In other words, it voltage waveform will be heavily distorted and dominated by the resonant frequency. The current, I_{cap} flowing in the capacitor bank and into the power system through the the transformer will also be magnified Q times, since

$$I_{cap} = \frac{V_p}{X_C} = \frac{QX_C I_h}{X_C} = QI_h \qquad (2.21)$$

Thus, this resonance phenomenon will possibly cause capacitor failure, fuse blowing, or transformer overheating.
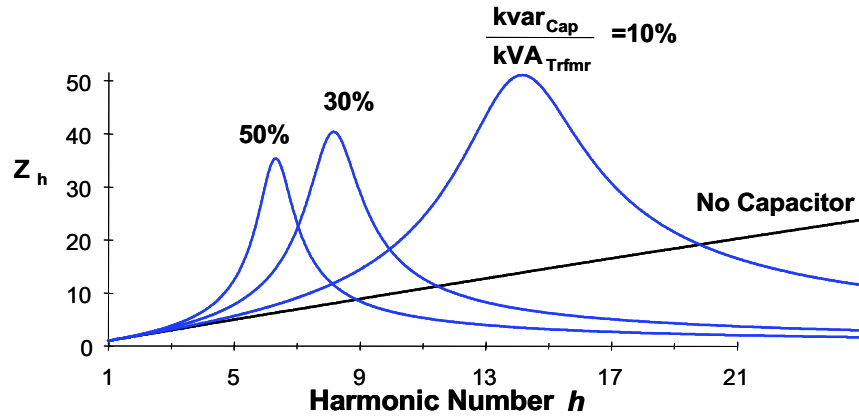
Figure 2.8: System frequency response as capacitor size is varied in relation to transformer (redrawn based on Figure 5.28 [2]).

The extent of voltage and current magnification is determined by the size of shunt capacitor bank. Figure 2.8 shows the effect of varying capacitor size in relation to transformer on the impedance seen from the harmonic source and compared with the case in which there is no capacitor.

There are two primary sources of exciting currents in distribution systems: harmonic currents from nonlinear loads and inrush currents during transformer energizing. These exciting currents are prevalent in distribution systems due to widespread use of power electronic devices in nonlinear loads and the frequent energization of distribution system transformers.

Consider a case where a distribution system is being energized in a relatively weak system. Prior to the energization, the total harmonic distortion is minimal and does not exhibit any sort of resonance problems. However, when a capacitor bank is energized, the current is damped out rather slowly
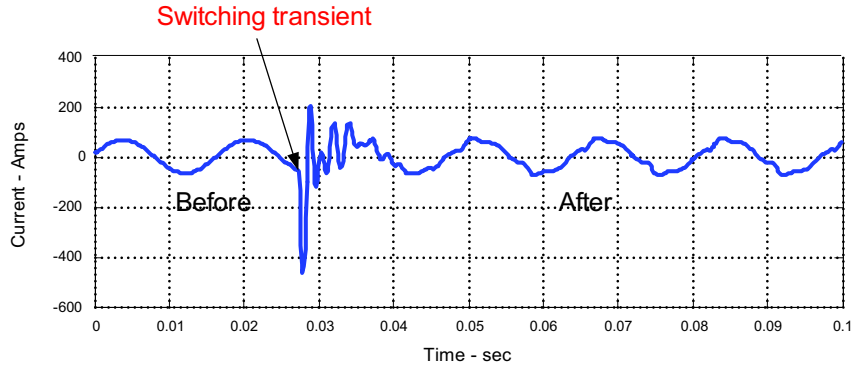
Figure 2.9: Capacitor energization resulting in increased harmonic distortion.

taking more than a quarter of a second. Furthermore, the current waveform exhibits clear signs of harmonic distortion. This is illustrated in Figure 2.9. This indicates that energizing a capacitor bank in the distribution system changes the system resonant frequencies. In this particular example, one of the system resonant frequencies coincides with harmonic currents of nonlinear loads on the system.

Note that parallel resonant frequencies must be properly accounted for when assessing power system harmonics. Otherwise, a filtering action using single-tuned filters to eliminate a characteristic harmonic at a given site may amplify the waveform distortion if the parallel peak (pole) of the filter coincides with with a lower order characteristic harmonic of the load. Active filters may overcome this hurdle but they must be well justified to offset their higher cost [2, 11, 22].

In some cases, energizing the transformer produces magnetizing inrush current that is rich in second to fifth-order harmonic currents. These magnetiz-

34

ing harmonic currents can excite the power system natural response frequencies as well. When this happens, a phenomenon called dynamic overvoltage occurs [23]. The following example illustrates an actual case where dynamic overvoltage occurs when a distribution system transformer is energized by a feeder recloser following a fault clearing operation. It is apparent in Figure 2.10 (a) that the feeder voltage (1.0 per unit is 25 kV) experiences dynamic overvoltage. The overvoltage magnitude is approximately 1.5 p.u and persists over the entire monitoring record. Note that the inrush current peaks for the first few cycles are very large and highly distorted. This appears vividly in Figure 2.10 (b), (c), and (d). Note that the magnitude of the inrush current in Figure 2.10 (b) exceeds the monitoring current setting of 200 amps – thus the current waveshape appears flat-topped. Due to the random fluctuating transient flux in the iron core, it is typical to observe that one phase experiences a more severe inrush than others. This also causes current and thus voltage imbalances.

One may also observe instances where a shunt capacitor and the inductance of a transformer or distribution line appear as a series LC circuit to harmonic sources. If the resonant frequency of this series LC circuit is in line with one of harmonic frequencies of the nonlinear loads, the circuit will draw large harmonic current around the resonant frequency in the power distribution system. Thus, customers having no nonlinear loads, but utilizing power factor correction capacitors, may in this way experience this series resonance problems due to neighboring harmonic sources [2]. As discussed in Section
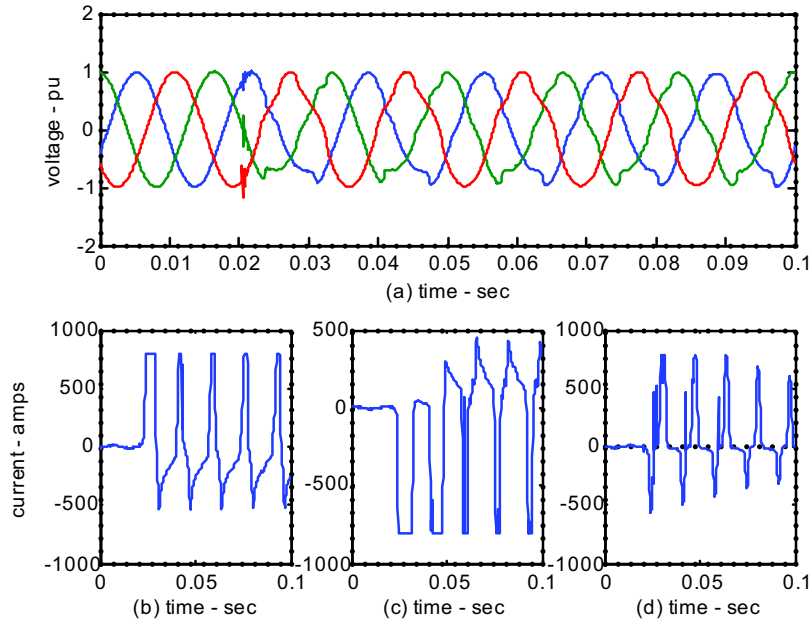
Figure 2.10: A dynamic overvoltage condition due to transformer energizing.

2.2.2, the series combination of the transformer inductance and the capacitor bank is very small (theoretically zero) and only limited by resistance in the system. This situation is depicted in Figure 2.11. During resonance, the power factor correction capacitor forms a series circuit with the transformer and harmonic sources. Thus, the harmonic current at the resonant frequency will flow freely in this circuit. The voltage at the power factor correction capacitor is magnified and highly distorted.

36
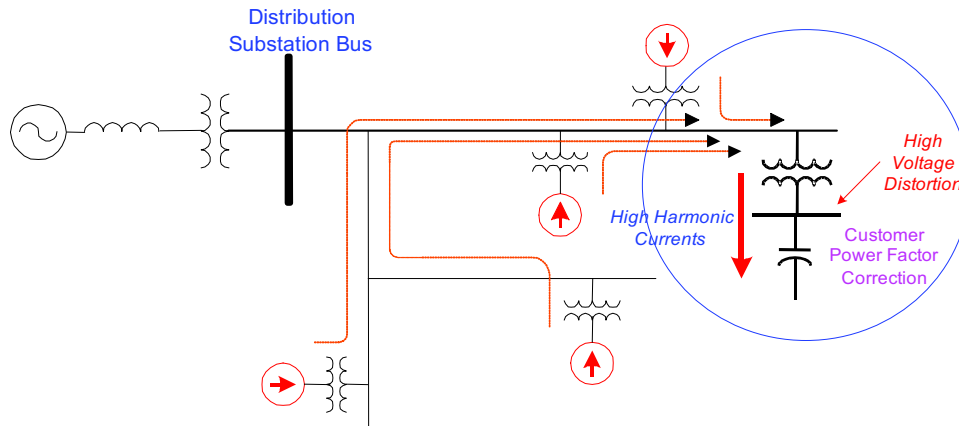
Figure 2.11: System with potential series resonance problems (redrawn based on Figure 5.29 [2]).

2.3.2 Oscillations in Power Transmission Systems

As discussed in Section 2.3, low frequency electromechanical oscillations[9] are one of the most serious concerns in transmission level. These oscillations are classified by the effective system components: [24, 25]:

- Intraplant mode oscillations: machines on the same power generation site oscillate against each other at 2.0 to 3.0 Hz depending on the unit ratings and the reactance connecting them.

- Local plant mode oscillations: one generator swings against the rest of the system at 1.0 to 2.0 Hz. The impact of the oscillation is localized to the generator and the line connecting ti to the grid.

---

[9]Since the term, oscillation is generally used to represent subsynchronous resonance, and other low frequency oscillatory instability phenomena in transmission levels, oscillations were chosen instead of resonance for this subsection title.

- Interarea mode oscillations: these phenomena are observed over a large part of the network and involve two coherent groups of generators swinging against each other at 1 Hz or less.

- Control mode oscillations: these are associated with complicated interactions between generators and poorly tuned exciters, governors, HVDC converters and SVC controls.

- Torsional mode oscillations (Subsynchronous oscillations): These oscillations are associated with a turbine generator shaft system in the frequency range of 10 to 50 Hz and are generally excited when a multi-stage turbine generator is connected to the grid system through a series compensated line. A mechanical torsional mode of the shaft system interacts with the series capacitor at the resonant frequency of the network. The resonance occurs when network natural frequency corresponds to synchronous frequency − torsional frequency.

In fact, these low frequency oscillations are inherent to electric power systems and appeared as soon as two synchronous generators operated in parallel[10]. These problems have become more outstanding, since interconnections and interchanges of energy have dramatically increased in transmission networks and power systems have been driven to operate very close to transient and

---

[10]The earliest problems in the form of spontaneous oscillations or hunting were experienced in 1920s [25].

small-signal rotor stability limits. Thus, a better understanding and suppression of low frequency oscillations could relax some of the constraints on larger bulk power transfers and increase power system security.

2.4 Power System Damping

In general, damping is a term broadly used to denote either the dissipation of energy in, and the consequent decay of, oscillations of all types or the extent of the dissipation and decay. Expanding the previous discussion on the role of damping in the case of forced oscillations in Section 2.1, this section discusses the term, damping used in electric power systems.

2.4.1 Damping in Power Distribution Systems

It is well known that the system damping from resistive components of the lengthy lines (cables) and loads often prevents catastrophic voltage and current distortions. This damping is equivalent to R in conventional X/R ratio of the utility distribution system. It is generally agreed that this is an adequate representation for many practical situations[11] in the distribution level [26]. Thus, X/R ratio or Q factor of the system should bee examined to design proper harmonic filters and coordinate protective devices for the power systems. The convention of using X/R ratio is also a motivation of

---

[11]There are instances where resistive components cannot effectively represent the system damping. These are related with fast transients like penetration of traveling waves into the ground. Corona is also one of these examples where energy is extracted from the circuit by currents flowing out from the conductor in small charges into the surrounding air.
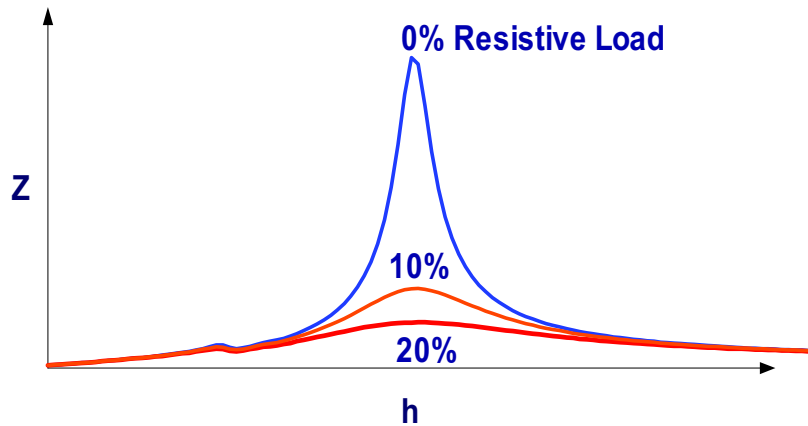
Figure 2.12: Effect of resistive loads on parallel resonance (redrawn based on Figure 5.31 [2]).

the proposed methodologies for quantifying the system damping in Chapters 4 and 5.

Figure 2.12 shows the parallel resonant circuit impedance characteristic for various amounts of resistive load in parallel with the capacitance. As little as 10% resistive loading can have a significant beneficial impact on peak impedance [2]. Note that the substation transformer dominates the system impedance and has a high X/R ratio, i.e. high Q value. High Q values indicates that the system has low damping. When resonance occurs in this system, the corresponding parallel resonant impedance peak is very sharp and high. Thus, the most problematic resonance phenomena may occur when capacitors are installed on substations buses, either utility substations or in industrial facilities.

Considerable loads of the utility distribution system is nowadays con-

trolled by power electronics to provide constant power to the loads. A constant power load, such as a motor variable speed drive or a switched mode power supply, presents a small-signal impedance or resistance to the power system that is negative, i.e. any rise in voltage causes the current to fall. This harms the system damping, or energy absorption capability, from the power system. Note also that motors are primarily inductive and provide little damping. In fact, they may increase distortion by shifting the system resonant frequency closer to a significant harmonic. Thus, it can be expected that the continuous addition of such loads to the power system will cause instabilities or poor performance in the future [2, 22].

2.4.2   Damping in Power Transmission Systems

System damping in the power transmission systems is frequently referred to in power system stability studies in terms of damping torque, since this damping torque plays a significant role of improving oscillatory stability in synchronous machines. This damping in transmission level basically represents the same function of restraining transient oscillatory disturbances as in distribution, since the performance of the damping torque is evaluated as the rate of decay of oscillations as well. It has been studied that power system damping consists of several types and components which should be modeled for stability studies, for example, damping due to turbine-generator torque vs. speed characteristics, damping due to load-frequency characteristics, electrical damping due to rotor amortisseur winding current, damping (or negative

damping) due to excitation system operation including the impact of power system stabilizer (PSS) to control excitation of generators, damping (or negative damping) due to speed governing, and transient losses associated with the network and generator stators following a transient, etc. One may find numerous research efforts in modeling or representing significant damping, in particular from dynamic loads [7,27] and identifying the power system in order to effectively design damping controllers [28–30].

It is also noteworthy that the analysis of transient behavior of power systems with FACTS devices has been the subject of extensive study in recent years. FACTS offer a powerful alternative to accommodate changes in operating conditions of an electric transmission system while maintaining sufficient steady-state and transient stability margins [4]. For example, the TCSC (tyristor controlled series compensator) has been introduced to provide flexible and controlled series compensation. Thus, TCSC can not only improve system stability by fast control action but also overcome the problem of subsynchronous resonance.

2.5   Discussion

Power quality and in particular, power system harmonics has become an important topic for utility and facility engineers. This has been be motivated by a growing need to design systems and interconnections with acceptable quality standards and to monitor the quality of electrical energy exchanges in the newly deregulated environment [31]. High-tech and knowledge-oriented

businesses are also demanding improved reliability and power quality expectations because newer equipment tends to be more sensitive to the electrical environment than older equipment[12].

On the other hand, the increasing use of nonlinear loads in industry increases harmonic distortion in utility distribution systems[13]. Waveform distortion levels in utility distribution systems have been raised even further by the application of capacitor banks used in industrial plants for power factor correction and by power utilities for increasing voltage profile along the utility feeders. The resulting resonant frequency of the system is likely to coincide with one of harmonics on the system, creating resonance. Thus, modern utility distribution systems are vulnerable to serious resonance phenomena.

Thorough harmonic studies, from the planning to the design stages of power utility and industrial installations, will prove to be an effective way to keep distribution systems and equipment under acceptable operating conditions and to anticipate potential problems with the installation or addition of nonlinear loads. However, this method works only for newly developed distribution systems. Unfortunately, most of the utility distribution systems were built long before the significance of PQ was recognized and have been

---

[12]It is estimated that more than 30% of the power currently being drawn from the utility companies is now heading for sensitive equipment. Forecasts suggest that figure will continue to increase, doubling by 2010 [32].

[13]Harmonic distortion is no longer a phenomenon confined to industrial equipment and processes, where the first power quality concerns developed. Uninterruptible power supplies (UPS), PCs, and electronic and entertaining devices proliferate nowadays in commercial and residential sectors. These loads represent formidable sources of harmonic currents [22].

43

expanded continuously to meet the continuously increasing demands without increased attention to these PQ issues. Thus, they are facing serious potential power quality problems and resort to remedial solutions when problems occur. This situation is an important motivation for the development of the methodologies presented in this dissertation, since successful implementation of these methodologies into modern PQ monitoring devices will provide significant system information on both older systems for which system studies were not considered in the planning stage and newer systems in which additional loads change system parameters. The methodologies presented in this dissertation will allow preventive and corrective solutions to various power quality problems in both cases.

Chapter 3

Empirical Estimation of Power System Parallel Resonant Frequencies using Capacitor Switching Transient Data

This chapter presents an efficient technique for estimating system parallel resonant frequencies using capacitor switching transient data. Unlike the previous method[1] where the resonant frequencies were estimated using the raw transient waveform, the proposed algorithm uses only the effective transient part of the disturbance waveform[2] and is thus robust to undesired background harmonic distortions. As such, the proposed method can be applied to data taken from any measurement point including a customer facility with significant nonlinear loads.

3.1   Introduction

Energizing a shunt capacitor bank shifts system resonant frequencies according to the effective capacitance and inductance of the system. When one of these frequencies corresponds to a frequency being produced by nonlinear

---

[1]The previous method refers to the method that Santoso proposed [33].

[2]This effective transient waveform can be regarded as empirical free response (zero input response) of the capacitor bank energizing. Thus, it is technically free from the fundamental and background harmonic excitation signals.

loads, resonance may develop in which the system voltage and current can be highly distorted [2]. Harmonic resonance and the associated magnification of harmonic levels can cause a number of different problems on power systems. Examples of harmonic resonance issues were reported in [34–36]. There are two common practical methods to prevent harmonic resonance problems, i.e., by keeping exciting harmonic currents from reaching the utility distribution system or by modifying the utility system natural resonant frequencies so that none of these frequencies lines up with harmonic frequencies produced by nonlinear loads. The first method may not be practical in many cases because of the wide variety of nonlinear loads that are now being used by virtually all classes of customers. In order for the second method to be effective, engineers must have information about the system resonant frequencies. This information can be estimated using the short-circuit impedance at the point on a circuit at which a capacitor bank is located. This estimate is generally precise for a simple system where there are only one or two capacitor banks in the system. For a more complex system having multiple capacitor banks, the natural frequency response is usually estimated by modeling the power system and carrying out an impedance scan [2, 11, 31]. Unfortunately, there are three issues with this application when harmonic studies are considered. First, the size of the admittance matrices (this calculation is repeated using discrete frequency steps throughout the range of interest) may be so large that an exact mathematical model of the system is not realistic. Second, the complexity of a rigorous and complete mathematical model of the system does

46

not necessarily explain the extent to which system components affect the frequency response characteristics in a specified location. Third, since the power system is constantly re-configured (by switching operations) to satisfy different operational constraints, the system model has to be modified or adjusted and impedance scans have to be redone. This is certainly a tedious and time-consuming task. Furthermore, the impedance scan only provides a snapshot of resonant frequencies for a particular system condition.

Thus, Santoso [33] presented an accurate empirical method to estimate the system parallel resonant frequencies using voltage and current waveforms from capacitor bank energizing events. This method provides a fundamentally sound alternative to monitor the existence of harmful resonance conditions using existing measurement data and power quality monitoring devices. Unlike the impedance scan method, this empirical method does not require any system short-circuit data. Capacitor switching transient data is all it needs. A profile of system parallel resonant frequencies can be obtained by applying the proposed methods to a series of capacitor switching transient events captured during a given monitoring period. The parallel resonant frequency profile is certainly more useful than a single snapshot of frequency estimates.

However, this method performs best when measurement data are taken at capacitor locations. Unfortunately, the estimate generates artificial non-resonant frequency components when measurement are taken elsewhere and also when the data exhibit significant harmonic distortions. Thus, the objective of this chapter is to extend this previous work so that the method can

47

be universally applied to data taken at any measurement location including a load bus where significant nonlinear loads may be present. The improved technique also utilizes capacitor switching transient data. However, instead of analyzing the entire waveform trace, it analyzes only the effective transient part of the waveform. Section 3.2 addresses the previous method to estimate the system parallel resonant frequencies and details the improved method, in particular how the effective transient segment is accounted for. Section 3.3 demonstrates the efficacy of the improved method and compares its results to those of the previous method.

3.2   Estimation of Parallel Resonant Frequencies

This section presents methodology to estimate the system parallel resonant frequencies using commonly available power quality data. This data is now commonly collected in many locations, i.e., at substations, end-user facilities, feeders, and other strategic locations. Power quality data of interest are the voltage and current waveforms due to capacitor switching events. Capacitor switching transient data typically provides accurate estimates of parallel resonant conditions. This is because when the capacitor bank is energized, its capacitance interacts with the system inductance at the point where the capacitor bank is located. The ringing frequencies, which usually last about $^1/_4$ to $^1/_2$ cycle following the switching operation, provide valuable information about new resonant frequencies introduced to the power system.
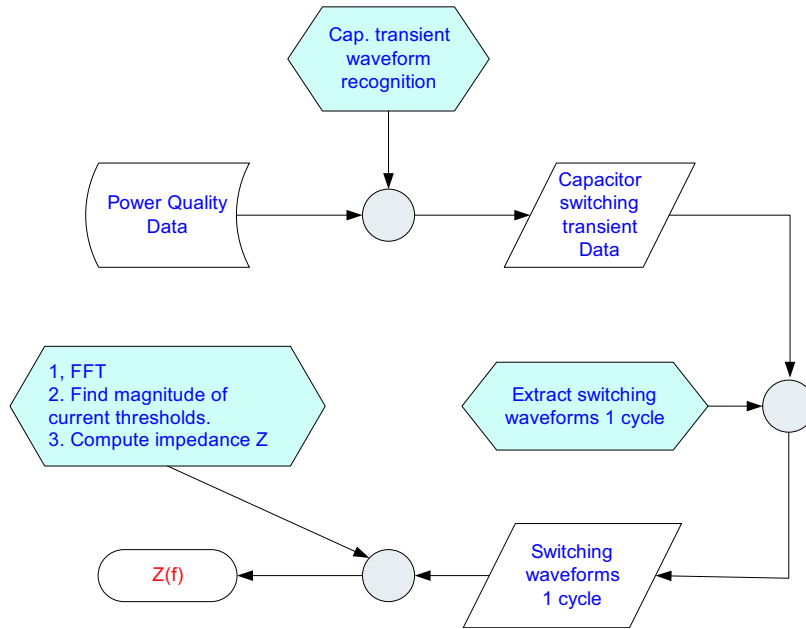
Figure 3.1: Data flow and process diagram of system parallel resonant frequency estimation using capacitor switching transient data.

3.2.1 Previous Estimation Method

Figure 3.1 illustrates the data flow and process of the previous estimation method. The method can begin with an existing power quality database or a real-time power quality data stream as used in web-based monitoring devices. Since typical power quality monitors capture a wide range of disturbance events, one needs to separate or identify capacitor switching event data from other PQ data before performing the estimation. The identification of the capacitor switching transient data can be done visually or automatically [37]. Once a single event of capacitor switching transient data (consisting of three phase voltage and current waveforms) is identified, transient portions of volt-
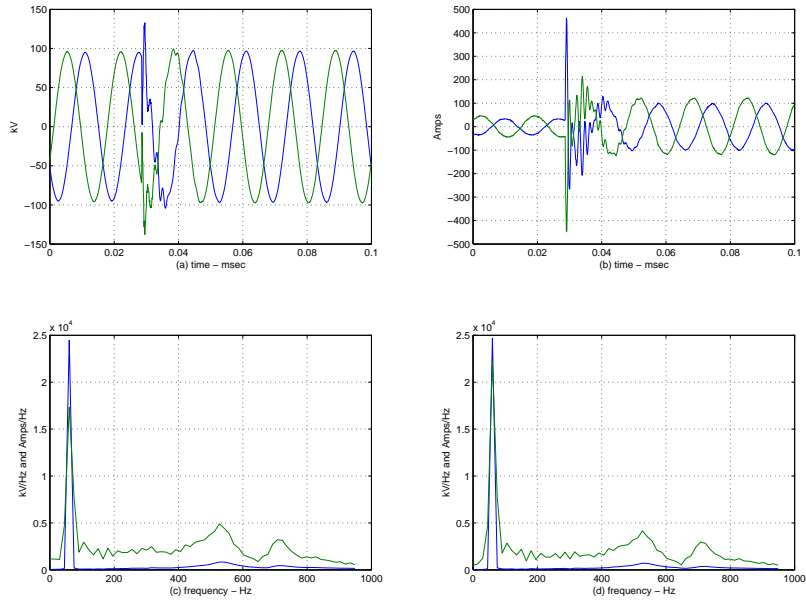
Figure 3.2: Capacitor switching transient waveforms measured at a 115 kV substation using a commonly available power quality monitor - only phases A and C (dashed line) waveforms are shown. (a) voltage waveforms, (b) current waveforms, (c) and (d) are FFTs of voltage and current in linear scales.

age and current waveforms will be extracted (only 1 cycle is needed). In order to extract the transient portion, the switching instant of the capacitor bank must be determined. A wavelet transform can be used to determine the exact switching instant effectively [38].

Fast Fourier transforms are then performed to find the spectra of transient waveforms for voltage and current of each phase. Let $V(f)$ and $I(f)$ be the Fourier transforms of the extracted voltage and current waveforms that contain the transient event. Figure 3.2(a) and (b) show voltage and current

waveforms of two phases (A and C) of a capacitor switching transient event. The transient event was captured using a power quality monitoring device at a 115 kV substation of a utility company in the Northeast (U.S.). Figure 3.2(c) and (d) present a pair of $V(f)$ and $I(f)$ waveforms shown in linear scales for phases A and C, respectively. Note that the current spectra $I(f)$ contains very small values over a wide range of frequencies since the current transient waveforms consist only of frequencies that correspond to transient frequencies. Figure 3.3(a) and (b) show voltage and current spectra in natural logarithmic scales. Frequencies of interest, approximately 525 Hz and 720 Hz, are now clearly seen in both voltage and current spectra. These are in fact the resonant parallel frequencies. They can be determined directly from voltage and current spectra by finding "bumps" or lobes of like frequencies. For the sake of brevity, this method is referred as the direct method.

Another method of estimating the resonant frequencies can be performed using the impedance estimation as follows,

$$Z_e(f) = \frac{V(f)}{I(f)}$$

Note that since $I(f)$ contains small values at non-transient frequencies, the impedance estimate at these non-transient frequencies will be large and are misleading. A way around this problem involves setting these large impedance values to zero for frequencies that satisfy $I(f) < xI(60 \text{ Hz})$, where x typically ranges between 5% to 15%. This will force any large artificial impedance values at non-transient frequencies to zero. The impedance estimate is shown

51
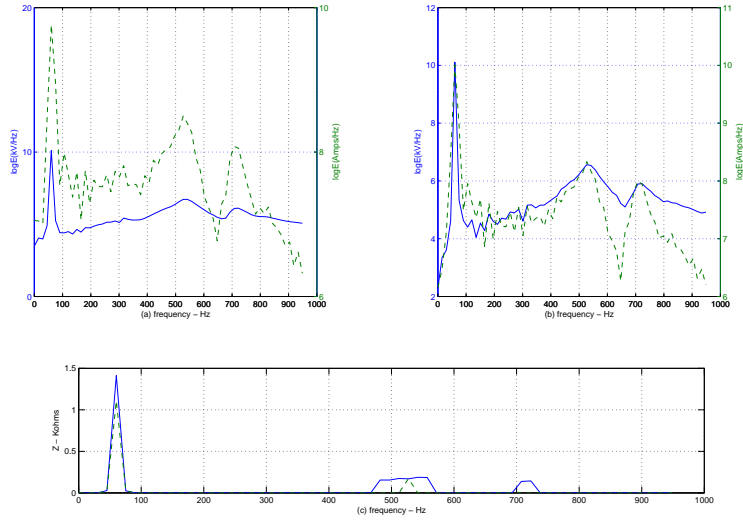
Figure 3.3: (a) Fourier transforms of phase A voltage and current (dashed line) waveforms, (b) Fourier transforms of phase C voltage and current (dashed line) waveforms in natural logarithmic scales, (c) frequency estimates using impedance (dashed line) method.

in Figure 3.3(c) where the resonant frequencies are from 480 to 580 Hz and 700 to 720 Hz. Both estimates (using the direct and impedance methods) correspond closely to the result obtained using the impedance/frequency scan method. However, there is an important weakness in this method that the proposed algorithm performs best when measurement data are taken at capacitor locations. The method is useful for measurements taken throughout the local system (i.e., same distribution system or nearby buses on the transmission system), even when the system is full of harmonic components. When measurements were not taken at the capacitor bank, the analysis results tend to contain harmonic artifacts that are misleading. These harmonic artifacts

52

will be illustrated in the following Section 3.2.2. However, it is noteworthy that weakness of the previous method always provides improvable opportunities. Thus, the following Section 3.2.2 presents an improved method which is robust against background harmonics and not restricted by locations.

3.2.2 Improved Estimation Method

The procedures of this algorithm can be described as follows. Once a single event of capacitor switching transient data is identified [39], the transient part of voltage and current waveforms after the switching instant, i.e., V_1 and I_1, respectively, are extracted. In order to obtain the effective transient segment, one cycle of voltage and current waveforms with the capacitor bank offline, V_2 and I_2, respectively, are constructed. Prony analysis [40] or phase detection and shifting methods are employed to construct one-cycle voltage and current waveforms using the waveform segment prior to the energizing instant. Voltage and current waveforms V_2 and I_2 may contain harmonic and any other frequency components that are not associated with the actual transient frequency. The effective voltage and current transient segments, ΔV and ΔI, are obtained by subtracting V_2 and I_2 from the original transient segments V_1 and I_1, respectively: $\Delta V = V_1 - V_2$ and $\Delta I = I_1 - I_2$. Figure 3.4 illustrates the aforementioned process for obtaining the effective current transient ΔI. The original current transient waveform I_1 is shown in tbe dotted line, while the reconstructed offline capacitor waveform I_2 is shown in the solid line. The effective transient segment ΔI is shown in Figure 3.4(b).

53

Estimates of parallel system resonant frequencies are then obtained using the spectral analysis of ΔV and ΔI. Note that the previous method utilizes the V and I instead of ΔV and ΔI. Let $\Delta V(f)$ and $\Delta I(f)$ be the Fourier transforms of ΔV and ΔI, and let $Z(f)$ be

$$Z(f) = \frac{FFT\ of\ \Delta V}{FFT\ of\ \Delta I} = \frac{\Delta V(f)}{\Delta I(f)}. \tag{3.1}$$

Note that $\Delta V(f)$ and $\Delta I(f)$ may contain small values at non-resonant frequencies which may lead to incorrect estimates. A way around this problem involves setting these erroneous impedance values to zero for frequencies that satisfy $\Delta V(f) < x \cdot \max[\Delta V(f)]$, where x typically ranges between 5% and 25%. Another heuristic method using a current threshold presented in the previous technique is also a viable alternative [33].

It should be emphasized that the proposed method is not intended to estimate the actual impedance of the system but to estimate the resonant frequencies.

3.3 Applications of the Proposed Method

A one-line diagram of a realistic test circuit is shown in Figure 3.5. This circuit is identical to the one investigated in [33]. It has a 40 Mvar capacitor bank and thus, it possesses one parallel resonant frequency at 325 Hz. Figure 3.6 illustrates voltage and current waveforms taken at 69 kV bus (capacitor bank bus) and 480 V bus (load bus). Figure 3.7 shows the estimated resonant frequency using the previous method. Notice that the previous method per-
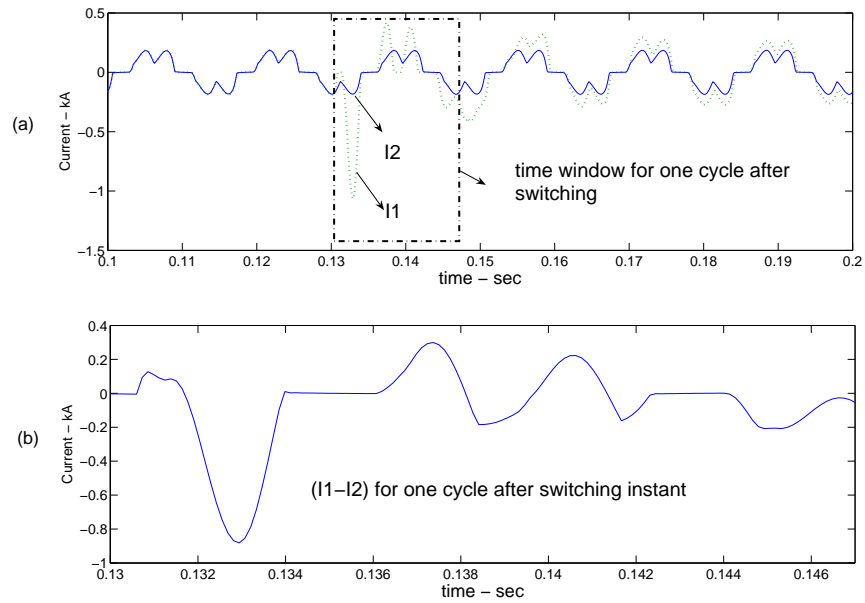
Figure 3.4: (a) Current waveforms when the capacitor bank is both in service (dotted line) and out of service (solid line), (b) Differential portion between them for one cycle.
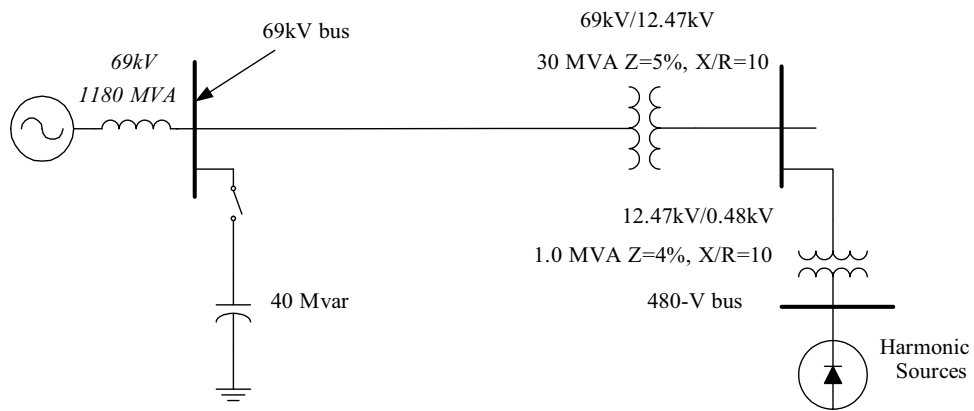
Figure 3.5: A one-line diagram for the test system .

55
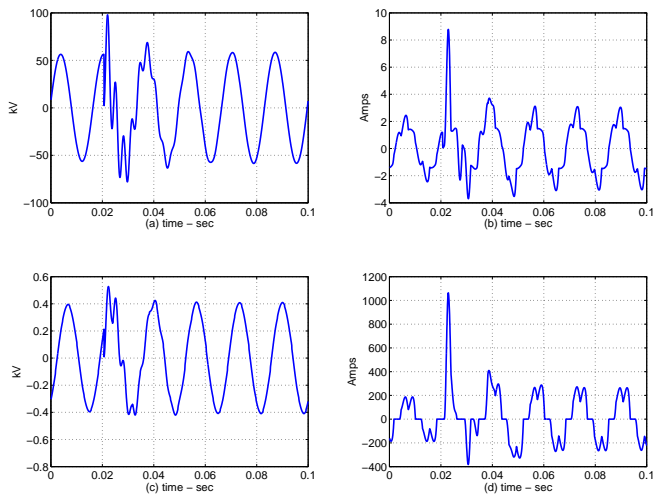
Figure 3.6: A capacitor switching transient event. (a-b) voltage and current waveforms measured at 69 kV bus, (c-d) voltage and current waveforms measured at 480 V bus.
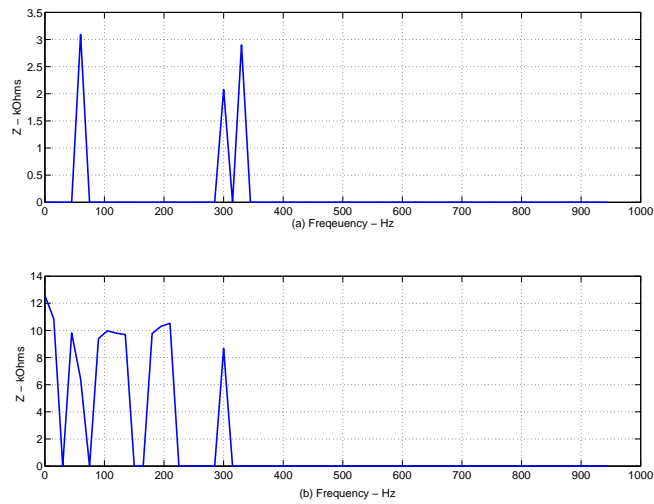
Figure 3.7: Resonant frequency estimates using (a) data measured at 69 kV substation and (b) data measured at 480 V bus
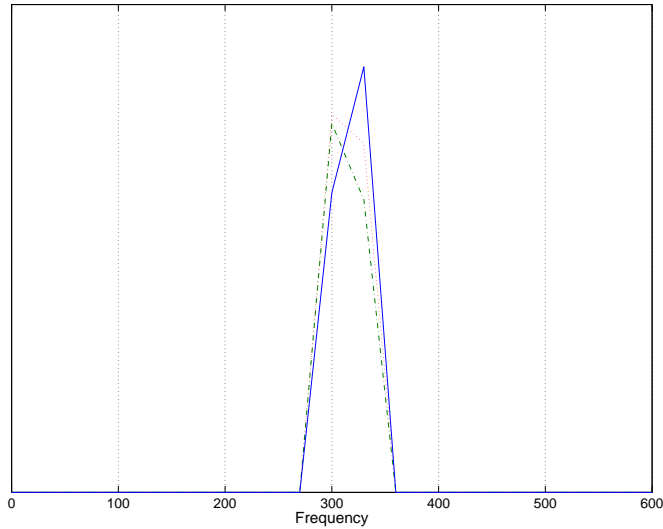
Figure 3.8: Resonant frequency estimates using data measured at 69 kV.

forms well with the measurement data taken at the capacitor bank location, i.e., 69 kV bus. Unfortunately, the resonant frequency estimated with the measurement data taken at the load bus is not satisfactory due to excessively high harmonic distortions (the current THD is 35.4%). As a result, the frequency estimate contains artificial frequency components around 100 and 200 Hz which are not associated with the actual resonant frequency.

The improved algorithm is applied to the same set of data. Figures 3.8 and 3.9 illustrate the resonant frequency estimate using the measured data taken at 69 kV bus and a load bus (480 V bus). In both cases, the non-resonant frequency components are removed and thus the method produces an accurate resonant frequency of 325 Hz for all three phases. Notice that the

57
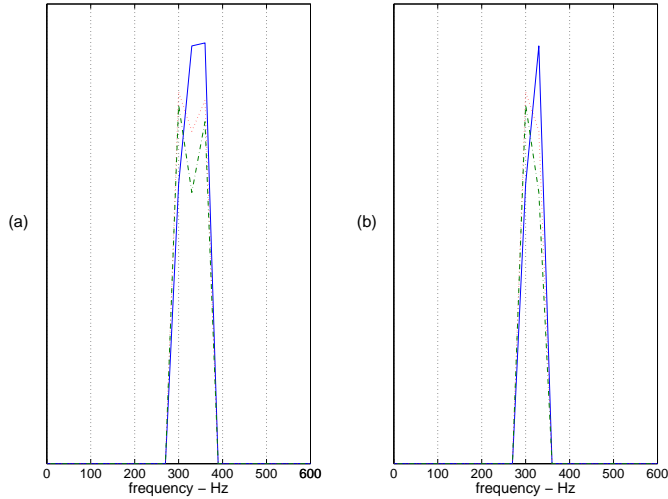
Figure 3.9: Resonant frequency estimation using data taken at 480V with threshold x of 15% (a) and (b) 25%; Solid, dashed and dotted lines correspond to phase A, B and C respectively.

new method also suppresses the 60 Hz component. Thus, it does not appear in the new resonant frequency estimate since no 60 Hz component exists in the effective voltage and current transient segments, $\Delta V(f)$ and $\Delta I(f)$. The result also indicates that appropriate choice of the threshold value, x, can better articulate the resonant frequency estimate

3.4 Discussion

In the above example, the parallel resonant frequency estimates are determined using a single capacitor-switching event with two phases of voltage and current waveforms. However, having a complete set of three-phase voltage and current waveforms provides better estimates and increases the confidence

58

level of the estimation results. In some cases, frequencies of interest may not be present. Furthermore, obtaining frequency estimates from a single switching event may not represent actual resonant frequencies as the system configuration may change over time due to various switching operations, and estimates from a single capacitor-switching event will not give an indication of the range of possible resonance frequencies. Thus, resonant estimates from multiple events should be used to provide consistent estimates and to capture all possible resonant frequencies for a given period of study. The method presented above is simple to construct and implement. In addition, they make use of existing data and equipment, and therefore are a valued-added application.

It should be noted that the method is intended for estimating resonant frequencies from a given period of measurement, thus any prestrike or restrike events will not be used in the estimation. On the other hand, capacitor switching events with delay pole closing can be used since its transient portion can be extracted in the same manner as in simultaneous closing since only 1 cycle of data is needed. This method presents a simple yet accurate empirical technique for estimating system parallel resonant frequencies. The technique does not require elaborate measurement data. Instead, it makes use of existing power quality data, specifically those of capacitor switching transients, to estimate parallel resonant frequencies.

3.5   Summary

The chapter presents an algorithm for estimating system parallel resonant frequencies. By utilizing only the effective transient voltage and current segments due to capacitor bank energizing, this technique can suppress misleading influence of harmonic currents from nonlinear loads and present accurate resonant frequency estimates, even when the data are not taken at the capacitor bank locations.

Chapter 4

On the Empirical Estimation of Utility Distribution Damping Parameters

This chapter describes an efficient and accurate methodology for estimating power system damping using capacitor bank switching transient data. This research proves that the free (zero-input) response[1] of a phase voltage due to a capacitor bank energizing can be nicely represented as an exponentially damped sinusoidal signal. The damping ratio of the damped sinusoidal signal can be exploited to obtain the X/R ratio of the power distribution system. This chapter also proposes an effective algorithm to extract the damping term and estimate the system X/R ratio, which includes contributions of loads, as well as the line impedances, based on the Hilbert transform and linear dynamic system theory. It is also found that this X/R ratio is independent of the measurement locations, provided they are along the same feeder. Therefore, one can examine the system vulnerability to various PQ disturbances, particularly resonance phenomena, with this quantified damping (X/R ratio) of the system.

---

[1]Refer to Section 2.1 for details of system response.

4.1 Background and Motivation

Harmonic resonance in a utility distribution system can occur when the system natural resonant frequency - formed by the overall system inductance and the capacitance of a capacitor bank - is excited by relatively small harmonic currents from nonlinear loads [2]. The system voltage and current may be amplified and highly distorted when resonance occurs. This scenario is more likely to occur while energizing capacitor bank in a system that has little or negligible resistive damping. During a resonance, the voltage drop across the substation transformer and current flowing in the capacitor bank is magnified by Q times. Q is the quality factor of a resonant circuit and is generally represented by X_L/R where X_L and R are the reactance at the resonant frequency and resistance of the distribution system Thevenin equivalent source and substation transformer at the resonant frequency. Note that during resonance, the magnitude of X_L is equal to but opposite in sign to that of X_C, the reactance of a capacitor bank. In addition, during a resonance, X_L and X_C reactances are h and $1/h$ multiple of their respective fundamental frequency reactance, where h is the harmonic order of the resonant frequency. Due to the highly distorted voltage and current, the impacts of harmonic resonance can be wide ranging, from louder noise to overheating and failure of capacitors and transformers [2, 41]. Refer to Chapter 2 for more descriptions on resonance concerns in power distribution systems.

Based on this background, it is desirable to predict the likelihood of harmonic resonance using system damping parameters such as the Q factor.

The Q factor is more commonly known as the X/R ratio. The reactance and resistance forming the Q factor should be effective impedance values that include the contributions of loads and lines to impedances from the equivalent Thevenin source and the substation transformer. In other words, the X/R ratio is influenced by the load level[2]. When the ratio is high, harmonic resonance is more likely to occur. Therefore, this chapter proposes an effective algorithm to estimate the X/R ratio based on linear dynamic system theory and the Hilbert damping analysis. The estimation technique requires only voltage waveforms due to the switching of capacitor banks to determine the overall system damping. It does not require system data and topology, and therefore it is practical to deploy in an actual distribution system environment.

4.2 Current Research

There has been very little research carried out on this subject. Most previous efforts have been exerted on power system stability issues in the transmission[3] system level, such as dynamic load modeling, and its impacts on inter-machine oscillations and designing damping controllers [21, 27, 28]. In particular, very little research has been conducted to quantify the damping level of the power system [27]. Research has shown that that the system damp-

---

[2]Motor loads are primarily inductive and provide little damping. In fact, they may increase distortion by shifting the system resonant frequency closer to a significant harmonic. Small, fractional hp motors may contribute significantly to damping because their apparent X/R ratio is lower than large 3-phase motors [2].

[3]Refer to Section 2.3 for more details on resonance and damping concerns in transmission levels.

ing supplied by resistive components of the lines and loads have a beneficial impact in preventing catastrophic resonance phenomena [2,41]. However, only a few research efforts have been undertaken to estimate the signal damping ratios using sophisticated signal processing algorithms based on the assumption that harmonic components can be represented as a sum of exponentially damped sinusoids. These techniques include ESPRIT [42], Prony analysis [28], and system identification based on the AR (all-pole) model [40,43]. These techniques can help better explain the characteristics of individual harmonic components. However, those techniques need post-processing procedures to solve significant problems: intrinsic spurious harmonics may mislead the evaluation of the results, the uncertainty of the system order and the computational burden may prevent real-world applications. Furthermore, no work has correlated the estimated damping ratios with the conventional X/R ratio of the system.

The organization of this chapter is as follows. Section 4.3 describes the scope of the problem and Section 4.4 develops a smart algorithm for estimating power system damping using capacitor switching transient data based on Hilbert transform and linear dynamic system theory. Sections 4.5 and 4.6 demonstrate the efficiency of the proposed technique using data from an IEEE Test Feeder [44] modeled in PSCAD [45] and actual measurement data.

4.3 Problem Description and Scope of the Problem

Let us consider a one-line diagram for a power distribution system in Figure 4.1, where a shunt capacitor bank is installed in the distribution feeder

64
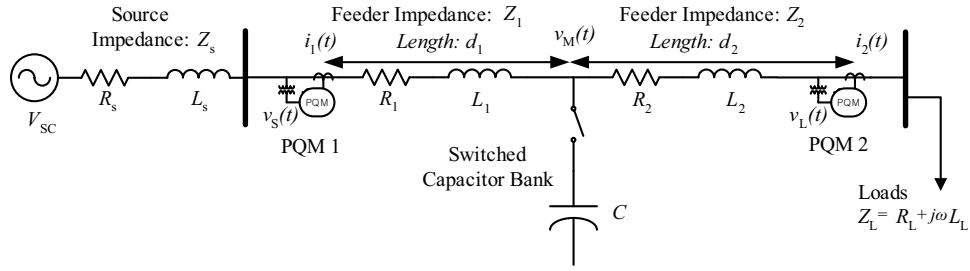
Figure 4.1: One-line diagram for a typical utility distribution feeder

and power quality monitoring devices are located on both sides of the capacitor bank. When the capacitor bank is energized, an oscillatory transient can be observed in the voltage and current waveforms captured by the power quality monitors. The oscillation frequency is indeed the new natural power system resonant frequency formed by the equivalent inductance and the capacitance of the switched capacitor bank.

The problem addressed in this chapter can be stated as follows. Given voltage waveforms as a result of capacitor energizing, determine the effective X/R ratio for the resonant frequency at the particular bus of interest. The proposed method makes use of the transient portion of capacitor switching transient waveforms captured anywhere in the system. Therefore, the capacitor banks considered in this work are those energized with mechanical oil switches and without any mechanism to reduce overvoltage transients. This is representative of the banks found in the majority of distribution feeders.

65

4.4   Power System Damping Estimation

The proposed estimation of the system damping quantified in terms of the X/R ratio requires the Hilbert transform and theoretical analysis of the distribution system. The Hilbert transform is used to extract the damping properties embedded in the envelope of the waveshape of the capacitor switching transient waveform. A brief review of the transform is described in Section 4.4.1. Section 4.4.2 derives a mathematical equation for the envelope of the transient waveform, correlates this equation with the system X/R ratio and discusses practical consideration.

4.4.1   Hilbert Transform

The Hilbert transform of a real-valued time domain signal $y(t)$ is another real-valued time domain signal, $\tilde{y}(t)$, such that an analytic signal $z(t) = y(t) + j\tilde{y}(t)$ exists [46]. This is a generalization of Euler's formula in the form of the complex analytic signal. It is also defined as a 90-degree phase shift system as shown below:

$$\tilde{y}(t) = H\left[y(t)\right] = \int_{-\infty}^{\infty} \frac{y(\tau)}{\pi(t-\tau)} d\tau = y(t) * (1/\pi t) \tag{4.1}$$

$$F\left[\tilde{y}(t)\right] = \tilde{Y}(f) = (-j\operatorname{sgn} f)\, Y(f) \tag{4.2}$$

where $\tilde{Y}(f)$ is the Fourier transform of $\tilde{y}(t)$. From $z(t)$, we can also write $z(t) = a(t)\cdot e^{j\omega(t)}$ where $a(t)$ is the envelope signal of $y(t)$ and $\omega(t)$ is the instantaneous phase signal of $y(t)$. The envelope signal is given by $a(t) = \sqrt{y(t)^2 + \tilde{y}(t)^2}$ and the instantaneous phase, $\omega(t) = \tan^{-1}\left(\frac{\tilde{y}(t)}{y(t)}\right)$. Using the property of Eq. (4.2),

66

one can easily obtain the Hilbert transform of a signal, $y(t)$. Let $Z(f)$ be the Fourier transform of $z(t)$ and one can obtain the following relationship:

$$Z(f) = F\left[z(t)\right] = F\left[y(t) + j\tilde{y}(t)\right] \tag{4.3}$$

$$= Y(f) + j\tilde{Y}(f)$$

$$= (1 + \mathrm{sgn}f)\,Y(f)$$

$$= \left\{ \begin{array}{ll} 2Y(f) & \text{for } f > 0 \\ 0 & \text{for } f < 0 \end{array} \right\}$$

Thus, the inverse Fourier transform of $Z(f)$ gives $z(t)$ as shown below in Eq. (4.4).

$$z(t) = F^{-1}\left[Z(f)\right] = y(t) + j\tilde{y}(t) \tag{4.4}$$

For the case of quadratic damping[4], the decaying transient and its Hilbert transform can be represented as Eqs. (4.5) and (4.6), respectively. Thus, the resulting envelope, $a(t)$ becomes $y_m e^{-\zeta\omega_n t}$, where y_m is an arbitrary constant magnitude, ζ is a damping ratio, and ω_n and ω_d are natural and damped natural frequencies which will be defined in the following Section 4.4.2. This is a unique property of the Hilbert transform applicable to envelope detection.

$$y(t) = y_m e^{-\zeta\omega_n t} \cos(\omega_d t + \phi) \tag{4.5}$$

$$\tilde{y}(t) = y_m e^{-\zeta\omega_n t} \sin(\omega_d t + \phi) \tag{4.6}$$

---

[4]Refer to Section 2.1 for more details. Damping coefficient, α in Section 2.1 is replaced by $-\zeta\omega_n$ based on the general nomenclature in signal processing and control systems.

4.4.2 Algorithm Development

4.4.2.1 Analysis of the Distribution System and Definition of the Effective X/R ratio

Let us consider a typical distribution system shown in Figure 4.1. Let us further assume that it is balanced. Therefore, the Thevenin equivalent source impedance is represented with R_s and L_s, while the line impedance for segments d_1 and d_2 are represented with its positive sequence impedance $(r + j\omega L_u)d_1 = R_1 + j\omega L_1$ and $(r + j\omega L_u)d_2 = R_2 + j\omega L_2$, where r and L_u are the line resistance and inductance in per unit length. The load impedance is represented with $Z_L = R_L + jX_L$. Let $v_s(t)$, $i_1(t)$ and $v_L(t)$, $i_2(t)$ be the instantaneous voltages and currents measured by PQM 1 and PQM 2, respectively, and $v_M(t)$ be the instantaneous voltage at the capacitor bank location.

Thus, one can set up the following differential equations for the equivalent circuit immediately following the energization of the capacitor bank, i.e., $t = t_s$. Note that currents $i_1(t)$ and $i_2(t)$ are measured by PQM 1 and 2 in the direction of the prevailing system loads as denoted in Figure 4.1. In the vector-matrix form, the state equations are expressed as

$$\dot{x}(t) = \mathbf{A}x(t) + \mathbf{B}u(t) \tag{4.7}$$

$$y(t) = \mathbf{C}x(t) \tag{4.8}$$

where $y(t)$ = output vector, $x(t)$ = state vector, and $u(t)$ = input vector, i.e.

$$x(t) = \begin{bmatrix} i_1(t) & i_2(t) & v_M(t) \end{bmatrix}^T \tag{4.9}$$

68

and

$$\mathbf{A} = \begin{bmatrix} \frac{-(R_s+R_1)}{L_s+L_1} & 0 & \frac{-1}{L_s+L_1} \\ 0 & \frac{-(R_2+R_L)}{L_2+L_L} & \frac{1}{L_2+L_L} \\ \frac{1}{C} & \frac{-1}{C} & 0 \end{bmatrix}, \ \mathbf{B} = \begin{bmatrix} 1 \\ 0 \\ 0 \end{bmatrix}, \ \mathbf{C} = \begin{bmatrix} 1 & 0 & 0 \\ 0 & 1 & 0 \\ 0 & 0 & 1 \end{bmatrix} \qquad (4.10)$$

The input vector, $u(t)$ of this system comprises only the equivalent voltage source. The state vector is regarded as the output vector. Thus, matrix $\mathbf{C}$ is a 3×3 identity matrix as shown in Eq. (4.10). Let the transfer function $G(s)$ – which describes the behavior between the input and output vectors – be expressed in the following form [47]:

$$G(s) = \mathbf{C}(s\mathbf{I} - \mathbf{A})^{-1}\mathbf{B} = [G_1(s), \ G_2(s), \ G_3(s)]^T \qquad (4.11)$$

where

$$G_1(s) = \left\{ C(L_2 + L_L)s^2 + (R_L + R_2)Cs + 1 \right\}/\Delta, \qquad (4.12)$$

$$G_2(s) = 1/\Delta \text{ and} \qquad (4.13)$$

$$G_3(s) = \left\{ (L_2 + L_L)s + (R_2 + R_L) \right\}/\Delta. \qquad (4.14)$$

The term $\Delta = |s\mathbf{I} - \mathbf{A}|$ is the characteristic equation of the system and is defined as follows:

$$\begin{aligned} \Delta = \ & (L_s + L_1)(L_2 + L_L)Cs^3 \cdots \\ & + \left\{ (L_s + L_1)(R_2 + R_L) + (L_2 + L_L)(R_s + R_1) \right\} Cs^2 \cdots \\ & + \left\{ (R_s + R_1)(R_2 + R_L)C + (L_s + L_1 + L_2 + L_L) \right\} s \cdots \\ & + R_s + R_1 + R_2 + R_L. \end{aligned} \qquad (4.15)$$

The s-domain representation of voltages $V_S(s)$ (PQM 1), $V_L(s)$ (PQM 2) and $V_M(s)$ across the capacitor can be obtained as follows:

$$V_S(s) = V_{sc}(s)\left\{G_1(s)(R_1 + sL_1) + G_3(s)\right\}, \qquad (4.16)$$

$$V_L(s) = V_{sc}(s)G_2(s)(L_L s + R_L), \text{ and} \qquad (4.17)$$

$$V_M(s) = V_{sc}(s)G_3(s). \qquad (4.18)$$

The input source voltage is considered constant as shown in Eq. (4.19) below because the power system fundamental frequency is substantially lower than a typical capacitor switching frequency [26]. Note that $v_{sc}(t_s^-)$ indicates a voltage level immediately before switching.

$$V_{sc}(s) = \frac{v_{sc}(t_s^-)}{s}. \qquad (4.19)$$

Note that the roots of the characteristic equation are the eigenvalues of the matrix $\mathbf{A}$, and the order of the characteristic equation is three. In linear dynamic system theory, the characteristic equation of the second-order prototype system is generally considered, i.e.,

$$\Delta(s) = s^2 + 2\zeta\omega_n s + \omega_n^2 \qquad (4.20)$$

where ω_n and ζ are the resonant frequency and the system damping ratio, respectively. The series RLC circuit is an example of the second-order prototype systems. Neglecting the circuit downstream from the capacitor bank[5],

---

[5]This capacitor bank is called isolated.

70

one can obtain the following characteristic equation:

$$\Delta(s) = s^2 + \left(\frac{R_s + R_1}{L_s + L_1}\right)s + \frac{1}{(L_s + L_1)C}. \qquad (4.21)$$

Thus, we obtain the following relations:

$$\omega_n^2 = \frac{1}{(L_s + L_1)C}, \qquad (4.22)$$

and

$$2\zeta\omega_n = \frac{R_s + R_1}{L_s + L_1}. \qquad (4.23)$$

From Eq. (4.23), we obtain the damping ratio of the system:

$$\zeta = \frac{1}{2\omega_n}\left(\frac{R_s + R_1}{L_s + L_1}\right). \qquad (4.24)$$

From Eq. (4.24) one can derive the conventional X/R ratio of the system at the resonant frequency. The system X/R ratio frequently appears in power system literature and is named as a quality factor, Q as well:

$$\frac{X}{R} = \frac{1}{2\zeta} = \omega_n\left(\frac{L_s + L_1}{R_s + R_1}\right). \qquad (4.25)$$

Note that the behavior of the transient voltage measured in the utility system after energizing the capacitor bank can be described by the general exponential function in the same form as Eqs. (4.5) and (4.6). Hence, transient voltage can be described as follows:

$$\begin{aligned}
v(t) &= e^{-\zeta\omega_n t}\left(p\cos\left(\omega_d t\right) + q\sin\left(\omega_d t\right)\right)\\
&= re^{-\zeta\omega_n t}\cos(\omega_d t + \phi)\\
&= a(t)\cos(\omega_d t + \phi)
\end{aligned} \qquad (4.26)$$

where $\omega_d = \omega_n\sqrt{(1 - \zeta^2)}$ is the damped resonant frequency, p and q are arbitrary constants, $r = \sqrt{p^2 + q^2}$ and $\phi = -\tan^{-1}(q/p)$.

71

Keep in mind that the aforementioned equations are based on the series RLC circuit without considering loads. Thus, the X/R ratio does not include damping contributions of the loads and the downstream lines to the whole system.

Note that the damping ratio is not strictly defined in the higher order system. However, thorough numerical experiments prove that the characteristic equation in Eq. (4.15) can be reasonably represented by a pair of complex conjugate dominant poles and one pole. This one pole is insignificant pole, since it is further away from $j\omega$ axis in the left half s-domain than those of dominant poles. Therefore, its effect on transient response is negligible, which corresponds to the fast-decaying time response. Application of the model reduction method [48] to the voltages of interest also confirms that the transfer functions of Eq. (4.16) and Eq. (4.17) can be reduced to Eq. (4.27). Similarly, the transfer function of Eq. (4.18) can be approximated by Eq. (4.28) by truncating the fast mode. Thus, these voltage functions, $V_S(s)$, $V_L(s)$ and $V_M(s)$ can be approximated as the following prototype quadratic equations:

$$V_S(s), V_L(s) \approx V_{sc}(s) \left(Q\frac{s^2 + 2\zeta_1\omega_{n1}s + \omega_{n1}^2}{s^2 + 2\zeta_2\omega_{n2}s + \omega_{n2}^2} \right), \text{ and} \qquad (4.27)$$

$$V_M(s) \approx V_{sc}(s)\frac{-Ks + P}{s^2 + 2\zeta\omega_ns + \omega_n^2} \qquad (4.28)$$

where Q, K and P are arbitrary constants.

Note that the damping term of the reduced second order system is a function of line parameters and loads. Thus, it should not be interpreted as the

conventional X/R ratio which is a function only of upstream lines and source parameters as defined in Eq. (4.25). However, the approximate damping term can indicate the relative X/R ratio of the whole system effectively and can quantify the overall contributions to the system damping by both lines and loads. Thus, we define $1/(2\zeta)$ from the reduced second order characteristic equation as the effective X/R ratio of the system.

What is worth noting is that the characteristic equation can vary according to the load composition. Hence, the X/R ratio is not a unique function of the parameters of the lines and loads but depends on the load composition and line configuration. Note that a parallel representation of the load elements results in a fourth order characteristic equation. However, the fourth order system can also be reduced to the second order prototype system by the model reduction technique with much bigger damping ratio than that from the series load representation even under the same loading condition. Therefore, the transient response of the whole system can be described by Eq. (4.26) as well. This is the motivation for detecting the envelope of the transient voltage by means of Hilbert transform. Consequently, the exponent, $-\zeta\omega_n$ of Eq. (4.26) can lead to the effective X/R ratio or $1/(2\zeta)$ if ω_n is available.

Since the aforementioned system parameters for determining the system damping level are not readily available, we propose an empirical method using conventional PQ data for evaluating the effective X/R ratio. The following section discusses how to obtain the effective X/R ratio of the system using conventional capacitor switching transient data.

73

4.4.2.2 Implementation and Practical Consideration

The implementation of the proposed damping estimation technique is illustrated in Figure 4.2. The implementation begins with an existing PQ database or a real-time PQ data stream as used in web-based monitoring devices. Since typical PQ monitors capture a wide range of disturbance events, a separate algorithm is needed to distinguish capacitor switching event data from other PQ data. The identification of capacitor switching transient waveforms can be done visually or automatically [39, 43]. Once a single event of capacitor switching transient data, i.e. three phase voltage, is identified, we extract transient portions of voltage waveforms after switching and construct extrapolated voltage waveforms based on the steady-state waveforms after capacitor energizing. This extrapolation can be done by concatenating a single period of waveforms captured 3 or 4 cycles after the switching operation on the assumption that voltage signals are considered to be (quasi-)stationary for that short period of time. If the number of samples after the detected switching instant is not sufficient to form a single period, steady-state voltage data before capacitor switching can be used alternatively. It is not uncommon to observe this situation since most of the PQ monitors store six cycles of data based on the uncertain triggering instant.

In this research, we assume that switching time instant can be accurately detected[6]. Then, we subtract the extrapolated data from the raw tran-

---

[6]Wavelet transform techniques, among others, are most frequently used for effectively determining the exact switching instant [39]. For example, there exists a commercial power

74

sient voltage data and obtain the differential portion. This differential portion can be interpreted as the zero-input (free) response of the system, whose behavior is dictated by the characteristic equation as discussed in Section 4.4.2.1. Note that this process minimizes the impacts of the system frequency component (forced input), the harmonics already inherent in the system and the voltage rise due to reactive energy compensation. The process of deriving this empirical free response of the capacitor bank energizing is described in [10].

The Hilbert transform is then performed to find the envelope signal, $a(t)$ of Eq. (4.26). In fact, the envelope from the Hilbert transform is not an ideal exponential function and is full of transients especially for those low-magnitude portions of the signal approaching the steady-state value (ideally zero). Thus, only a small number of data are utilized in order to depict the exponential satisfactorily: one cycle of data from the capacitor switching instant is generally sufficient to produce a good exponential shape. The number of data will depend on the sampling rate of the PQ monitoring devices and should be calibrated by investigating the general load condition, especially when the method is applied to a new power system in order to optimize the performance. The obtained data is now fitted into an exponential function. The direct way to fit the data into the exponential function is possible through iteration-based nonlinear optimization technique. However, the exponential function is namely an intrinsic linear function, such that the $\ln a(t)$ produces

---

quality monitoring system equipped with singularity (switching) detection based on the wavelet transform.
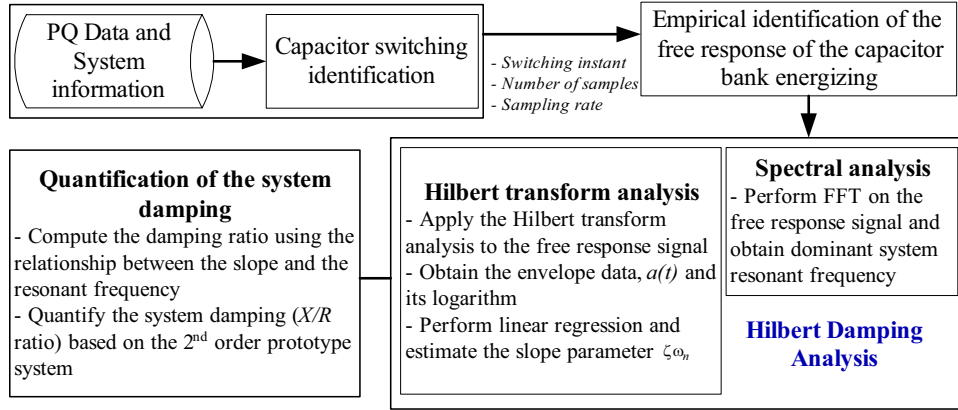
Figure 4.2: Data flow and process diagram of the system damping estimation

a linear function, i.e.

$$\ln\{a(t)\} = \ln r - \zeta\omega_n t \qquad (4.29)$$

As a result, we can apply standard least squares method to approximate the optimal parameters more efficiently. The solution is not optimal in minimizing the squared error measure, due to the logarithmic transformation. However, except for very high damping cases, this transformation plus the least square estimation method, creates a very accurate estimate of $a(t)$. Since the FFTs of the differential voltages provide very precise spectral information of the system [10, 33], one can obtain the effective X/R ratio that quantifies the system damping level, including impacts from lines and loads. The proposed algorithm is very practical and ready to be implemented in modern PQ monitoring systems since the conventional capacitor switching transient data is all it needs and the method is not computationally intensive.

76

4.5 Method Validation using IEEE Test Models

This section demonstrates the application of the damping estimation method using the IEEE power distribution test feeder [44] modeled in PSCAD [45]. The test system is a 12.47 kV radial distribution system served by a 12 MVA 115/12.47 kV delta-Yg transformer. The Thevenin equivalent impedance is largely due to the transformer leakage impedance, i.e., $Z(\%) = 1 + j10$ on a 12 MVA base. Thus, the equivalent source inductance L_s would be 3.4372 mH. The evaluation of distance estimates is carried out under both unbalanced $[Z_{012}]_{UB}(\Omega \text{ /mi})$ and balanced $[Z_{012}]_B(\Omega \text{ /mi})$. Their sequence impedance matrices in ohms per mile are as follows, respectively,

$$[Z_{012}]_{UB} = \begin{bmatrix} 0.7737 + \text{j}1.9078 & 0.0072 \text{ - j}0.0100 & \text{ - }0.0123 \text{ - j}0.0012 \\ \text{ - }0.0123 \text{ - j}0.0012 & 0.3061 + \text{j}0.6334 & \text{ - }0.0488 + \text{j}0.0281 \\ 0.0072 \text{ - j}0.0100 & 0.0487 + \text{j}0.0283 & 0.3061 + \text{j}0.6334 \end{bmatrix}$$
(4.30)

$$[Z_{012}]_B = \begin{bmatrix} 0.7737 + \text{j}1.9078 & 0 & 0 \\ 0 & 0.3061 + \text{j}0.6333 & 0 \\ 0 & 0 & 0.3061 + \text{j}0.6334 \end{bmatrix}$$
(4.31)

The positive sequence line inductance per mile, L_u, for both balanced and unbalanced feeders is 1.6801mH/mi. The efficacy of the proposed technique is evaluated under the following conditions:

- (A) ignore loads and circuits downstream from the switched capacitor bank when all lines are assumed balanced,

- (B) include loads and circuits downstream from the bank and vary the loading conditions when the loads and lines are assumed balanced, and
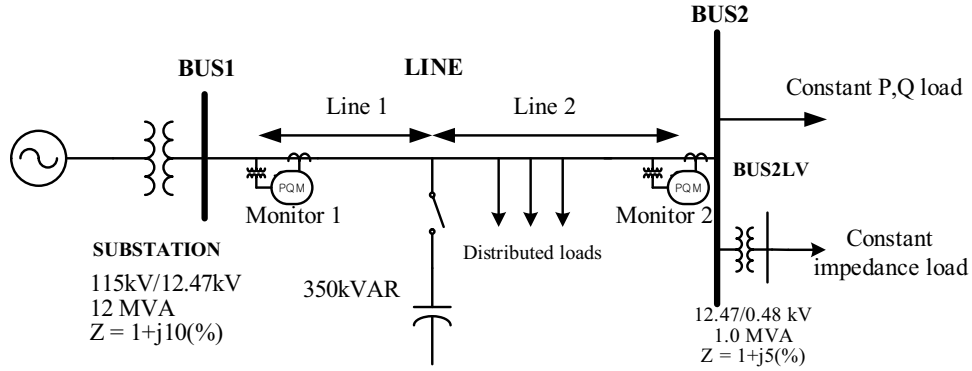
Figure 4.3: IEEE distribution system test case with modification and additional capacitor bank

investigate the feasibility of the proposed method when harmonic currents are injected from the nonlinear loads and resonance occurs as well, and

- (C) evaluate the same system as in (B), however, loads and lines are unbalanced.

Loads illustrated in Figure 4.3 are modeled as a combination of fixed impedance and dominant complex constant power loads which are appropriately modeled as variable R and L in parallel. They are connected at the 12.47 kV as well as at the 0.48 kV level through a 1 MVA service transformer $(Z(\%) = 1 + j5)$. A 350 kVar three-phase switched capacitor bank is located d_1 miles out on the feeder. Two PQ monitors are installed both at the BUS 1 (substation) and BUS 2. Note that the conventional sampling rate of 256 samples/cycle is applied in the following studies.

78

Table 4.1: Estimation results when downstream loads and circuits are excluded.

Parameters	$f_{res} = \omega_d/2\pi$	ζ	X/R
Theoretical results	707.36	0.0139	35.96
Empirical estimates	706.42	0.0135	35.96

4.5.1 Evaluation Cases with Downstream Loads and Circuits Omitted

The damping estimation technique is first evaluated for a balanced feeder without loads and circuits downstream from the capacitor bank. The estimated parameters are compared with the theoretical results derived from the characteristic equation in Eq. (4.15) and summarized in Table 4.1 (for d_1 = 3 miles).

The above results show that the proposed techniques provide reasonably accurate estimates of resonant frequency, damping ratio and effective X/R ratio. Note that the resonant frequency in the resulting table indicates a damped resonant frequency, which is the frequency obtainable from the measurement data. However, the damped resonant frequency is very close to the natural resonant frequency since in general the damping ratio is very small. It should also be noted that the fractional numbers are not included to indicate the high accuracy of the estimates but to present the same significant figures as those of the analytical values. The frequency interval, Δf, between two closely spaced FFT spectral lines is 15.03 Hz based on the number of samples (1024) and sampling rate of the PQ data (256 samples per cycle).

4.5.2 Evaluation Cases for Balanced Lines and Balanced Loads

4.5.2.1 Linear load

This section examines the case where three phase balanced lines and loads downstream from the capacitor bank are included. The lines are configured as $d_1 = 3$ miles and $d_2 = 1$ mile. Note that loads are modeled with series R and L in an aggregate manner and connected to BUS 2. The proposed technique is applied to quantify the system damping level for varying load sizes and power factors. The resulting parameters are compared with the theoretical results using the characteristic equation in Eq. (4.27) and summarized in Table 4.2 through Table 4.4. The results demonstrate that the proposed technique can provide very accurate estimates of resonant frequency, damping ratio, and effective X/R ratio, since the estimated parameters are very close to theoretical values. It is also observed that the overall system damping level is more influenced by the power factor of the load than the load size, since the effective X/R ratio of a moderate load with 0.95 pf is even less than that of heavy load with 0.90 pf. Note the change in resonant frequency according to the load condition.

Table 4.2: Estimation results when load power factor is 0.95.

Loading cond.	Moderate, 3.16MVA			Heavy, 7.37MVA		
Parameters	$f_{res} = \omega_d/2\pi$	ζ	X/R	$f_{res} = \omega_d/2\pi$	ζ	X/R
Theoretical results	772.28	0.0293	17.08	845.97	0.0387	12.92
Estimates	766.55	0.0286	17.47	841.70	0.0373	13.38

Table 4.3: Estimation results when load power factor is 0.90.

Loading cond.	Moderate, 3.16MVA			Heavy, 7.37MVA		
Parameters	$f_{res} = \omega_d/2\pi$	ζ	X/R	$f_{res} = \omega_d/2\pi$	ζ	X/R
Theoretical results	758.51	0.0217	23.00	818.11	0.0273	18.31
Estimates	751.52	0.0214	23.38	811.64	0.0266	18.80

Table 4.4: Estimation results when load power factor is 0.87.

Loading cond.	Moderate, 3.16MVA			Heavy, 7.37MVA		
Parameters	$f_{res} = \omega_d/2\pi$	ζ	X/R	$f_{res} = \omega_d/2\pi$	ζ	X/R
Theoretical results	754.58	0.0198	25.23	810.24	0.0242	20.69
Estimates	751.52	0.0194	25.74	811.64	0.0234	21.38

The Eq. (4.32) below describes an example of system model reduction process for a moderate loading condition with 0.95 pf. The rapid mode truncation reduces the order of transfer function from Eq. (4.16) to Eq. (4.27). The resulting characteristic equation is presented in the following Eq. (4.34) by taking appropriate numeric values for line parameters according to the positive sequence equivalent circuit. Note that the transient voltage response in any monitoring location in the power system of interest is governed by the same characteristic equation. In fact, the estimates and the theoretical results for the system damping level at PQM 1, 2 and over capacitor location are identical. Figure 4.4 illustrates the damping estimation procedures of (a) extracting the transient voltage differential, (b) detecting envelope by way of the Hilbert transform, (c) performing linear regression for the natural logarithms
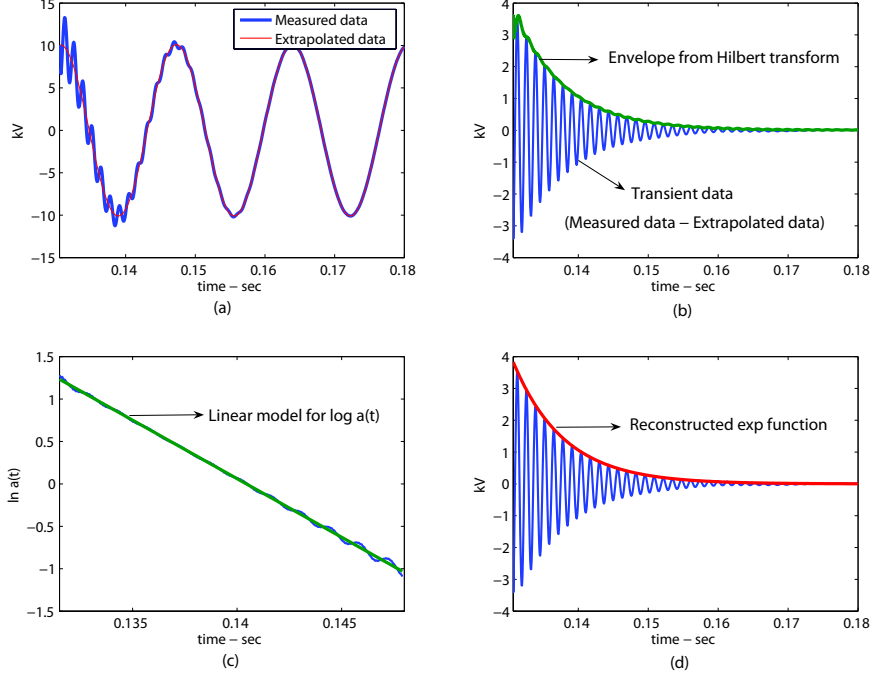
Figure 4.4: Step-by-step procedures of the proposed damping estimation method. (a) extracting the transient voltage differential between the measured data (bold) and the extrapolated data (solid), (b) detecting envelope by way of Hilbert transform, (c) performing linear regression for the natural logarithms of the envelope, which results in the effective X/R ratio, and (d) reconstructing exponential function that perfectly fits in the voltage transient response.

of the envelope, which results in the effective X/R ratio, and (d) reconstructing the exponential function that perfectly fits in the voltage transient response. The damped resonant frequency is accurately determined using the parallel resonant frequency estimation method addressed in [10, 33].

$$\frac{V_S(s)}{V_{sc}(s)} = \frac{1.278s^3 + 1.495e3s^2 + 4.778e7s + 48.02e9}{2.15s^3 + 2.65e3s^2 + 5.125e7s + 48.15e9} \tag{4.32}$$

$$\Rightarrow \frac{0.59455\left(s^2 + 132.6s + 3.732e7\right)}{s^2 + 284.2s + 2.357e7} \tag{4.33}$$

82
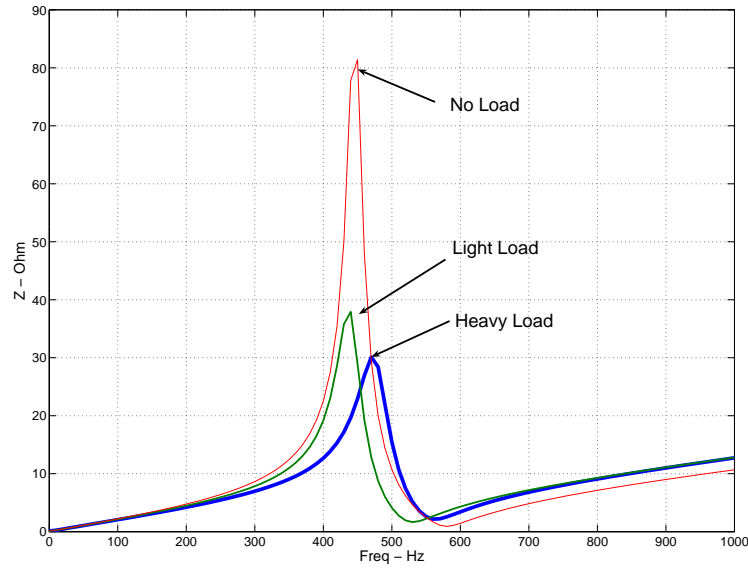
Figure 4.5: System impedance scan results of a typical 12.47 kV system for two different loading conditions

$$\Delta(s) = s^2 + 284.2s + 2.357e7 \qquad (4.34)$$

4.5.2.2 Nonlinear load

The load model is modified to inject the fifth and seventh harmonic currents by 3% of the 60 Hz component and the capacitor bank size is increased to 850 kVar to support the resonance condition near the seventh harmonic. The distribution feeder is balanced with $d_1 = 4$ miles and $d_2 = 1$ mile. Both moderate and heavy loading conditions with the same power factor are investigated. The impedance scan results and the voltage and current waveforms are illustrated in Figures 4.5 and 4.6 to emphasize the load impact on the system
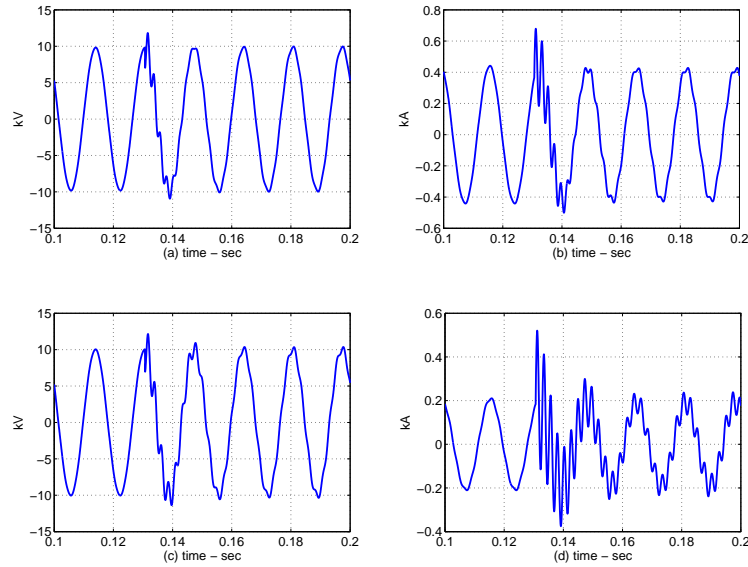
Figure 4.6: Voltage and current waveforms at a simulated 12.47 kV substation: (a), (b) voltage and current for a system under heavy loading condition and (c), (d) voltage and current when resonance occurs due to loading condition change

damping and resonant frequency.

The change from a heavy to a moderate load condition causes a system resonance phenomenon due to the new resonant frequency formed near the seventh harmonic as well as the increased peak impedance level. Thus, injecting the same amount of harmonic currents can result in different levels of distorted voltage and current waveforms. However, it is often neglected that change in the load condition shifts the resonant frequency. This can be more influential in mitigating the resonance phenomena in many cases than lowered peak impedance level. The estimation results presented in Table 4.5

84

Table 4.5: Estimation results for nonlinear load with 0.87 pf.

Loading cond.	Moderate, 3.16MVA			Heavy, 7.37MVA		
Parameters	$f_{res} = \omega_d/2\pi$	ζ	X/R	$f_{res} = \omega_d/2\pi$	ζ	X/R
Theoretical results	439.58	0.0374	13.38	476.94	0.0454	11.02
Estimates	439.27	0.0370	13.50	476.45	0.0437	11.43

demonstrate that the performance of the proposed technique is independent of the load type, i.e., whether it is linear or nonlinear, as long as the steady-state voltage waveforms are considered to be (quasi)-stationary during the observation period immediately after the capacitor bank operation. The estimated parameters are very close to those theoretical values calculated from a positive-sequence equivalent circuit as well.

4.5.3 Evaluation Case for Unbalanced Lines and Loads

This section investigates a case where the system is modeled with unbalanced lines and loads with $d_1 = 3$ miles and $d_2 = 2$ miles. The resulting voltage unbalance is 0.5%. Note that only a moderate load size is considered in this case, since the dominant complex constant power load is modeled by a combination of RL in parallel. The damping from the load then becomes significantly higher compared to that from the combination of RL in series which are employed in the previous case study. Although the lines and loads are unbalanced, the positive sequence equivalent circuit is analyzed to provide approximate theoretical values using three-phase active and reactive power

85
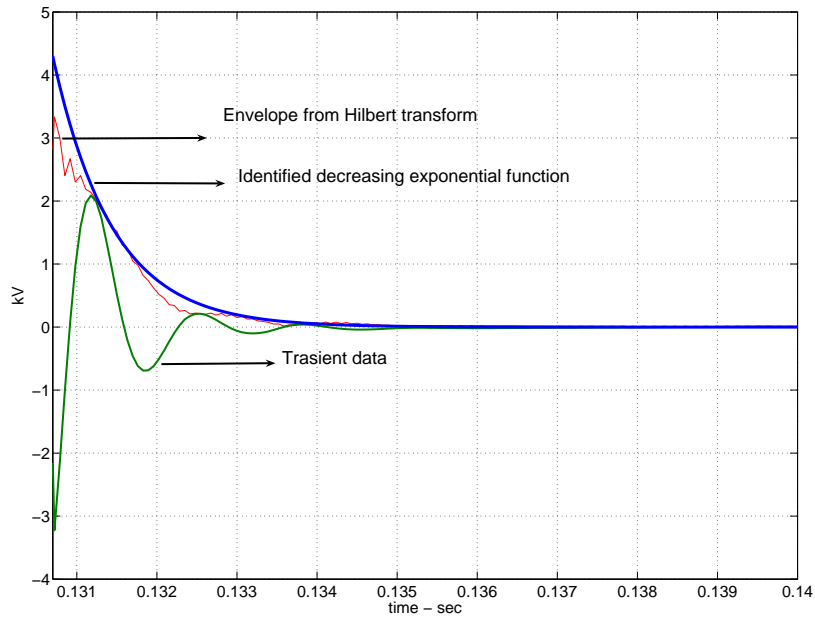
Figure 4.7: Hilbert damping analysis of the phase A transient voltage of a moderately loaded system

measured at the substation - 2.91 MVA, 0.92 lagging pf. Although the estimates from each phase show slight deviations, it should be judged that the results are reasonably accurate since they are in the region of expected theoretical values as presented in Table 4.6. It is also observed that the method is independent of the load composition since only the waveform data is needed. As illustrated in Figure 4.7, the voltage transient is much shorter than that of the balanced line case. Thus, care must be taken to select the observation period to guarantee the optimal envelope from the Hilbert transform: empirical study recommends less than a half cycle data for this high damping case.

Table 4.6: Estimation results with unbalanced lines and loads.

	Phase A	Phase B	Phase C	Theoretical value
$f_{res} = \omega_d/2\pi$	766.55	766.55	766.55	762.30
ζ	0.2918	0.2097	0.3732	0.3459
X/R	1.713	2.356	1.340	1.446

Note that the effective X/R ratio is very small, since they are less than 2. The X/R ratio is approximately 5% of the isolated capacitor bank case, which has been conventionally employed for harmonic studies. Therefore, thorough understanding of the load type, composition and condition is required in advance to perform any mitigation measures against harmonic issues and the proposed technique provides system impedance characteristic in a very practical but precise manner.

4.6   Method Application using Actual Measurement Data

The performance of the damping estimation technique is also validated using actual data of a capacitor switching transient event. The transient event was captured using a widely available power quality monitoring device at a 115 kV substation of a utility company.

Figure 4.8 illustrates the measured voltage waveforms and the results from the Hilbert damping analysis while Table 4.7 summarizes the resulting estimated parameters. As shown in Figure 4.8(d), there are two prominent frequency components at 526 Hz and 721 Hz. However, the lower component
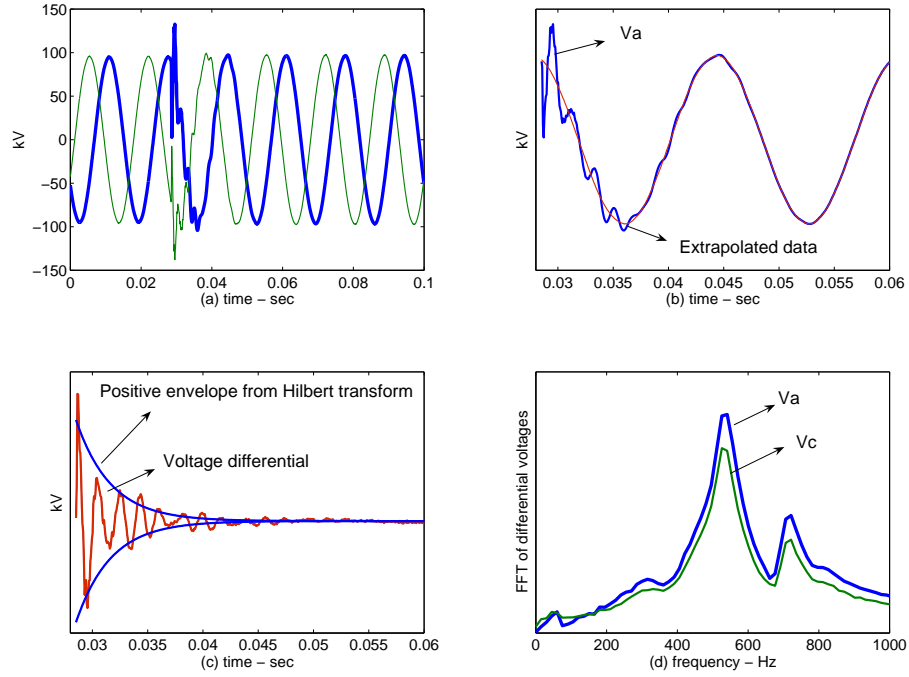
Figure 4.8: Application of the damping estimation method to actual data: (a) voltage waveform of phase A (bold) and C, (b) Phase A voltage transient and the extrapolated voltage after capacitor switching, (c) positive and negative envelope of voltage A detected by Hilbert damping analysis, (d) spectral information of the differential voltage A and C

Table 4.7: Estimation results for actual data.

Parameters	Estimates
$f_{res} = \omega_d/2\pi$	526
ζ	0.0154
X/R	32.50

at 526 Hz is selected to estimate the effective X/R ratio since the magnitude at 526 Hz is much bigger. Although there are no theoretical values to evaluate the estimation results, the obtained values are considered to be reasonable in that the system is at a subtransmission level whose X/R ratio is generally known to be in the order of 30, and the envelope nicely matches the transient voltage as shown in Figure 4.8(c).

The Hilbert damping analysis may cause considerable estimation errors for the following possible two scenarios: (1) the PQ data is significantly corrupted by noises such that the stationarity assumption on the PQ data is no longer valid. (2) the extracted free response possess multiple comparable resonant frequency components such that there is no single dominant mode. One may consider the following ways around these problems.

- Reinforce the signal preprocessing stages by adding the high frequency noise rejection filters and adding the band-pass filters. Thus, one can appropriately select important resonant frequencies based on the system studies followed by the Hilbert damping analysis.

- Exploit the wavelet transform which inherently embeds the band-pass filtering can provide a unified algorithm to estimate the damping ratios of multiple modes as presented in Chapter 5.

- Apply methodology known to be robust to ambient noise signals such as ESPRIT which includes the noise term in its original mathematical model. Thus, one can even extract important system information even

from the heavily distorted data at the cost of increased computational burden [43].

4.7 Conclusions

This chapter proposed a novel method to estimate utility distribution system damping. The proposed method is derived using linear dynamic system theory and utilizes the Hilbert system damping analysis to extract circuit signatures describing the system damping embedded in the voltage waveforms. The efficacy of the integrated signal processing and system theory was demonstrated using data obtained from simulations of a representative utility distribution system and an actual power system. The results show that the proposed method can accurately predict the utility distribution system damping parameters.

Chapter 5

Estimation of System Damping Parameters using Analytic Wavelet Transform

This chapter presents a novel methodology for estimating the damping information of a power system in which multiple resonant frequency components exist. The proposed method was developed using the analytic wavelet transform and requires only the intrinsic transient portion of the voltage waveform, i.e. the free response of the capacitor bank energizing. The method can estimate damping ratios of the selected resonant frequencies and is free from the uni-modal restriction of the previous Hilbert damping analysis. Thus, the method can provide more accurate system modal information.

5.1 Introduction

The main problem of the Hilbert damping analysis is that it does not perform as well for multi-modal cases[1] as for uni-modal cases, as illustrated in Chapter 4. Thus, the previous chapter suggested an alternative to this problem by exploiting a single dominant mode in order to quantify the overall

---

[1]Two or more energized shunt capacitor banks and feeders may interact and form two or more modal (resonant) components. These cases correspond to multi-degree-of-freedom (MDOF) systems in mechanical or structural engineering [49].

system damping. Unfortunately, it is not uncommon to find many practical cases for which this technique fails to work, since multiple modal components are comparable in size such that there is no conspicuous mode to choose. As suggested in Section 4.4, one may reinforce the signal preprocessing stages by adding high-frequency noise rejection filters and /or adding band-pass filters and thus appropriately selecting the important resonant frequencies based on the system studies followed by the Hilbert damping analysis. The proposed wavelet transform based damping analysis can replace this complex procedure in an efficient and systematic way. It requires only capacitor switching waveforms. Thus, the proposed method provides more accurate knowledge of system modal characteristics. Accurate system modal information can be utilized to evaluate the system's vulnerability to power quality disturbances, particularly resonance phenomena, so that a utility can take preventive measures and improve the PQ of the system.

One may find a great number of wavelet applications in power systems engineering, particularly in power quality problems. Most of this research has focused on utilizing features of the wavelet transform to detect singularities of the signals. Thus, one may pinpoint starting and ending instants of PQ events and switching instants of system equipment. Unique distribution of the wavelet transform output by scales can be utilized to identify PQ disturbances as well. One can also compress the large amount of PQ data effectively by keeping only the significant wavelet coefficients (essential features of the data) [38, 43, 50]. It is also interesting to note that the continuous wavelet transform can be

92

applied to identify the dynamic system modal parameters. These research problems have been encountered in civil and mechanical engineering and have shown very promising results [49, 51]. The vibration data, acoustic data, and ambient noise have been utilized to identify system modal parameters, from which one can detect any damage of the system in order to prevent further damage.

Power systems engineers are aware of the significant impact of the system damping[2] on system operations and controls. However, they lack in such an effective method to accurately quantify the system damping. Only few methods, such as computationally-intensive Prony analysis and ESPRIT, have been addressed [40, 43]. Thus, the main purpose of this chapter can be stated as follows: Apply the wavelet based system identification method to electric power systems and develop an effective power system damping estimation technique using only capacitor switching transient data. The system modal parameters to be estimated are the same as those parameters (resonant frequency and system damping ratio) defined in Chapter 4. However, this method has been developed based on an assumption that the whole system transfer function can be decomposed into a sum of prototype quadratic transfer functions which effectively represent system modes of interest. In essence, this is the same assumption on which Prony and other harmonic analysis tools were developed.

---

[2]In this chapter, damping refers to the general capability of the power distribution system to restrain oscillatory voltage and current (resonance) by dissipating energy. Utility engineers commonly use X/R ratio to indicate this system damping.

The organization of this chapter is as follows. Section 5.2 develops a smart algorithm for estimating power system damping using capacitor switching transient data based on the analytic wavelet transform. Section 5.3 demonstrates the accuracy and efficiency of the proposed technique for the same simulation data used in Chapter 4, and Section 5.4 presents applications to actual measurement data with reference to values from the Prony analysis. This chapter discusses practical implementation issues and pitfalls of the proposed method in Section 5.6 and concludes in Section 5.7.

5.2 Wavelet Transform

The wavelet transform represents a signal via time-scale basis functions that are dilated and translated versions of a mother wavelet, $\psi(t)$ [52]. A wavelet function $\psi(t)$ is a normalized ($\|\psi\| = 1$) zero average function, centered in the neighborhood of $t = 0$. A family of these basis functions is obtained by scaling ψ by s and translating it by u:

$$\psi_{u,s}(t) = \frac{1}{\sqrt{s}}\psi\left(\frac{t - u}{s}\right) \tag{5.1}$$

Then, the wavelet transform of a signal $f(t)$ at scale s and position u is computed by correlating $f(t)$ with a wavelet, $\psi(t)$, as presented below:

$$Wf(u, s) = \langle f, \psi_{u,s}\rangle = \int_{-\infty}^{+\infty} f(t)\frac{1}{\sqrt{s}}\psi^*\left(\frac{t - u}{s}\right) dt \tag{5.2}$$

Dilation by the scale s is inversely proportional to frequency and represents the periodic (harmonic) nature of the signal. This is an important characteristic of

the wavelet transform that enables time-frequency localization of the signal, since the mother wavelet can be considered to be a window function. The wavelet coefficients, $Wf(u,s)$ measures the similarity between the dilated and translated mother wavelet and the target signal at time (u) and scale (s). It should be noted that the Parseval theorem can be used to obtain the wavelet transform in the frequency domain:

$$Wf(u,s) = \langle f, \psi_{u,s} \rangle \tag{5.3}$$

$$= \int_{-\infty}^{+\infty} f(t) \frac{1}{\sqrt{s}} \psi^* \left(\frac{t-u}{s} \right) dt$$

$$= \frac{1}{2\pi} \int_{-\infty}^{+\infty} \hat{f}(\omega) \frac{1}{\sqrt{s}} \hat{\psi}_{u,s}^* (\omega) \, d\omega$$

Combined with the characteristics of the analytic wavelet transform, which will be detailed in the following Section 5.2.1, Eq. (5.3) presents an efficient method to obtain the wavelet coefficients.

In essence, the wavelet transform provides good time resolution at high dilations (low frequencies) but good high-frequency resolution sacrifices its time resolution due to the Heisenberg uncertainty principle [52]. The time (Δt) and frequency (Δf) resolutions of the wavelet transform are $\Delta t = s\Delta t_\psi$ and $\Delta f = \Delta f_\psi / s$ [52], where subscript ψ indicates the mother wavelet. Thus, two modal components in time cannot be identified unless they are more than Δt apart. Similarly, two distinct spectral components cannot be discriminated unless they are more than Δf apart. However, since window functions, in particular Gaussian window functions, lack measurable duration, effective

95

duration in the time domain and effective bandwidth in the frequency domain are determined based on Gabor's definition for mean square measures [52]. The bandwidth of this Gaussian window based wavelet, i.e. the Gabor wavelet, is discussed further in the Appendix A.

Calculating wavelet coefficients at every possible scale requires a fair amount of work and a subset of scales and positions may be sufficient in many applications. If we choose scales and positions based on powers of two, i.e. dyadic scales and positions, then analysis will be much more efficient. This computationally efficient version of the wavelet is called a Dyadic Discrete Wavelet Transform (DWT) [38,52]. DWT, however, does not work well in this system damping estimation, since low-frequency resolution prevents accurate modal separation. Thus, this dissertation does not consider DWT.

5.2.1 Analytic Wavelet Transform

An analytic wavelet can be constructed by the frequency modulation of a real and symmetric window $g(t)$, i.e. $\psi(t) = g(t)\exp(j\eta t)$ [52]. The Fourier transform of $\psi(t)$ is then $\hat{\psi}(\omega) = \hat{g}(\omega - \eta)$. Thus, $\hat{\psi}(\omega) = 0$ for $\omega < 0$ if $\hat{g}(\omega) = 0$ for $|\omega| > \eta$. Hence, ψ is analytic as defined in Eq. (4.1) of Chapter 4. Specifically, a Gabor wavelet is a representative of the analytic wavelet transform and is obtained from a Gaussian window [52]:

$$g(t) = \frac{1}{(\sigma^2\pi)^{1/4}} \exp\left(\frac{-t^2}{2\sigma^2}\right) \tag{5.4}$$

The Fourier transform of this window is then computed as follows:

$$\hat{g}(\omega) = \frac{1}{(4\sigma^2\pi)^{1/4}} \exp\left(\frac{-\sigma^2\omega^2}{2}\right) \tag{5.5}$$

Thus, if $\sigma^2\eta^2 \gg 1$, $\hat{g}(\omega) \approx 0$ for $|\omega| > \eta$. Hence, Gabor wavelets are considered to be analytic. The Fourier transform of $\psi_{u,s}$ is a dilation of $\hat{\psi}(\omega)$ by $1/s$, and can be obtained as $\hat{\psi}_{u,s}(\omega) = \sqrt{s}\hat{\psi}(s\omega)e^{-j\omega u}$. Thus, the AWT of $f(t)$, i.e. $Wf(u,s)$ is the inverse Fourier transform of the frequency function obtained by multiplying $\hat{f}(\omega)$ by $\sqrt{s}\hat{\psi}(s\omega)$. Thus, given the Fourier transform of the chosen analytic wavelet transform, computational complexity can be reduced. This is because the Fourier and inverse Fourier transforms of the signal, $f(t)$ at each scale, s can be calculated efficiently via FFT [3] [53]. Note that the spectral range of interest will determine the number of required scales.

An analytic wavelet transform defines a local time-frequency energy density named as a scalogram:

$$P_W f(u,s) = |Wf(u,s)|^2 \tag{5.6}$$

The instantaneous frequency, $\omega(u)$ is related to the ridges [4] of the normalized scalogram, $s^{-1}P_W f(u,s)$ and defined as $\omega(u) = \eta/s(u)$ [52]. There are several methods to extract ridges [52,54]. The cross section method has been used in

---

[3]The discrete Fourier transform of a circular convolution is the product of the two discrete Fourier transforms. For two signals f and h with a length $M \geq 32$, computing their convolution with an FFT is faster than using the straightforward formula.

[4]The time-scale representation of the energy concentration of the continuous wavelet transform is called the ridge. Ridges represent the frequency content of the analyzing signal with a high density of energy that is a function of u [52].

the present research based on the pre-known damped resonant frequency (ω_d). Note that the scalogram is linear on the time axis but logarithmic on the scale axis. To obtain a linear frequency spectrogram, logarithmic interpolation is required to obtain $\omega(u)$.

5.3 System Damping Estimation based on Analytic Wavelet Transform

Let a multi-modal signal $v(t)$ be represented as a weighted sum of N individual signals, $v_i(t)$. In particular, each $v_i(t)$ can be interpreted as a damped sinusoidal as:

$$v(t) = \sum_{i=1}^{N} \alpha_i v_i\left(t\right) = \sum_{i=1}^{N} \alpha_i a_i\left(t\right) \cos\theta_i\left(t\right) = \sum_{i=1}^{N} \alpha_i e^{-\zeta_i \omega_{ni} t} \cos\left(\omega_{di} t + \phi_i\right) \quad (5.7)$$

Utilizing a linearity property of the wavelet transform, the wavelet transform of $v(t)$ is then represented as follows:

$$W\left(\sum_{i=1}^{N} \alpha_i v_i\right)\left(u,\ s\right) = \alpha_i \sum_{i=1}^{N} W v_i\left(u,\ s\right) \quad (5.8)$$

Eq. (5.8) makes it possible to analyze each ith component of a multi-modal signal, $v(t)$ and thus separate amplitude and phase components.

5.3.1 Algorithm Development

Let us represent a signal, $v(t)$ as $v(t) = a(t)\cos\theta(t)$. This may represent a whole single mode signal or a single modal component of a multi-modal signal. The Gabor wavelet transform of this signal is obtained as follows [55]:

$$W v\left(u,s\right) = \frac{1}{2} a\left(u\right) \hat{\psi}_{u,s}\left(\omega\left(u\right),\sigma,\eta\right) e^{j\theta(u)} + \varepsilon\left(a'\left(t\right),\omega'\right) \quad (5.9)$$

where $\omega = \theta'(u) = \frac{d\theta(u)}{du}$, $\omega'(u) = \frac{d\omega(u)}{du}$ and $\hat{\psi}_{u,s}$ is a dilated and translated version of Eq. (5.5),

$$\hat{\psi}_{u,s}(\omega, \sigma, \eta) = \frac{1}{(4\sigma^2 s^2 \pi)^{1/4}} \exp\left(\frac{-(\omega - \eta/s)^2 \sigma^2 s^2}{2}\right) \exp(-j\omega u) \qquad (5.10)$$

The last term, $\varepsilon(a'(t), \theta''(u))$ in Eq. (5.9) is an approximation error and can be neglected if the derivative of the phase is greater than the bandwidth $\Delta\omega$ [52], i.e $\theta'(u) \geq \Delta\omega$. The derivation for this Gabor wavelet function is presented in the Appendix A.

As discussed in Section 5.2, the following condition should be met in order to identify any two components, for example the ith and jth components of a multi-modal signal [52]:

$$\left(\theta'_i(u) - \theta'_j(u)\right) \geq \max\{\Delta\omega(s_i), \Delta\omega(s_j)\}$$

In general, the signal $v(t)$ can be represented as a damped sinusoidal: $v(t) = ae^{-\zeta\omega_n t} \cos(\omega_d t + \phi)$ where $\omega_d = \omega_n \sqrt{(1 - \zeta^2)}$ and ω_n is a system natural frequency as discussed in Chapter 4. The algorithm for estimating the power system damping ratios based on AWT can be developed as follows:

1. The signal utilized for estimating the system damping is the same capacitor bank switching transient as used in Chapter 4. Thus, the same preprocessing steps should be taken to extract the empirical free response of the system.

2. Perform FFT on this free response of the system and determine the salient ω_d's. Note that ω_d's replace ω_n's in this algorithm development,

99

since the observable resonant frequency components are ω_d's. However, small damping ratios make the numerical difference between them negligible.

3. Obtain the Gabor wavelet coefficients using Eqs. (5.9) and (5.10). The error term in Eq. (5.9) will be neglected. However, it should be noted that this error term may mislead the estimation results if the condition, $\theta'(u) \geq \Delta\omega$ is not satisfied.

4. The angular velocity of the Gabor wavelet function ($\omega = \eta/s$ is equal to the angular velocity of the signal, i.e. ω_d as far as the ridge is concerned. Therefore, $\exp\left(-\left(\omega - \eta/s\right)^2 \sigma^2 s^2/2\right)$ will be 1.

5. Consequently, the following relation can be derived:

$$\ln\left(\frac{2\left|Wv\left(u, s(u)\right)\right|}{\left(4\pi\sigma^2 s(u)^2\right)^{1/4}}\right) \approx -\zeta\omega_d u + \ln a \tag{5.11}$$

It should be noted that Eq. (5.11) and Eq. (4.29) have the same form. Thus, the standard linear squares method can be applied to find the slope of Eq. (5.11). As to a multi-modal signal, this linear regression analysis should be performed for all modal components of interest. The ridge is considered to be constant, since a constant instantaneous angular velocity is assumed. Since $s(u) = \frac{\eta}{\omega_d}$ where η denotes the frequency center of the base wavelet, the frequency center of a dilated wavelet is η/s.

100

5.4 Method Validation

This section illustrates procedures of the AWT based damping estimation technique and demonstrates its efficacy for a synthetic signal, IEEE test system, and actual PQ data.

5.4.1 Method Validation for a Synthetic Multi-Modal Signal

A synthetic voltage signal, $v(t)$ is composed of three damped sinusoidal components and can be represented as follows:

$$v(t) = \sum_{i=1}^{3} a_i e^{-\zeta_i \omega_{ni} t} \cos\left(\omega_{di} t + \phi_i\right)$$

This signal is composed of the 5th, 7th, and 11th harmonics (modes) with reference to the system frequency (60 Hz). The magnitudes of modal components are selected based on our experience in harmonic analysis with reference to the magnitude of the 5th harmonic voltage, a_1. Thus, $a_1 = 100$ (selected arbitrarily), $a_2 = 100 \cdot 5/7 = 71.43, a_3 = 100 \cdot 5/11 = 45.45$. The damping ratios, ζ_i's for these harmonic components are randomly selected as 0.03, 0.05, and 0.1, respectively. The phase angles, ϕ_i's are chosen arbitrarily as $\pi/3$, $-\pi/4$ and $\pi/6$, respectively. Figure 5.1 shows (a) the synthetic waveform and (b) FFT result for this signal. Figure 5.2 illustrates the linear regression analysis based on Eq. (5.11) for (a) the 5th mode, (b)the 7th mode, and (c) the 11th mode of the signal. Note that the solid lines are fitted into the bold lines. Based on Eq. (5.11), linear regression analysis finds the slopes of each mode, $(-\zeta_i \omega_{di})$. Using ω_{di}'s obtained from the spectral analysis of the signal, we can
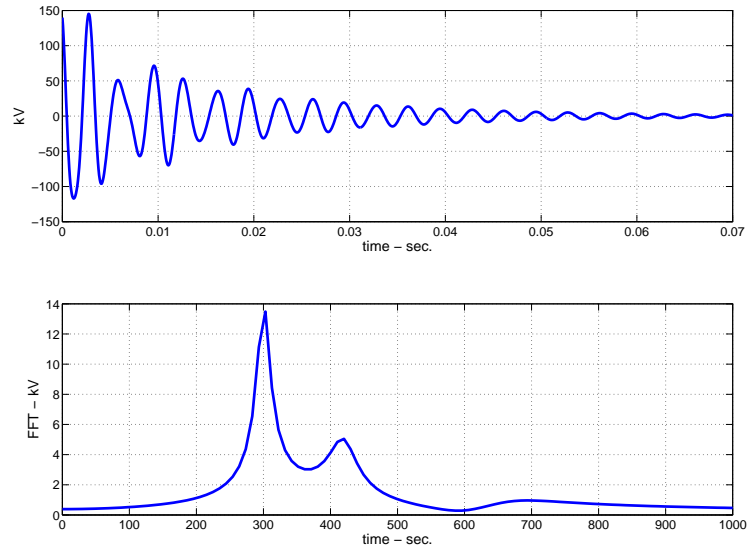
Figure 5.1: (a) Synthetic voltage transient waveform and (b) FFT of the waveform
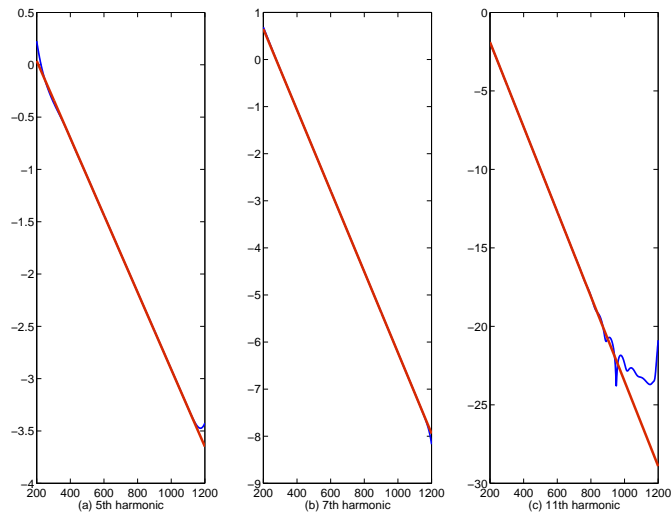
Figure 5.2: Linear regression analysis for (a) 5th harmonic, (b) 7th harmonic and (c)11th harmonic

102

Table 5.1: Estimation results for a synthetically composed signal

Parameters	$f_d = \omega_d/2\pi$	ζ	X/R
Theoretical values	300, 420, 660	0.030, 0.050, 0.100	16.81, 10.00, 5.00
Estimates using AWT	303, 420, 694	0.030, 0.050, 0.095	16.67, 10.00, 5.26

obtain the multi-modal damping ratios ($\zeta_i's$). Based on the assumption that the voltage in s-domain can be represented by a sum of quadratic equations whose characteristic equation is the same form as Eq. (4.21), we can interpret $(\frac{1}{2\zeta_i})$ as the effective X/R ratio at ω_{di} as defined in Eq. (4.25).

As described in Table 5.1 above, the estimated damping ratios are very close to the theoretical values. However, there is a need to adjust the parameters (η and σ) of the Gabor wavelet, since the estimated damping ratio of the 11th mode is not as accurate as those of other modal components. This research found that η should be adjusted around 6 and σ should be in the range between 7 and 10 in order to obtain accurate modal parameters.

Table 5.2: Estimation results when load power factor is 0.95.

Loading cond.	Moderate, 3.16MVA			Heavy, 7.37MVA		
Parameters	$f_{res} = \omega_d/2\pi$	ζ	X/R	$f_{res} = \omega_d/2\pi$	ζ	X/R
Theoretical results	772.28	0.0293	17.08	845.97	0.0387	12.92
Hilbert transform	766.55	0.0286	17.47	841.70	0.0373	13.38
AWT	766.55	0.0286	17.47	841.70	0.0376	13.29

Table 5.3: Estimation results when load power factor is 0.90.

Loading cond.	Moderate, 3.16MVA			Heavy, 7.37MVA		
Parameters	$f_{res} = \omega_d/2\pi$	ζ	X/R	$f_{res} = \omega_d/2\pi$	ζ	X/R
Theoretical results	758.51	0.0217	23.00	818.11	0.0273	18.31
Hilbert transform	751.52	0.0214	23.38	811.64	0.0266	18.80
AWT	751.52	0.0218	22.89	811.64	0.0270	18.53

Table 5.4: Estimation results when load power factor is 0.87.

Loading cond.	Moderate, 3.16MVA			Heavy, 7.37MVA		
Parameters	$f_{res} = \omega_d/2\pi$	ζ	X/R	$f_{res} = \omega_d/2\pi$	ζ	X/R
Theoretical results	754.58	0.0198	25.23	810.24	0.0242	20.69
Hilbert transform	751.52	0.0194	25.74	811.64	0.0234	21.38
AWT	751.52	0.0191	26.04	811.64	0.0227	21.99

5.4.2   Method Validation for IEEE Test Model

The proposed damping estimation method can also be applied to the IEEE test system that has been discussed in Section 4.5.2. The proposed technique is applied to quantify the system damping level for varying load sizes and power factors. The resulting estimates are summarized in Tables 5.2 through 5.4 above, along with the theoretical results using the characteristic equation in Eq. (4.27) and the results from the Hilbert damping analysis. These tables demonstrate that the proposed technique can estimate resonant frequency and damping ratio (or effective X/R ratio) accurately.

104

5.5 Method Validation using Actual Measurement Data

The performance of the damping estimation technique was also validated using actual data of a capacitor switching transient event. The transient events were captured by widely available power quality monitoring devices.

It should be noted that the reference values are those of the Prony analysis [40, 56], since the analytical results are not available. Given accurate system parameters, eigenvalues from linear matrices arising from the dynamic model of a system may provide analytical modal parameters. In practice, the system may be too complex to model or may have parameters that drift with time or operating condition. In these cases, it may be desirable to replace the actual dynamic model with an estimated linear model that is derived from the system output waveform. The estimated linear model may be used for control design, for example, to design power system stabilizers [21].

One approach to estimate the system modal parameters is Prony analysis [28]. The system order is carefully chosen to be 100 through numerous simulations for the following case studies[5]. In general, the larger the number of specified eigenvalues, the more accurate the results are. However, if too many eigenvalues are specified, the resulting set of eigenvalues has a tendency to contain spurious eigenvalues, i.e. those eigenvalues that are highly damped and highly oscillatory. Thus, they help the estimated waveform fit the ac-

---

[5]The eigenvalues of interest are almost invariable with this system order and higher. Thus, the estimated modal parameters are considered to be accurate within negligible error bounds.

Table 5.5: Estimation results for actual data measured at a 115kV substation.

Parameters	Estimates (AWT)	Estimates (Prony)
$f_{res} = \omega_d/2\pi(Hz)$	526, 721, 310	533, 705, 456
ζ	0.0714, 0.0309, 0.1081	0.0667, 0.0335, 0.1176

tual waveforms more closely, but do not provide any useful information. More description on Prony analysis is provided in Appendix B.

5.5.1 PQ data at a 115 kV substation of a utility company

This transient event was captured at a 115 kV substation of a utility company in the Northeast (U.S.) and is the same event illustrated in Figure 4.8. The Hilbert damping analysis was utilized to estimate the overall system damping using the most dominant mode. However, the Hilbert damping analysis is insufficient for identifying individual modal components according to the following Table 5.5. There is a clear discrepancy between the overall system damping ratio in Table 4.7 using only the most dominant resonant frequency (526 Hz) and the damping ratio of this mode estimated by the AWT based method. The overall system damping was found to be 0.0154 in Section 4.4. This may be not a surprising result, since the second dominant mode is considerable in magnitude in this case study. Note that the estimated modal parameters of the AWT based method correspond to those of the Prony analysis. Figure 5.3 shows how closely the estimated waveform fits to the actual waveform. However, the computation time of the AWT based method is less than a third of that of Prony analysis under the same computing environment.

106
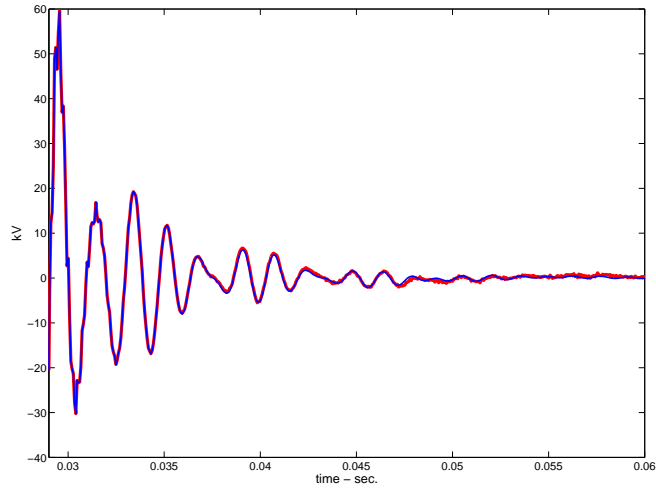
Figure 5.3: Original voltage transient (bold line) and Prony estimate (solid line) from 115kV line.

5.5.2 Actual PQ data

In the following, examples are presented using a distribution feeder with capacitor banks as illustrated in Figure 5.4. Actual PQ measurements were taken at three locations (PQM A, PQM B and PQM C). A capacitor switching event recorded at approximately 13:00 on December 3, YYYY is used for the data from A and B. The data from C was recorded at 17:48 on December 2, YYYY.

107
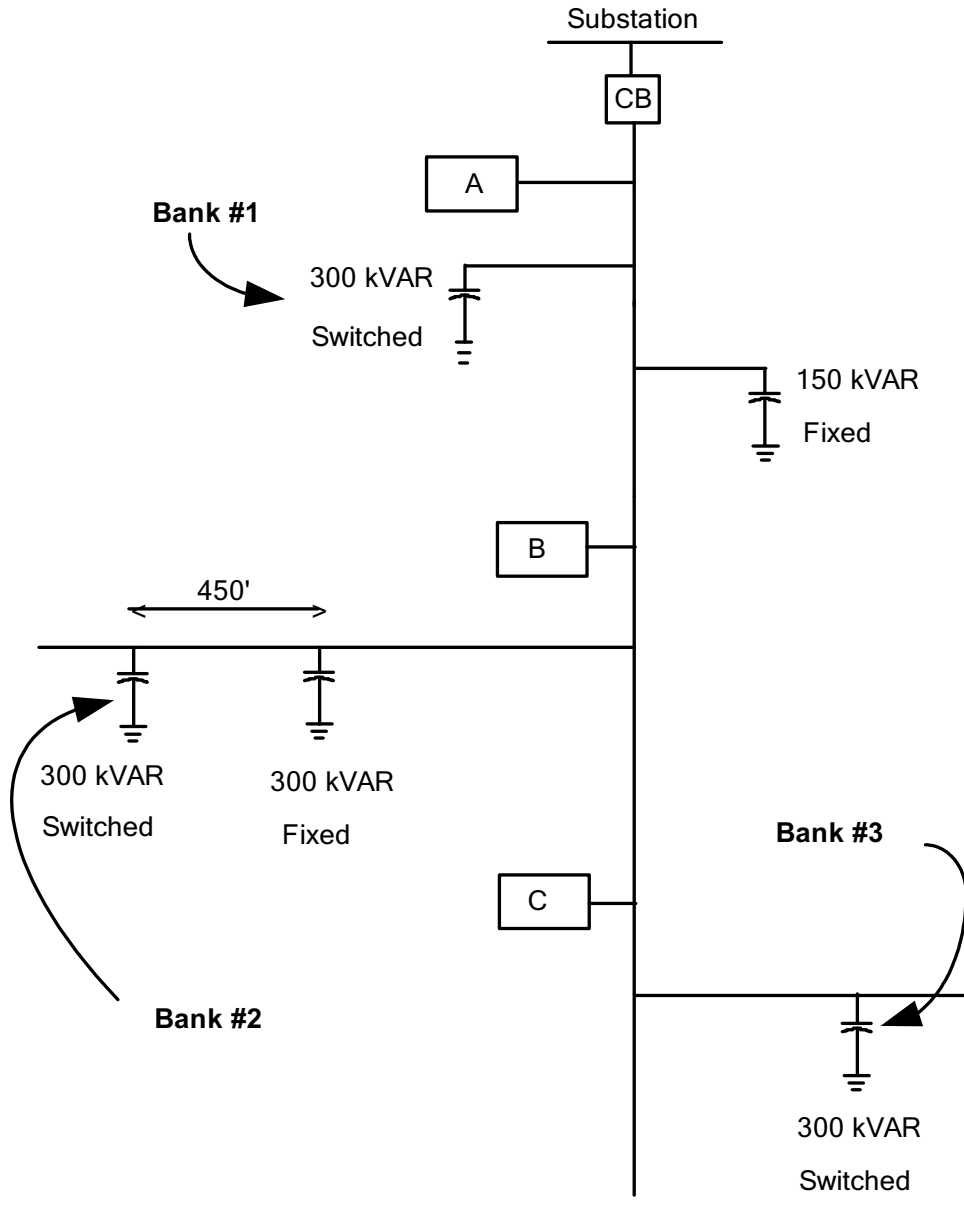
Figure 5.4: A feeder with several capacitor banks.
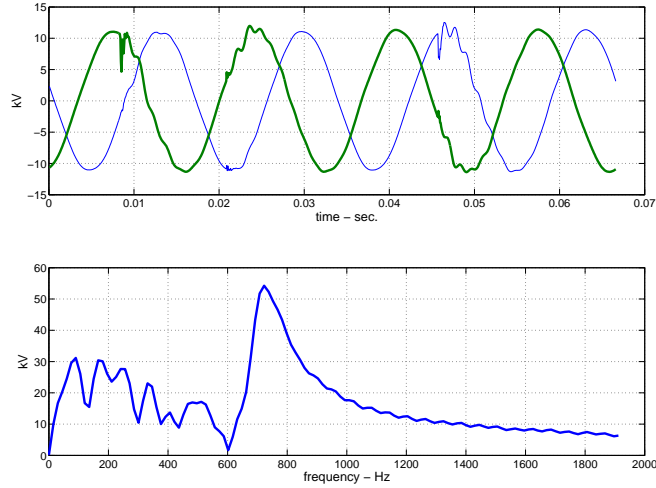
Figure 5.5: (a) Voltage waveforms (Phase A, B from PQM A) and (b) FFT analysis of the voltage transient (Phase A).

5.5.2.1   Analysis using PQM A

The phase voltage waveforms at PQM A and the spectrum of phase A voltage are illustrated in Figure 5.5. Three modal components of interest are selected from Figure 5.5(b) based on their magnitudes. It is also clear that the modal parameters from the Prony analysis can be used as references, since the signal generated by the Prony method matches well with the actual signal according to Figure 5.6. The resulting modal parameters in Table 5.6 demonstrate the efficacy of the proposed method. Thus, we can conclude that the AWT method provides as accurate results as Prony analysis with much less computational power.

109
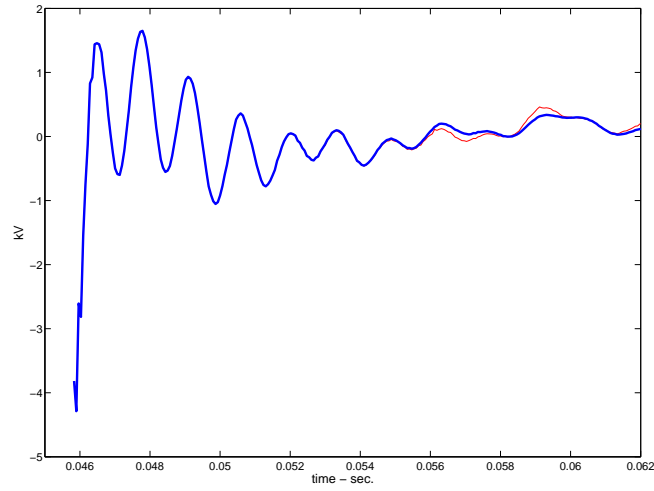
Figure 5.6: Original voltage transient (bold line) and Prony estimate (solid line) from PQM A.

Table 5.6: Estimation results for actual data (PQM A).

Parameters	Estimates (AWT)	Estimates (Prony)
$f_{res} = \omega_d/2\pi(Hz)$	721, 331, 510,185	708, 295, 492, 204
ζ	0.0660,0.0316, 0.1591,0.8752	0.0615, 0.0272, 0.1011,0.8403
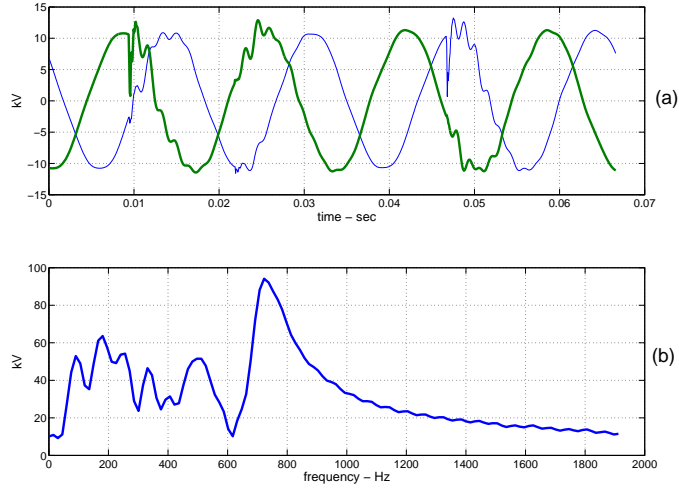
Figure 5.7: (a) Voltage waveforms (Phase A, B from PQM B) and (b) FFT
analysis of the voltage transient (Phase A).

5.5.2.2 Analysis using PQM B

The phase voltage waveforms at PQM B and the spectrum of phase A
voltage are illustrated in Figure 5.7. Three modal components of interest are
selected from Figure 5.7(b) based on their magnitudes. The Prony analysis
provides an accurate approximation of the empirical free response according
to Figure 5.8.

Based on the result from the Table 5.7, the AWT based method provides
precise system modal parameters.

111
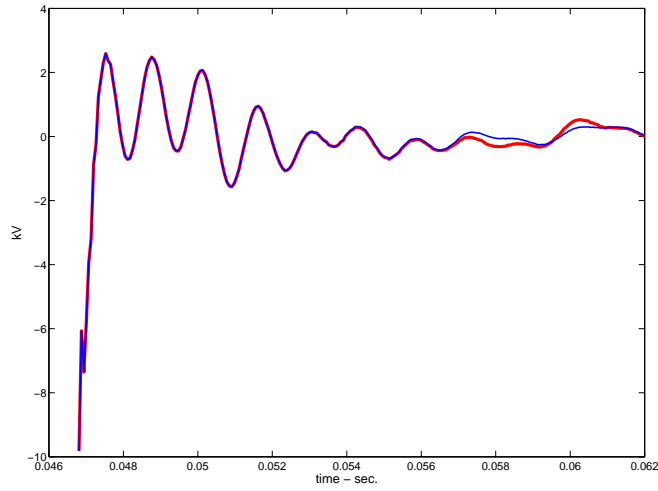
Figure 5.8: Original voltage transient (bold line) and Prony estimate (solid line) from PQM B.

Table 5.7: Estimation results for actual data (PQM B).

Parameters	Estimates (AWT)	Estimates (Prony)
$f_{res} = \omega_d/2\pi(Hz)$	721, 331, 481,185	710, 297, 490,189
ζ	0.0703, 0.0291, 0.1062,0.5327	0.0679, 0.0268, 0.0942,0.4719

112
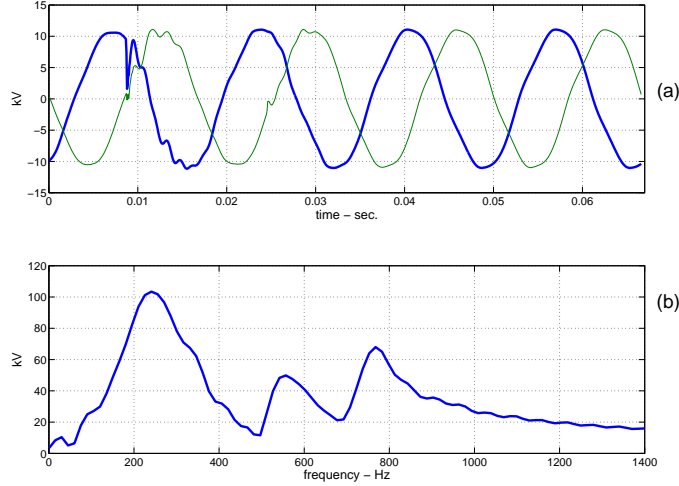
Figure 5.9: (a) Voltage waveforms (Phase A, B from PQM C) and (b) FFT analysis of the voltage transient (Phase A)

Table 5.8: Estimation results for actual data (PQM C).

Parameters	Estimates (AWT)	Estimates (Prony)
$f_{res} = \omega_d/2\pi(Hz)$	240, 766, 556	233, 748, 532
ζ	0.2320, 0.0618, 0.0592	0.2672, 0.0529, 0.0626

5.5.2.3   Analysis using PQM C

The phase voltage waveforms at PQM C and the spectrum of phase A voltage are illustrated in Figure 5.9. Three modal components of interest are selected from Figure 5.9(b) based on their magnitudes. It is also clear that the Prony analysis for the empirical free response provides an accurate approximation of the measured signal according to Figure 5.10.

We should also note that these estimated resonant frequencies corre-

113
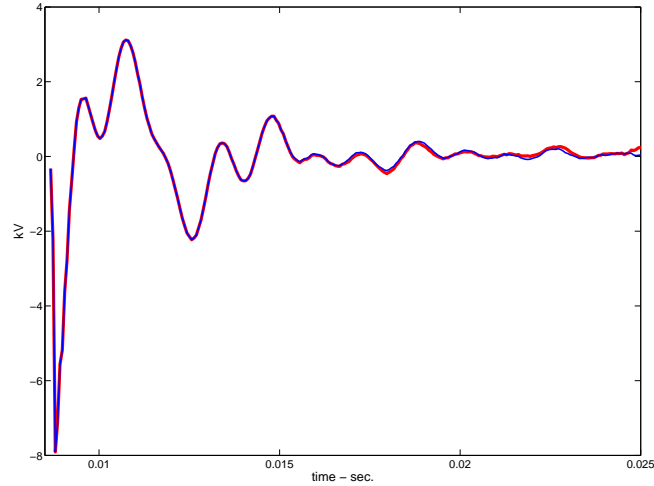
Figure 5.10: Original voltage transient (bold line) and Prony estimate (solid line) from PQM C

spond to those of a paper which dealt with the same system [33]. On top of this frequency information, the corresponding damping ratios can indicate the geographical information of the PQM devices and the switched capacitor bank contributing to a specific modal component. When it comes to the resonant frequency around 710 Hz, the damping ratios are almost in the same order. However, the damping ratios for a frequency component around 500 Hz from PQM A and B are in the similar order but the damping ratio from PQM C is lower than these values. It should be noted that the resonant frequencies were shifted to higher values when the PQM C was triggered. Thus, one may monitor the changed loading condition and its impact on the resonant frequencies and damping.
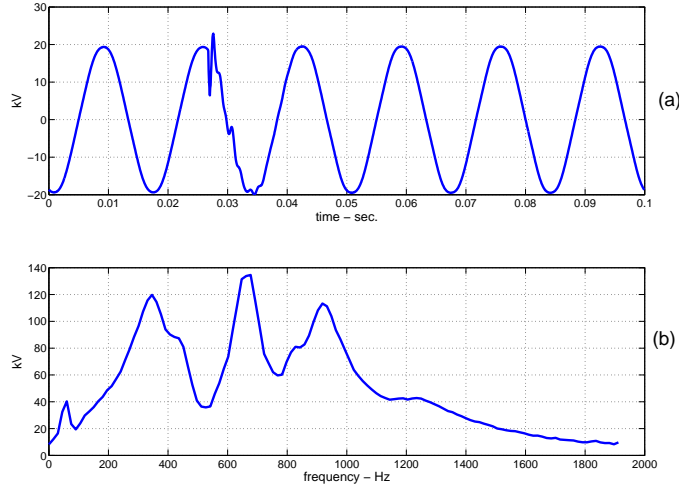
Figure 5.11: (a) Voltage waveforms (Phase A) and (b) FFT analysis of the voltage transient (Phase A).

Table 5.9: Estimation results for actual data.

Parameters	Estimates (AWT)	Estimates (Prony)
$f_{res} = \omega_d/2\pi (Hz)$	676, 346, 916	663, 350, 911
ζ	0.0595, 0.1591, 0.0626	0.0660, 0.1619, 0.0634

5.5.3 PQ data due to a back-to-back energizing

The proposed algorithm was applied to the same event that will be presented in Figure 6.15. A 1.8 Mvar capacitor bank (Bank 1) is energized in close proximity to a bank that is already in service (Bank 2). The two banks are located in the middle of a distribution feeder and separated by approximately 2,500 feet. A power quality monitor is installed downstream from Bank 1 but upstream from Bank 2.

115
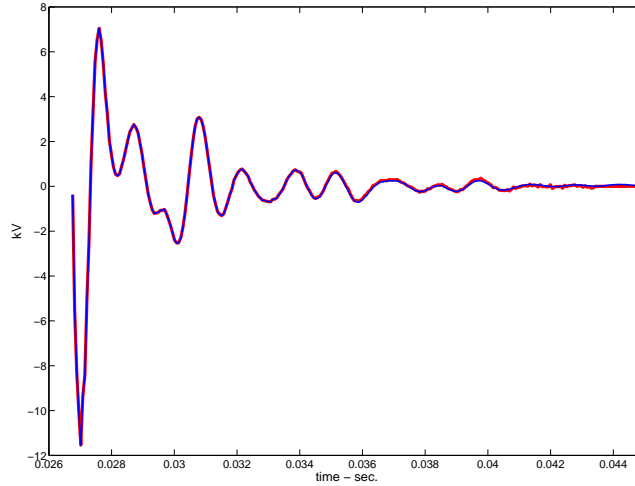
Figure 5.12: Original voltage transient (bold line) and Prony estimate (solid line) from PQ monitor.

5.6 Discussion

As presented in this chapter, the proposed AWT based method has been proven to be a viable tool for identifying system modal parameters. We expect its promising contribution to power systems identification problems based on our preliminary research results. However, there are several research opportunities in line with this research effort.

- A systematic and adaptive technique should be developed to provide the parameters of the Gabor wavelet transform. A trial and error selection scheme has been used in this research. However, as indicated in Section 5.3.1 and illustrated in Figure 5.2(c), inappropriately chosen wavelet parameters may result in erroneous estimates. Another good way to

116

overcome this issue would be to build a better analytic wavelet function that best identifies power systems.

- A systematic method is needed to minimize the end-effects of the window function on the estimation accuracy, which is closely related with the above problem.

- The instantaneous frequencies easily computed from the wavelet transform are neglected in this research due to their low resolutions. This computational loss should be avoided by developing an improved algorithm to truly stick to the philosophy of time-frequency analysis and utilize this byproduct.

5.7   Conclusions

This chapter proposed a computationally efficient method to estimate multi-modal system damping ratios using the analytic wavelet transform. The efficacy of the proposed method was demonstrated using simulated and actual PQ data. The estimated damping ratios can be estimated to be as correct as those of the Prony analysis. But, the measured computation time of the wavelet based method is less than a third of that of the Prony analysis in the same computing environment. In addition to this, this method is free from the spurious high-energy harmonic components of the Prony method. Thus, the proposed AWT based method can predict the utility distribution system damping parameters efficiently and precisely.

Chapter 6

On Two Fundamental Signatures for Determining the Relative Location of Switched Capacitor Banks

This chapter describes two fundamental signatures of shunt capacitor bank switching transient phenomena from which one can accurately determine the relative location of an energized capacitor bank whether it is upstream or downstream from the monitoring location. Mathematical analysis of a capacitor bank energizing proves that: (1) the energized capacitor bank affects only the upstream reactive power flow and (2) at the energizing instant, the gradients (time-derivatives) of voltage and current waveforms measured upstream from the capacitor location will have opposite signs. The reverse is true in that at the energizing instant gradients of voltage and current waveforms measured downstream from the same capacitor location will have equal signs. Thus, we can precisely determine the relative location of the switched capacitor bank by simply evaluating power factor changes and the signs of voltage and current waveform gradients at the switching instant. The efficacy of our practical direction finding technique is demonstrated analytically, and by way of time-domain simulation models and actual data.

118

6.1 Introduction

Capacitor banks are widely used in both transmission and distribution systems to provide reactive power, increase system capacity, voltage support, and also reduce power losses [57]. They are also very effective in reducing billing charges in distribution systems. Unfortunately, overvoltage transients resulting from capacitor switching operations can cause adverse impacts both on the power system and within customer facilities. Examples of these disturbances include harmonic resonance, voltage magnification at low voltage capacitor banks, and nuisance tripping of adjustable-speed drives. With the large number of capacitors on most power systems, it is important to identify such problems and correlate them to the specific capacitor bank that has been energized. Unfortunately, most utilities have very limited methods for identifying transient switching problems and correlating them with the capacitor switching operation [2, 41].

To address this problem, this chapter proposes and develops a precise and practical algorithm capable of determining the relative location of an energized capacitor bank on a power distribution system. This technique is based on two fundamental physical phenomena of capacitor bank energizing operation. First, only reactive power flow upstream of the capacitor bank is reduced by the injected reactive power. Reactive power flow downstream of the capacitor bank is not affected at all. Thus, we will observe the power

119

factor improvement only at the upstream[1] PQ monitors. Second, when an uncharged capacitor bank is energized, it behaves like an instantaneous short-circuit element since the initial voltage at the capacitor terminal is zero. As a result, the instantaneous system voltage at the energizing instant is pulled towards zero voltage. If a measurement is available at the source-side of capacitor bus, the instantaneous system voltage would be zero. Due to the instantaneous short-circuit phenomenon, current measured at the substation (or upstream from the capacitor location) will have a significantly large but short-lived magnitude (i.e., inrush capacitor currents). On the other hand, current measured downstream from the capacitor sees little of the inrush current. As the capacitor is being charged, the instantaneous voltage rises and overshoots its system peak voltage momentarily. Thus, the relative location of a switched capacitor bank can be determined by observing the polarities of initial voltage and current change, i.e. the signs of voltage gradient, dv/dt and current gradient, di/dt at the monitoring locations. Figure 6.1 illustrates these phenomena clearly. These two fundamental phenomena have rarely been noted in the previous extensive literature on capacitor bank energizing. Several techniques have been proposed to determine the relative location of switched capacitors. Parsons [58] investigated the disturbance energy flow during the transient period and the polarity of the initial peak of the disturbance power to find out the relative location of the switched capacitor bank. The technique requires a provision that the disturbance energy must be greater than or equal

---

[1]Upstream or downstream corresponds to the designation illustrated in Figure 6.2
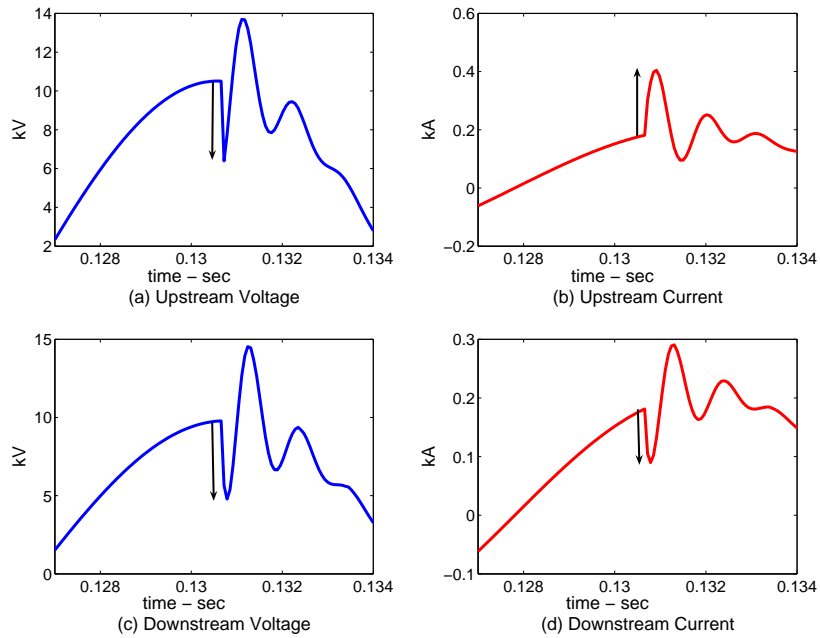
Figure 6.1: Voltage and current waveforms recorded from power quality monitors which are upstream (a and b), and downstream (c and d) from the switched capacitor bank. Note that initial changes of current on b and d are dissimilar.

to a certain percentage of the peak excursion of the disturbance energy. If this condition is satisfied, the technique subsequently compares polarities of final values of disturbance energy and power. Unfortunately, the technique requires three-phase voltage and current waveforms and assumes a constant steady-state instantaneous power. Furthermore, [58] does not provide theoretical analysis of its method. Kim [59] applied a backward Kalman filter to find the location of a switched capacitor bank by estimating the voltage rise of the capacitor bank. Unfortunately, this solution is also impractical to im-

121

plement because it is based on the assumption that an exact power system dynamic model exists, which is not the case. Chang [60] proposed a method using voltage-disturbance energy index and current branch current phase-angle variations for tracking transients. However, [60] argued that the phase angle variation is only related to distance from the disturbance source without going into the basic physics and directional information that this phase angle variation conveys.

Unlike these efforts, the proposed method is based on the underlying physics of capacitor action. It is also practical in that our technique will check initial transient waveshapes of voltage and current and steady-state power factor changes without being confused by certain man-made indexes. Thus, both the analysis procedures and results are manifest to everyone without being confused by artificial quotients that need another interpretation process.

The scope of the problem is described in Section 6.2. Analytical expressions for voltages and currents in the transient and steady state at the promising monitoring locations due to capacitor bank energizing are derived and our algorithm to determine the relative location of the switched capacitor bank is presented in Section 6.3. The efficacy of the proposed technique is demonstrated using data generated by simulating IEEE Test Feeder [44] in PSCAD [45] and actual system data in Section 6.4
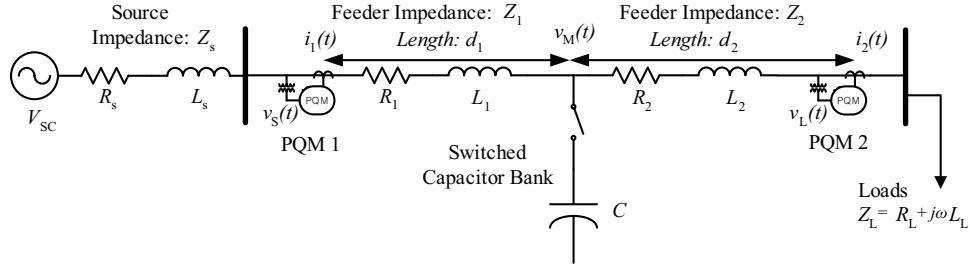
Figure 6.2: The switched capacitor bank is downline from power quality monitor PQM 1 and upline from PQM 2. The CT direction is in the direction of feeder current flow.

6.2 Problem Description and Definition

Let us consider a one-line diagram illustrated in Figure 6.2 above where a capacitor bank is energized. A power quality monitoring device (PQM) is located on both sides of the capacitor bank with its CT (current transformer) direction pointing to the direction of the feeder current. In this arrangement, the switched capacitor bank is physically downstream of PQM 1, but upstream of PQM 2. The problem addressed in this chapter can be stated as follows: Given voltage and current waveforms resulting from the capacitor energizing event, determine the relative direction of the switched capacitor bank. However, the capacitor bank can be considered to be electrically upstream of PQM 1 but downstream of PQM 2 when both CTs are reversed upon installation. Nevertheless, its physical location is unchanged. Thus, we determine only the physical location of the switched capacitor bank in order to be consistent in presenting the direction. When the CT is found to be installed reversely, the measured current must be flipped in the preprocessing stage.

123

As indicated before, our method comprises two independent direction finding algorithms:

1. **Algorithm utilizing the steady state PQ data**: This algorithm is based on the phase angle change between voltage and current, i.e. power factor improvement is achieved only upstream of the switched capacitor bank. In fact, this power factor information has been provided by the conventional monitoring of the power factor of the system. However, this power factor monitoring has not previously been utilized to locate the switched capacitor bank.

2. **Algorithm utilizing the transient state PQ data**: This algorithm is based on the initial signs of dv/dt and di/dt immediately after the capacitor switching operation, i.e. we observe the different polarity upstream from the capacitor bank and the same polarity downstream from the capacitor bank.

However, these two independent algorithms can work together and avoid any erroneous conclusions, especially when the power factor change is too small to be detected or the transient voltage and current waveforms do not clearly show the initial polarity changes due to limited resolution of PQMs. The implementation of the proposed estimation technique is illustrated in Figure 6.3 below. The implementation begins with an existing power quality database or a real-time power quality data stream as used in web-based monitoring devices. Since typical PQ monitors capture a wide range of disturbance events,

124
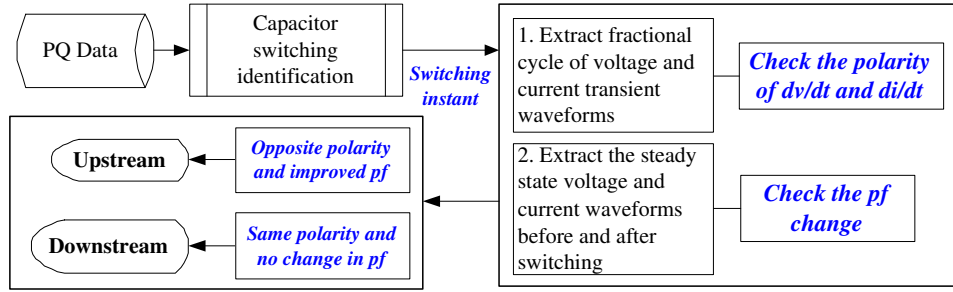
Figure 6.3: Flowchart for the proposed direction finding algirthms.

a separate algorithm is needed to identify capacitor switching event data from other PQ data. The identification of capacitor switching transient waveforms can be done visually or automatically [38]. Once a single event of capacitor switching transient data (three phase voltage and current waveforms) is identified, the transient and steady-state portions of the voltage waveforms are extracted. Wavelet transform techniques are used to determine the exact switching instant effectively. The time instant is used to extract the transient portion of data, the fractional cycle right after the capacitor energizing, and the steady-state data before and after the switching operation. The steady-state data is considered to be one or two cycles of voltage and current right before switching and two or three cycles after switching. Thereafter, the proposed two algorithms are applied to these extracted data to determine the relative location of the capacitor bank. The directional decision is made if any of two algorithms clearly provide the signatures discussed above. Note that the flowchart in Figure 6.3 does not include the ambiguous case that one of two algorithms cannot make its own decision because the decision will be

125

made using a clear signature from any of the two methods.

The following section supports the aforementioned two signatures from shunt capacitor bank switching utilized in our proposed algorithms by the mathematical analysis of switching operation.

6.3   Analysis of Shunt Capacitor Bank Energizing

The following analysis is based on the same mathematical model of capacitor bank energizing presented in Chapter 4. Thus, this section adopts the same parameter notations, dynamic equations, and analysis procedures and results described in Section 4.4.2.1. However, it should be noted that the purpose of using these equations is different. This chapter is intended to investigate instantaneous behaviors of current and voltage immediately after capacitor bank energizing and to prove the empirical observation that their behaviors are unique depending on the monitoring location. Note also that we are also interested in phase angle change between voltage and current due to capacitor bank energizing.

Based on the previous analysis of the equivalent utility feeder diagram shown in Figure 6.2, the currents $i_1(t)$ at PQM 1 and $i_2(t)$ at PQM 2 in s-domain immediately after capacitor bank energizing can be obtained as follows:

$$I_1(s) = V_{sc}(s)G_1(s), \text{ and} \tag{6.1}$$

$$I_2(s) = V_{sc}(s)G_2(s). \tag{6.2}$$

where $G_{1,2}(s)$ are transfer functions for an input voltage source $V_{sc}(s)$ and

output currents, $I_1(s)$ and $I_2(s)$.

Consequently, the voltages at PQM 1, 2 and across the switched capacitor bank in s-domain can be represented as follows:

$$V_S(s) = V_{sc}(s) \left\{ G_1(s)(R_1 + sL_1) + G_3(s) \right\}, \tag{6.3}$$

$$V_L(s) = V_{sc}(s) G_2(s)(L_L s + R_L), \text{ and} \tag{6.4}$$

$$V_M(s) = V_{sc}(s) G_3(s). \tag{6.5}$$

where $G_3(s)$ is a transfer function for an input voltage source and output voltage over a capacitor bank.

The analysis of the equivalent circuit for $t \leq t_s$ (before switching) is quite straightforward in its simple structure (linear RL circuit) and is thus omitted. However, it should be noted that i_1 is equal to i_2 before switching.

6.3.1 Algorithm 1 based on power factor change

Let $Z_1(s)$ and $Z_2(s)$ be the impedance functions at PQM 1 and PQM 2, respectively as expressed in Eq. (6.6) and Eq. (6.7).

$$Z_1(s) = V_S(s)/I_1(s), \text{ and} \tag{6.6}$$

$$Z_2(s) = V_L(s)/I_2(s). \tag{6.7}$$

According to Eqs. (6.1) through (6.4), the impedance functions before and after the switching operation can be presented as in Table 6.1. Note that capacitor bank energizing doest not affect $Z_2(s)$. However, the term $\frac{G_3(s)}{G_1(s)}$ is added to inductive impedance (load) term in $Z_1(s)$ after switching. This

term is the ratio of numerator functions of $G_3(s)$ and $G_1(s)$: note that the characteristic equations of $G_1(s)$ and $G_3(s)$ are the same but the numerator of $G_1(s)$ has higher system order than that of $G_3(s)$. Consequently, this term includes an inverse of polynomial equations and contributes to the phase angle reduction [47]. In order to illustrate the impact of the capacitor bank operation on impedance $Z_1(s)$, Bode plots are drawn by varying the system parameters of the equivalent circuit such as line lengths, capacitor bank size, and load size and power factor as shown in Figure 6.2. The line parameters are based on the IEEE test system [44]. Each plot validates the improved power factor at PQM 1, which is installed upstream from the capacitor bank. As there is no change in $Z_2(s)$, there should be no power factor change around PQM 2, which is installed downstream from the capacitor bank. Figure 6.4 below illustrates Bode plots of $Z_1(s)$ under typical operating conditions.

Each graph demonstrates the improved power factor, i.e. reduced phase angle between voltage and current, thanks to injected reactive power. Figure 6.4(a) and (b) shows considerable phase reductions, by $7.5\,^\circ$ and $13.5\,^\circ$, respectively. Even an insensibly chosen small capacitor bank can change the upstream power factor: note the small phase angle reductions by $0.1\,^\circ$ and $1.5\,^\circ$ as depicted in Figure 6.4(c) and (d), respectively. This phenomenon can be clearly summarized by phase diagrams as shown in Figure 6.5. Improvement in power factor occurs only at PQM 1. In fact, we can frequently observe even a leading power factor near PQM 1. This leading power factor is not indicated in Figure 6.5. However, this leading power factor is true because

128

Table 6.1: Impedance functions at PQM 1 and 2 before and after capacitor bank switching

Z(s)	Before switching	After switching
$Z_1(s)$	$R_1 + R_2 + R_L + s(L_1 + L_2 + L_L)$	$\frac{G_3(s)}{G_1(s)} + sL_L + R_L$
$Z_2(s)$	$sL_L + R_L$	$sL_L + R_L$
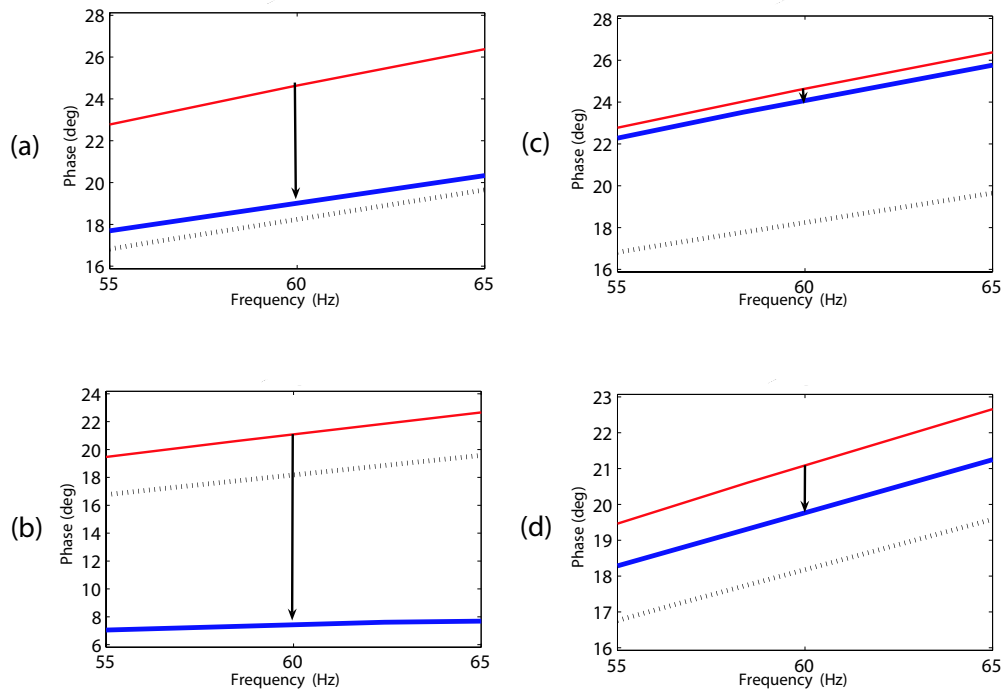
Figure 6.4: Bode phase plots of the resulting transfer functions for serving (a) 7MVA, (b) 3MVA 0.95 power factor load with 750kVar and (c) 7MVA, (d) 3MVA, 0.95 power factor load with 75kVar: Note that $Z_1(s)$ is a solid line before switching, but $Z_1(s)$ is a bold line after switching and $Z_2(s)$ is a dotted line. The levels of decreased phases are indicated by arrows.
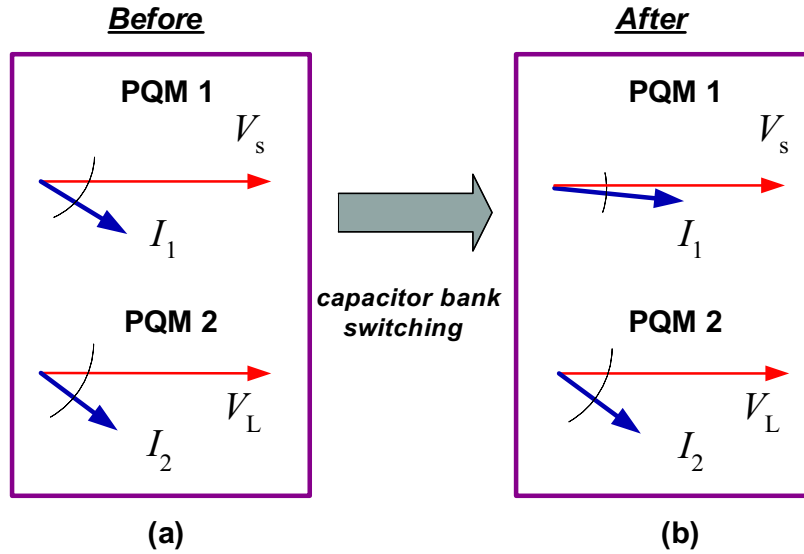
Figure 6.5: Change in the phase angle relationship between voltage and current waveforms before and after the capacitor bank energizing. Only PQM1 can detect the phase angle jump.

we are advised to inject larger reactive power than needed at the installation siting from a perspective of optimal sizing and siting of capacitor banks [6].

6.3.2 Algorithm 2 based on the initial signs of dv/dt and di/dt

The initial instantaneous change of voltage and current right after capacitor bank switching both at PQM 1 and 2 are analyzed in this section. Two approaches in s-domain and time-domain are provided. Applying the initial value theorem to the transfer functions in Eqs. (4.12), (4.13), and (4.14), one

can obtain the following results:

$$g_1(t_s^+) = \lim_{s \to \infty} sG_1(s) = \frac{1}{L_s + L_1},$$

$$g_2(t_s^+) = \lim_{s \to \infty} sG_2(s) = 0, \text{ and}$$

$$g_3(t_s^+) = \lim_{s \to \infty} sG_3(s) = 0.$$

Thus, immediately after a capacitor bank switching at $t = t_s$, the magnitude of $i_1(t)$ should be instantaneously increased with a gain of $\frac{1}{L_s + L_1}$ and those of $i_2(t)$ and $v_M(t)$ should be decreased toward zero, since $i_1(t_s^+) = v_{sc}(t_s^-)g_1(t_s^+)$, $i_2(t_s^+) = v_{sc}(t_s^-)g_2(t_s^+)$ and $v_M(t_s^+) = v_{sc}(t_s^-)g_3(t_s^+)$. Note that we are interested in voltage and current behaviors at the switching instant and thus this impulse response works effectively for determining the instantaneous current and voltage direction. Based on this analysis, it is clear that initial sign of di/dt is an important signature for determining the relative location of the capacitor bank.

An effective way to prove these initial behaviors of voltage and current is to obtain analytical equations in the time-domain and observe their behaviors graphically. As it is impossible to analyze those higher order functions of interest as shown in Eq. (6.1) through Eq. (6.4) in the time-domain, the system order reduction method, using Gramian-based input-output balancing [48] are applied to the above s-domain transfer functions. Numerical analysis using various real-world data [44] finds that we can reasonably express transfer functions in the prototype quadratic forms[2] as was done for drawing Bode plots in

---

[2]Note that the corresponding second order representation may vary according to our

131

the previous section. Thus, transfer functions can be reduced to the following forms without losing important system characteristics:

$$G_1(s) \approx \left(\frac{a_1 s^2 + b_1 s + c_1}{s^2 + 2\zeta\omega_n s + \omega_n^2} \right), \tag{6.8}$$

$$G_2(s) \approx \left(\frac{a_2 s^2 - b_2 s + c_2}{s^2 + 2\zeta\omega_n s + \omega_n^2} \right), \text{ and} \tag{6.9}$$

$$G_3(s) \approx \left(\frac{-a_3 s^2 + b_3 s + c_3}{s^2 + 2\zeta\omega_n s + \omega_n^2} \right) \tag{6.10}$$

where $a_{1,2,3}$, $b_{1,2,3}$, and $c_{1,2,3}$ are positive constants and ω_n and ζ are the resonant frequency and the system damping ratio, respectively. Note that $a_{1,2}$ of $G_{1,2}(s)$, are negligible compared with $b_{1,2}$ and $c_{1,2}$. $a_{1,2}$ do not appear under certain operating conditions. a_3 in $G_3(s)$ is also much smaller than b_3 and c_3 but a_3 should be kept to preserve the important transient characteristics of $G_3(s)$. However, it should be noted that these small constants can help transfer functions match for the original transfer functions more accurately. The following Figures 6.6 through 6.8 illustrate how closely the original transfer functions (solid lines) can be approximated by the reduced functions (bold lines).

Based on the Eqs. (6.3) through (6.5), the following order reduced voltage functions in s-domain can be obtained:

$$V_S(s) \approx V_{SC}(s) \left(\frac{f_1 s^2 + g_1 s + h_1}{s^2 + 2\zeta\omega_n s + \omega_n^2} \right) \tag{6.11}$$

$$V_M(s) \approx V_{SC}(s) \left(\frac{-f_2 s^2 + g_2 s + h_2}{s^2 + 2\zeta\omega_n s + \omega_n^2} \right) \tag{6.12}$$

---

state elimination method. However, this does not affect the general behavior of the resulting voltage and current waveforms.
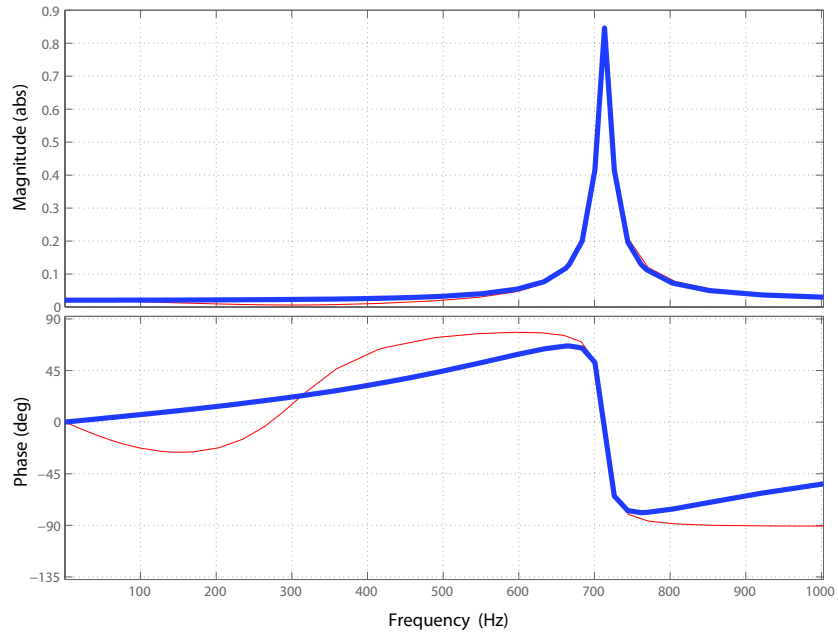
Figure 6.6: Bode plots of original $G_1(s)$ and reduced $G_1(s)$.
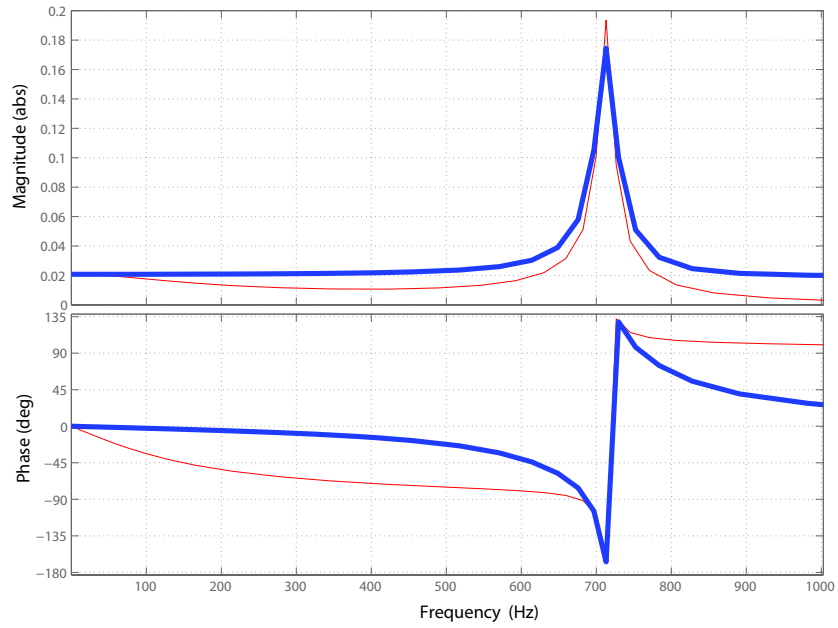
Figure 6.7: Bode plots of original $G_2(s)$ and reduced $G_2(s)$.

133
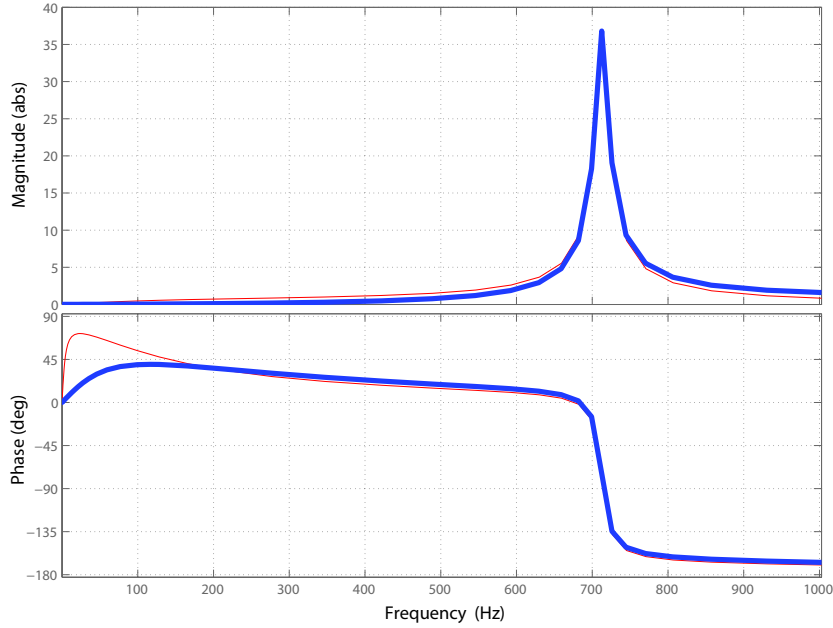
Figure 6.8: Bode plots of $G_3(s)$ and reduced $G_3(s)$.

where $f_{1,2}, g_{1,2}$, and $h_{1,2}$ are positive constants. $V_L(s)$ can be reduced to the same form as $V_M(s)$. Note that the magnitudes of $v_S(t)$ and $v_L(t)$ should be instantaneously decreased toward zero voltage right after capacitor bank energizing at $t = t_s$. Chapter 7 provides derivation and more descriptions on this property. Thus, initial instantaneous changes in voltage waveforms alone do not provide any directional signatures, since both of them move toward zero after switching. However, it should be noted that the direction of current right after switching depend on the sign of voltage at switching.

These s-domain representations can be easily transformed to the time-domain quantities as shown Eq. (6.13) where $\theta = \cos^{-1} \zeta$, $\eta = (1 - \zeta^2)$ and

134

the damped resonant frequency, $\omega_d = \omega_n\sqrt{\eta}$.

$$v_S(t) = \frac{v\left(t_s^-\right)}{\omega_d}\left[A(t) + B(t) + C(t)\right] \qquad (6.13)$$

where

$$A(t) = -f_1 e^{-\zeta\omega_n t}\sin\left(\omega_d t - \theta\right),$$

$$B(t) = g_1 e^{-\zeta\omega_n t}\sin\left(\omega_d t\right), \text{ and}$$

$$C(t) = h_1\frac{\eta - \sqrt{\eta}e^{-\zeta\omega_n t}\sin\left(\omega_d t + \theta\right)}{\omega_d}.$$

Note that $v_L(t)$ and $v_M(t)$ have the similar format as follows:

$$\frac{v\left(t_s^-\right)}{\omega_d}\left[-A(t) + B(t) + C(t)\right].$$

However, constant parameters, f_1, g_1 and h_1 should be replaced by the corresponding parameters of $v_L(t)$ and $v_M(t)$.

Since the transfer functions of $I_1(s)$ and $I_2(s)$ resemble those of voltage functions in a reduced form, $i_1(t)$ and $i_2(t)$ can also be represented in the same form as $v_S(t)$ and $v_L(t)$. However, care must be taken for assigning signs to the terms corresponding to $A(t)$, $B(t)$ and $C(t)$ above. Therefore, time-domain voltages and currents at PQM 1 and 2 can be drawn based on the system parameters used in Section 6.3.1. This time-domain studies confirm the analytical proof above and lead to the following conclusions.

If the the switched capacitor bank is physically downstream from PQM 1 and the CT of the PQM 1 points to the direction of the load current flow, the following is true:

135
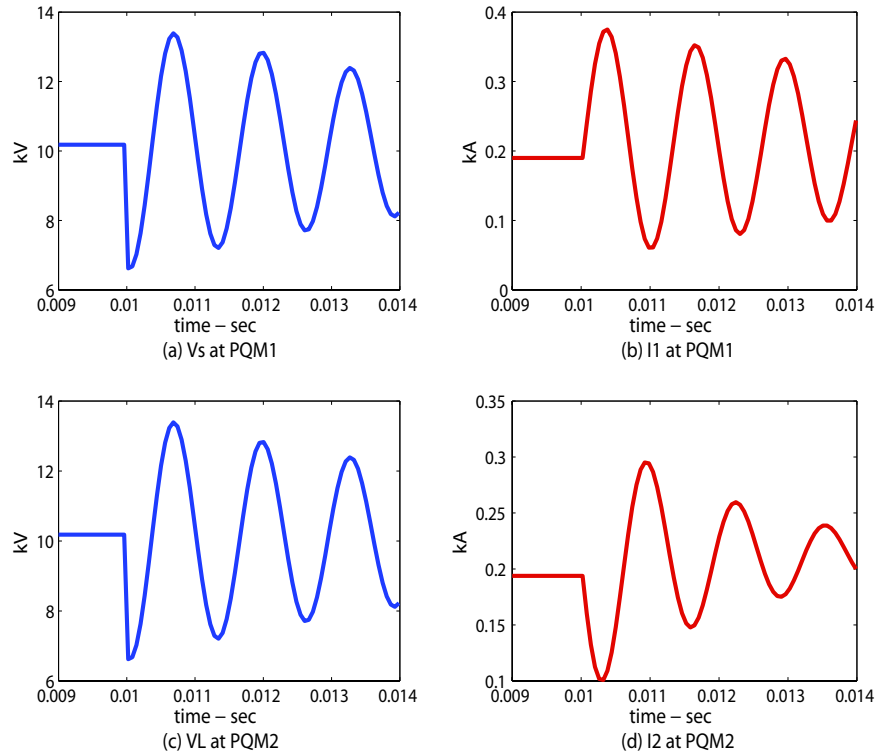
Figure 6.9: Voltage and current waveforms when the source voltage is positive. (a) Upstream voltage, (b) Upstream current, (c) Downstream voltage, (d) Downstream current.

1. When the gradient of voltage, $v_S(t)$ immediately after the switching instant (t_s) is negative, its corresponding gradient of current $i_1(t)$ will be positive (see Figure 6.9).

2. When the voltage gradient is positive, its corresponding gradient of current $i_1(t)$ will be negative (see Figure 6.10).

3. This means the voltage and current gradient immediately after the switching instant are opposites of each other.

136
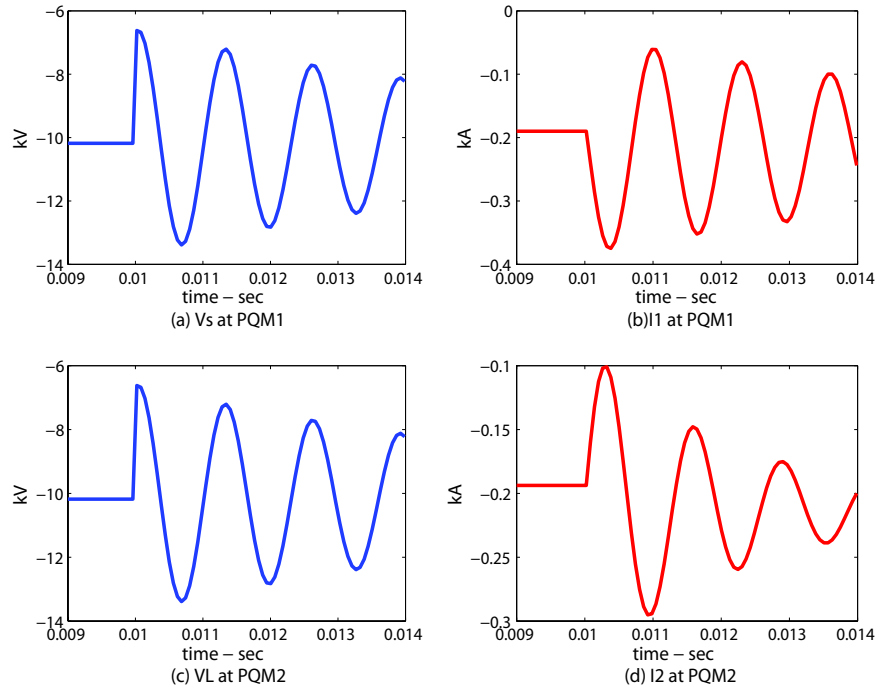
Figure 6.10: Voltage and current waveforms when the source voltage is negative.(a) Upstream voltage, (b) Upstream current, (c) Downstream voltage, (d) Downstream current.

If the the switched capacitor bank is physically upstream from PQM 2 and the CT of the PQM 2 points to the direction of the load current flow, the following is true:

1. When the gradient of voltage $v_L(t)$ immediately after the switching instant (t_s) is negative, its corresponding current gradient $i_2(t)$ will be also negative (see Figure 6.9).

2. When the voltage gradient $v_L(t)$ immediately after the switching instant (t_s) is positive, its corresponding current gradient $i_2(t)$ will be also pos-

137

itive (see Figure 6.10).

3. This indicates that the voltage and current gradient for a capacitor bank that is upstream from the PQ monitor is identical.

6.4 Evaluation and Applications

This section demonstrates the application of the proposed direction finding method. The efficacy of our method is validated first using a modified 12.47 kV IEEE power distribution test feeder [61] and then through actual PQ data.

6.4.1 Method validation through simulations

The modified IEEE test feeder is illustrated in Figure 6.11. Three selected cases are presented in this chapter:

- Case 1 considers energizing capacitor bank 1 only by temporarily removing capacitor bank 2 and line 2 under peak (7MVA) and moderate (4MVA) load conditions.

- Case 2 investigates switching of capacitor bank 2 while capacitor bank 1 was already energized under moderate load condition. Line 2 is still not energized.

- Case 3 considers powering nonlinear loads through line 2 as well. Capacitor bank 2 is switched while capacitor bank 1 was already energized

138
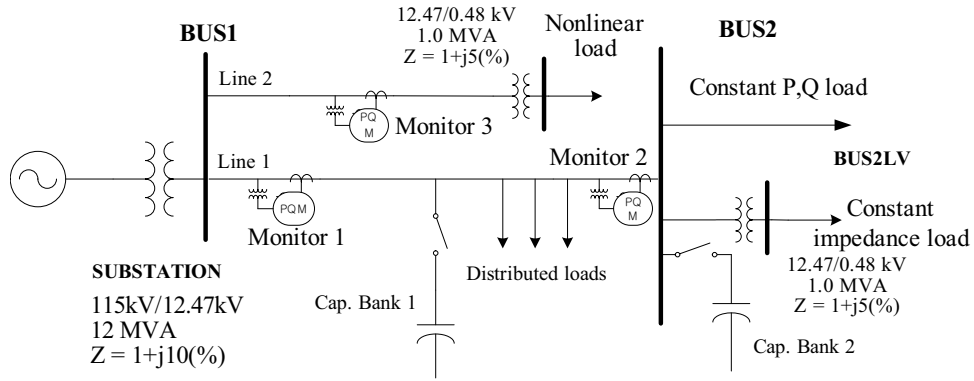
Figure 6.11: Modified IEEE distribution system test case with modification and two capacitor banks (1: 350kVar and 2: 100kVar).

under moderate load condition. Thus, measured data by PQM 3 is also studied in this case study.

As we can see in the resulting Tables 6.2 through 6.4, only PQM 1 sees the power factor improvement after capacitor bank 1 energizes. However, both PQM 1 and PQM 2 record power factor changes when the capacitor bank 2 is energized because both of them are upstream from capacitor bank 2. Even with severe harmonic currents flowing in the power system, as in Case 3, the result is consistent. PQM 1 and 2 can observe the power factor improvement but PQM 3 cannot, i.e. there is no phase angle jump between voltage and current at PQM 3 since PQM 3 is the only monitor downstream from capacitor bank 2. In addition to this power factor related signature, the polarities of voltage and current gradients immediately after the switching instant support our conclusions. As presented in Figures 6.12 through 6.14 obtained from Case 3, PQM 3 is the only one monitor where voltage and

139

Table 6.2: Phase angle differences in degree between voltage and current waveforms (Case 1): Capacitor Bank 1 is energized.

	PQM 1		PQM 2	
Load	Peak Load	Moderate Load	Peak Load	Moderate Load
Before	30.9°	30.5°	28.3°	26.6°
After	28.8°	24.1°	28.3°	26.6°

Table 6.3: Phase angle differences in degree between voltage and current waveforms (Case 2): Capacitor Bank 2 is energized.

	PQM 1	PQM 2
Before	25.6°	25.0°
After	21.0°	20.5°

current behave in the same direction right after capacitor bank switching. We can clearly observe opposite polarities of voltage and current at PQM 1 and 2 right after the switching instant.

6.4.2 Validation through actual measurement

A 1.8 Mvar capacitor bank (Bank 1) is energized in a close proximity to a bank that is already in service (Bank 2). The two banks are located in the middle of a distribution feeder and separated by approximately 2,500 feet.

Table 6.4: Phase angle differences in degree between voltage and current waveforms (Case 3): Capacitor Bank 2 is energized.

	PQM 1	PQM 2	PQM 3
Before	26.0°	25.0°	21.8°
After	21.6°	20.7°	21.8°

140
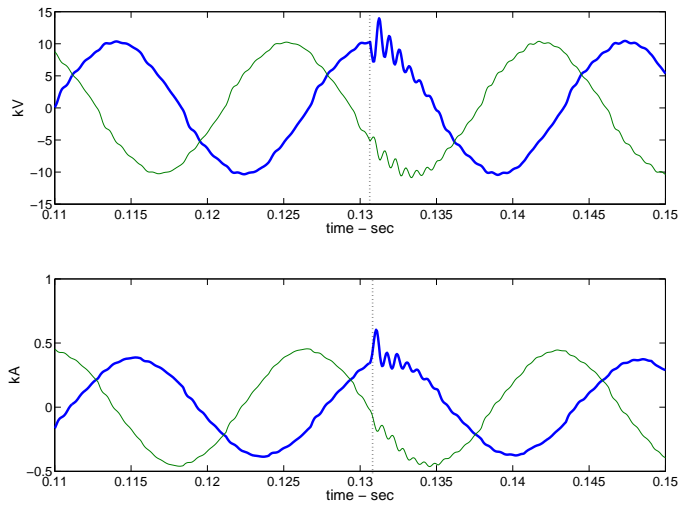
Figure 6.12: Voltage and current waveforms measured by PQM 1: Phase A (bold line), Phase C (solid line).
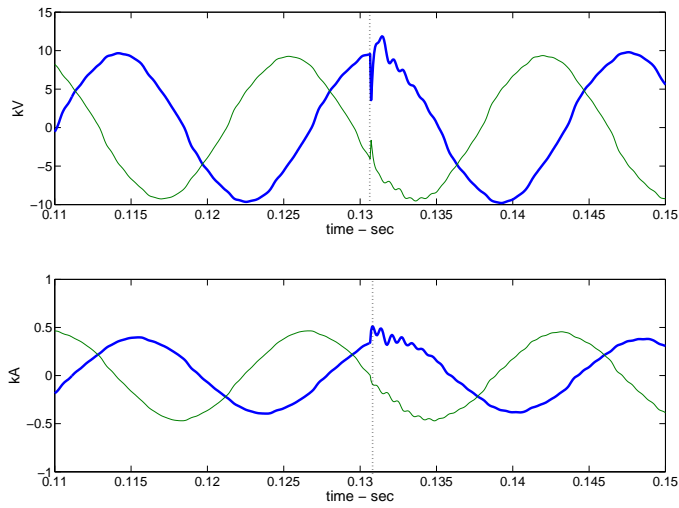
Figure 6.13: Voltage and current waveforms measured by PQM 2: Phase A (bold line), Phase C (solid line).

141
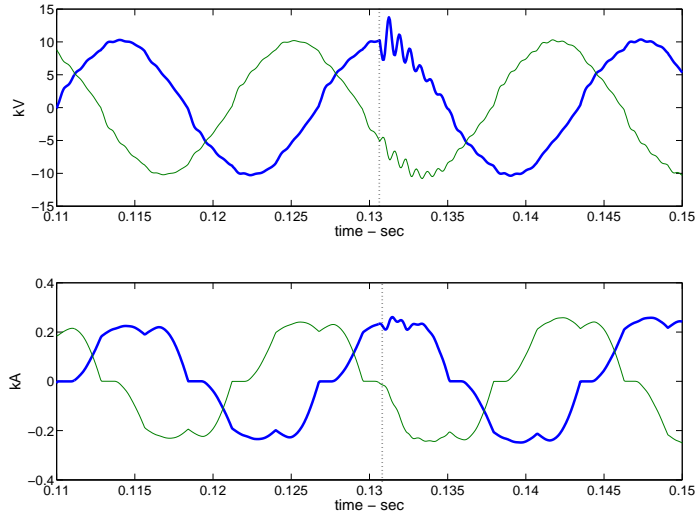
Figure 6.14: Voltage and current waveforms measured by PQM 3: Phase A (bold line), Phase C (solid line).

A power quality monitor is installed downstream from Bank 1 but upstream from Bank 2. Figure 6.15 illustrates the voltage and current waveforms. The reduced phase angle difference (from $17.3\,°$ to $2.2\,°$) between voltage and current after the capacitor bank switching indicates that the power factor of the line has been improved, which informs that the monitor is upstream from the capacitor bank. From this figure, it is also clear that the polarity of dv/dt is < 0, and the polarity of di/dt is > 0. This opposite polarity of voltage and current confirms that the switched capacitor bank is bank 1 because it is downstream from the monitor.

142
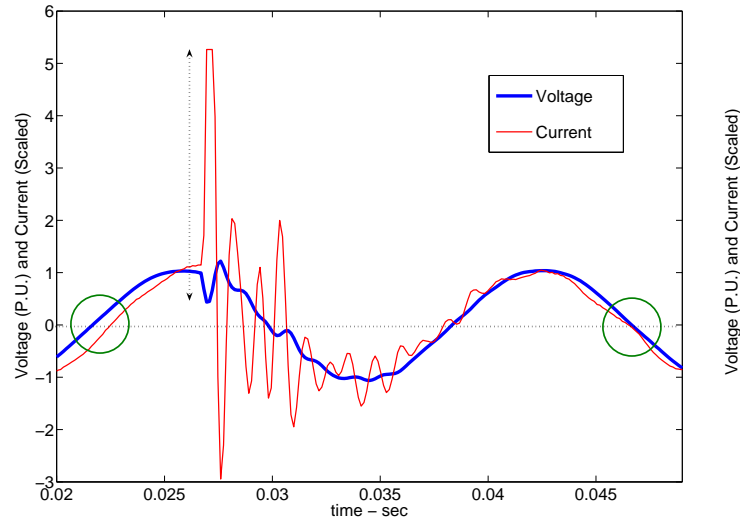
Figure 6.15: Voltage and current waveforms of an actual back-to-back capacitor switching event

6.5   Conclusion and Discussion

This chapter investigates two fundamental phenomena caused by the capacitor bank energizing: reactive power change (power factor change) occurring only on the upstream lines from the capacitor bank and the signs of initial voltage and current change right after the capacitor bank switching, i.e. those are opposite on the upstream lines and the same on the downstream lines. It has been demonstrated that we can use these physics to determine accurately the relative location of the switched capacitor bank for IEEE test cases and actual data. Our method implies an academic importance as well since it is based on the fundamental physics of the capacitor bank operation, which have been neglected in numerous previous studies. It is important to note that our

143

algorithm is far more practical than the other sophisticated signal processing-based techniques addressed because this easy-to-implement method does not impose any more computational burdens on the modern PQ monitoring devices: we use already built-in functionalities such as identification of capacitor switching event and conventional data acquisition and processing.

Chapter 7

Distance Estimation of Switched Capacitor Banks in Utility Distribution Feeders

This chapter describes an efficient and accurate technique for estimating the location of an energized capacitor bank downline from a monitoring equipment. The proposed technique is based on fundamental circuit theory and works with existing capacitor switching transient data of radial power distribution systems. Once the direction of a switched capacitor bank is found to be downstream from a power quality monitoring point, the feeder line reactance is estimated using the initial voltage change, which provides distance of the capacitor bank from the monitor based on the unit line reactance. The efficacy of the proposed technique is demonstrated with system data from IEEE test feeders modeled in a commercial time-domain modeling software package.

7.1 Introduction

Capacitor banks have long been used to provide voltage support and to correct displacement power factor on utility distribution systems. Due to their widespread applications, capacitor switching transients are the most common transient events on the power system, second only to voltage sag disturbances.

Capacitor switching operations are frequently correlated with problems such as nuisance tripping of adjustable speed drives, process controls, and any load that cannot tolerate sub-cycle overvoltage transients [2, 41]. Unfortunately, most utilities have very limited resources to identify these problems and correlate them with the capacitor switching operations. Moreover, among for those that have the capability, the switched capacitor bank involved in the problem cannot be determined since the necessary methodology is not available. In order to solve this problem, this chapter proposes and develops a smart algorithm capable of identifying which capacitor bank is switched by estimating the location of the capacitor bank on the distribution feeders. The proposed algorithm can also help diagnose capacitor problems, such as determining the exact bank having restrike problems, blown fuses, or can/unit failures [62].

There has been very little research done on this subject. However, a few relevant works are worth to mention. Parsons [58] investigated the disturbance energy flow during the transient period and the polarity of the initial peak of the disturbance power to find out the relative but not the exact location of the switched capacitor bank. Sochuliakova [63] presented an analytical expression of the position of a switched capacitor as a function of transient frequency. Unfortunately, this method does not lend itself to real-world applications as it needs to find eigenvalues from system dynamic equations established based on an assumption that all equivalent circuit elements, such as line inductance, resistance and capacitor bank size, and load levels, are already known. Furthermore, the interpretation of distance as a function of transient frequency

146

is ambiguous. Kim [59] applied a backward Kalman filter to find the location of a switched capacitor bank by estimating the voltage rise of capacitor bank. Unfortunately, this solution is also impractical to implement because it is based on the assumption that an exact power system dynamic model exists, which is not the case.

Unlike these efforts, this chapter proposes an analytical method for pinpointing the location of a switched capacitor bank using conventional power quality data, i.e., capacitor switching transient voltage waveforms. The proposed technique is developed based on the empirical observation that the degree of the initial voltage change due to capacitor energizing is determined by the distance between the monitoring location and the capacitor bank. Upon finding that the capacitor bank is downstream from the monitoring location [58, 64], our method estimates the feeder line impedance. This quantity is then utilized to estimate the location of the switched bank with respect to the monitoring location. This capability will be especially beneficial for substation power quality monitors since all switched capacitor banks are downstream from them. The chapter describes the scope of the problem in Section 7.2 and develops analytical expressions for the transient voltages at the promising monitoring locations followed by estimated distance in Section 7.3. The efficacy of the proposed technique is demonstrated using data from IEEE Test Feeder [44] modeled in PSCAD [45] in Sections 7.4 and 7.4.

7.2 Problem Description and Definition

Note that this chapter is developed based on the same nomenclature used in Chapters 4 and 6. This chapter adopts the one-line diagram and parameter definitions in these chapters.

7.2.1 Problem Description

Let us consider a one-line diagram shown in Figure 6.2 where a capacitor bank is energized and power quality monitoring devices are located on both sides of the capacitor bank. In this arrangement, the switched capacitor bank is downstream from PQM 1, but upstream from PQM 2. When a capacitor bank is energized, the oscillatory switching transient is captured by PQM 1 and 2. The problem addressed in this chapter can be stated as follows: Given voltage waveforms resulting from the capacitor energizing event, determine the distance (d_1), between PQM 1 and the switched capacitor bank. Note that the voltage waveforms captured by PQM 2 cannot be used to determine the distance (d_2) to the switched capacitor bank since it is upstream from the power quality monitor.

7.2.2 Scope of the Problem

In order to determine the distance (d_1), one must consider the characteristics of capacitor switching transients. It is obvious that these characteristics depend on the manner in which a capacitor is energized. Some capacitors - especially substation banks - are energized using synchronous closing controls,

pre-insertion inductors and resistors, and with inrush or outrush reactors. In this work, we only consider capacitor banks energized without any mechanism to reduce overvoltage transients and inrush currents. Switching transients without control mechanisms are more likely to cause power quality problems than those with control mechanisms. Switching without control mechanisms is representative of most banks in the majority of distribution feeders.

7.2.3 Hypothesis

In a normal capacitor bank energizing, the voltage across the capacitor at t_s^-, immediately prior to the energizing instant, is zero, i.e., the capacitor has no initial charge. Immediately after the energizing moment, t_s^+, the system voltage at the capacitor location is briefly pulled down to zero since the capacitor voltage cannot change instantaneously. The capacitor voltage then rises as the capacitor begins to charge toward the system voltage.

What is worth noting is that at the monitoring location PQM 1, the initial change in voltage will not reach completely to zero because of the impedance between PQM 1 and the switched capacitor. If the capacitor were moved closer to PQM 1, the voltage seen at PQM 1 at t_s^+ would be closer to zero. If PQM 1 were installed at the capacitor bank bus, the voltage seen at PQM 1 at t_s^+ would be zero. This observation suggests that the initial voltage change during the switching can be used to estimate the distance between PQM 1 and the capacitor location, d_1. Figure 7.1 illustrates the voltage waveform during the switching instant.

149
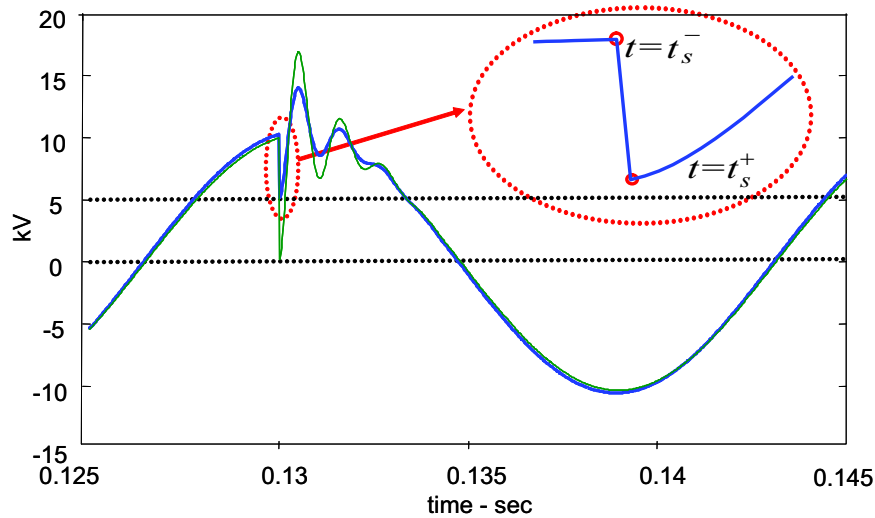
Figure 7.1: System voltage waveforms measured both at PQM 1 (bold line) and the capacitor location (solid line). The portion of the initial voltage change at PQM 1 is zoomed in to indicate key switching instants.

7.3   Estimation of Distance to a Switched Capacitor Bank

The distance estimate will be derived first without consideration of the loads and circuits downstream from the capacitor bank and with this consideration, respectively.

7.3.1   Distance Estimation: neglecting circuit and loads downstream from the switched capacitor bank

Let us begin the distance estimation without considering circuits and loads downstream from the capacitor bank. The voltage $v_S(t)$ measured by PQM 1 at the substation bus can be analytically determined by way of the s-domain representation. The s-domain representation of the substation voltage

150

$v_S(t)$ for $t \geq t_s^+$ is as follows:

$$V_S(s) = V_{sc}(s) \left\{ \frac{L_1 C s^2 + R_1 C s + 1}{(L_1 + L_s)C s^2 + (R_s + R_1) C s + 1} \right\} \tag{7.1}$$

$$\approx \frac{v_S(t_s^-)}{s} \left\{ \frac{L_1 C s^2 + R_1 C s + 1}{(L_1 + L_s)C s^2 + (R_s + R_1) C s + 1} \right\}$$

$$= \frac{v_S(t_s^-)}{s} - \frac{v_S(t_s^-)}{(L_1 + L_s)} \left\{ \frac{(L_s s + R_s)}{s^2 + \left(\frac{R_s + R_1}{L_s + L_1} \right) s + \frac{1}{(L_s + L_1)C}} \right\}$$

Note that $v_S(t_s^-)$ is the system voltage measured by PQM 1 immediately before the energization t_s and supersedes the source voltage, $v_{sc}(t_s^-)$, in Eq. (7.1) since the actual monitoring location is at PQM 1 and there should be a negligible voltage drop between them. The input source voltage is considered constant since the power system fundamental frequency is substantially lower than a typical capacitor switching frequency [26]. The above equation can be recast into a simple time-domain form since $V_S(s)$ can be interpreted as a transient response of a quadratic transfer function for a unit-step function [47]. The system voltage $v_S(t)$ measured by PQM 1 is

$$v_S(t) = v_S\left(t_s^-\right) - K v_S\left(t_s^-\right) e^{-\zeta \omega_n (t - t_s^+)} B(t) \tag{7.2}$$

where ω_n is the natural resonant frequency and ζ is the system damping ratio, i.e.,

$$\omega_n^2 = \frac{1}{(L_s + L_1)C}, \text{ or } f_n = \frac{1}{2\pi \sqrt{(L_s + L_1)C}} \tag{7.3}$$

$$2\zeta \omega_n = \frac{R_s + R_1}{L_s + L_1} \text{ or } \zeta = \frac{1}{2\omega_n} \left(\frac{R_s + R_1}{L_s + L_1} \right) \tag{7.4}$$

151

Parameter K, ω_d and $B(t)$ in Eq. (7.2) are defined as follows:

$$K = \frac{L_s}{L_1 + L_s}, \quad \omega_d = \omega_n \sqrt{(1 - \zeta^2)}, \quad \text{and}$$

$$B(t) = \left(\frac{\zeta}{\sqrt{(1 - \zeta^2)}} - \frac{1}{K} R_s C \frac{\omega_n}{\sqrt{(1 - \zeta^2)}} \right) \sin \left(\omega_d (t - t_s^+) \right) + \cos \left(\omega_d (t - t_s^+) \right).$$

The instantaneous voltage $v_S(t)$ measured by PQM 1 at the switching instant, t_s^+, can be obtained from Eq. (7.2). Therefore, $v_S(t_s^+)$ is as follows:

$$v_S(t_s^+) = \frac{L_1}{L_s + L_1} v_S(t_s^-) \tag{7.5}$$

It is important to keep in mind that $v_S(t_s^-)$ and $v_S(t_s^+)$ are the instantaneous voltages measured by PQM 1 immediately before and after the switching instant t_s as illustrated in Fig. 7.1 above. Voltage $v_S(t_s^+)$ cannot be zero since the switched capacitor bank is some distance away from PQM 1. This fact is exploited to estimate the distance between PQM 1 and the switched capacitor bank. Using Eq. (7.5), the distance to the switched bank can be estimated in terms of the line inductance, $\hat{L}_1 = d_1 L_u$:

$$\hat{L}_1 = \frac{|v_S(t_s^+)|}{|v_S(t_s^-) - v_S(t_s^+)|} L_s = \frac{|v_S(t_s^+)|}{\Delta v_{S,t_s}} L_s = \kappa L_s \tag{7.6}$$

The distance to the switched capacitor bank is then

$$d_1 = \frac{\hat{L}_1}{L_u} = \kappa \frac{L_s}{L_u} \tag{7.7}$$

From this result, it is obvious that estimating the distance requires only the voltage waveforms from PQM 1, the positive sequence line inductance in per

152

unit length, and the Thevenin equivalent source inductance. The first two parameters are usually readily available. The Thevenin equivalent inductance can be approximated from the leakage impedance of the substation transformer. It should be emphasized that voltage $v_S(t_s^-)$ is the system voltage without considering the loads and circuits downstream from the switched bank.

7.3.2 Distance estimation: including downstream circuit and loads

This section expands on the above analysis by considering circuits and loads downstream from the capacitor bank. Clearly, the addition of the downstream circuits and loads increases the complexity of the analysis considerably. Refer to Chapter 4 for derivation of voltages $V_S(s)$ at PQM 1, and $V_L(s)$ at PQM 2 in the s-domain. They are as follows:

$$
\begin{aligned}
V_S(s) &= \frac{V_S(s)}{\Delta} \left[\begin{array}{l} L_1(L_2 + L_L)Cs^3 + \{L_1(R_2 + R_L) + R_2(L_2 + L_L)\}Cs^2 + \cdots \\ \{CR_1(R_2 + R_L) + R_1 + R_2 + R_L\}s + R_1 + R_2 + R_L \end{array} \right] \\
&= \frac{V_S(s)}{\Delta} N(s) \tag{7.8}
\end{aligned}
$$

$$
V_L(s) = V_S(s)\frac{(L_L s + R_L)}{\Delta} \tag{7.9}
$$

where Δ is the characteristic function of the system, i.e.,

$$
\begin{aligned}
\Delta = &(L_s + L_1)(L_2 + L_L)Cs^3 + \\
&\{(L_s + L_1)(R_2 + R_L) + (L_2 + L_L)(R_s + R_1)\}Cs^2 + \\
&\{(R_s + R_1)(R_2 + R_L)C + (L_s + L_1 + L_2 + L_L)\}s + \\
&R_s + R_1 + R_2 + R_L
\end{aligned}
$$

and $V_S(s) = v_S(t_s^-)/s$

The s-domain representation of $V_S(s)$ and $V_L(s)$ is cumbersome to invert to the time-domain representation. Fortunately, the inverse transformation is not necessary, since we are interested only in the voltage magnitude at the switching instant t_s^+, i.e., $v_S(t_s^+)$ and $v_L(t_s^+)$. The initial-value theorem [47] is used to determine these voltage magnitudes. They are as follows:

$$v_S(t_s^+) = \lim_{s \to \infty} sV_S(s) = \frac{L_1}{L_s + L_1} v_S(t_s^-) \tag{7.10}$$

$$v_L(t_s^+) = \lim_{s \to \infty} sV_L(s) = 0 \tag{7.11}$$

The result given in Eq. (7.10) is identical to that in Eq. (7.5). It suggests that the system voltage seen at a monitoring location immediately after the switching instant $v_S(t_s^+)$ depends on the system voltage immediately before the switching instant, $v_S(t_s^-)$ and the Thevenin equivalent source inductance L_s. Therefore, the distance estimate is

$$d_1 = \frac{\hat{L}_1}{L_u} = \frac{|v_S(t_s^+)|}{\Delta v_{S,t_s}} \cdot \frac{L_s}{L_u} = \kappa \frac{L_s}{L_u} \tag{7.12}$$

This analytical result also applies to a more general case where significant capacitive loads or secondary capacitor banks should be considered. This capacitive components can be aggregately represented as a single fixed capacitor bank: suppose a secondary capacitor bank, C_2 installed in parallel with the load in Figure 6.2. Now the original capacitor bank is denoted as C_1. The following shows the dynamic equations for this case based on the same

154

conventions as used in Chapter 4:

$$\begin{bmatrix} \frac{di_1}{dt} \\ \frac{di_2}{dt} \\ \frac{di_L}{dt} \\ \frac{dv_M}{dt} \\ \frac{dv_L}{dt} \end{bmatrix} = \begin{bmatrix} -\frac{R_s+R_1}{L_s+L_1} & 0 & 0 & -\frac{1}{L_s+L_1} & 0 \\ 0 & -\frac{R_2}{L_2} & 0 & \frac{1}{L_2} & -\frac{1}{L_2} \\ 0 & 0 & -\frac{R_L}{L_L} & 0 & \frac{1}{L_L} \\ \frac{1}{C_1} & -\frac{1}{C_1} & 0 & 0 & 0 \\ 0 & \frac{1}{C_2} & -\frac{1}{C_2} & 0 & 0 \end{bmatrix} \begin{bmatrix} i_1(t) \\ i_2(t) \\ i_L(t) \\ v_M(t) \\ v_L(t) \end{bmatrix} + \frac{1}{L_s+L_1}\begin{bmatrix} 1 \\ 0 \\ 0 \\ 0 \\ 0 \end{bmatrix} v_{sc}(t)$$

Thus, transfer function can be represented as follows:

$$G(s) = \mathbf{C}(s\mathbf{I} - \mathbf{A})^{-1}\mathbf{B} = [G_1(s),\ G_2(s),\ G_3(s), G_4(s), G_5(s)]^T$$

The voltage at PQM 1 in s-domain becomes as follows:

$$V_S(s) = V_{sc}(s)\left\{G_1(s)(R_1 + sL_1) + G_4(s)\right\}$$

Note that the system state transition matrix $\mathbf{A}$ now becomes a 5×5 matrix and all of the derived equations become much more complicated than before. However, based on the initial value theorem discussed above, one can still prove the following relationship.

$$v_S(t_s^+) = \lim_{s \to \infty} sV_S(s) = \frac{L_1}{L_s + L_1}v_S(t_s^-)$$

Consequently, the same estimation equation in Eq. (7.12) is applicable to this case.

It should be noted that $v_S(t_s^-))$ and $v_S(t_s^+)$ in Eq. (7.10), and $v_S(t_s^-)$ and $v_S(t_s^+)$ in Eq. (7.5) are different since the former is the system voltage with loads, while the latter is the system voltage without loads. Furthermore, the result given in Eq. (7.10) should not be interpreted as meaning that the voltage $v_S(t_s^+)$ is independent of the system load. Voltage $v_S(t_s^+)$ indeed depends

155

on system loads since voltage, $v_S(t_s^-)$, immediately before the switching is load dependent. However, κ in Eq. (7.6) is independent of loads and circuits downstream from the capacitor bank because is the ratio of estimated L_1 and L_s, and therefore it must be a constant.

It is interesting to note that the instantaneous voltage captured at PQM 2 immediately after the switching instant, $v_L(t_s^+)$ is zero. This is indeed expected since at the system voltage at the capacitor bank at the switching instant is zero (assuming the voltage has no initial charge). This phenomenon is equivalent to having an instantaneous short circuit condition. Therefore, the system voltage downstream from the capacitor bank location is zero at the energizing instant. Given this fact, the voltage measurement from PQM 2 - which is downstream from the switched capacitor bank - cannot be used to estimate distance to the bank. However, it can be used to determine the relative location of the capacitor bank from the PQ monitor.

7.4   Implementation and Practical Considerations

The implementation of the proposed estimation technique is illustrated in Fig. 7.2 below. The implementation begins with an existing power quality database or a real-time power quality data stream as used in web-based monitoring devices. Since typical PQ monitors capture a wide range of disturbance events, a separate algorithm is needed to identify capacitor switching event data from other PQ data. The identification of capacitor switching transient waveforms can be done visually or automatically [62]. Once a single event of
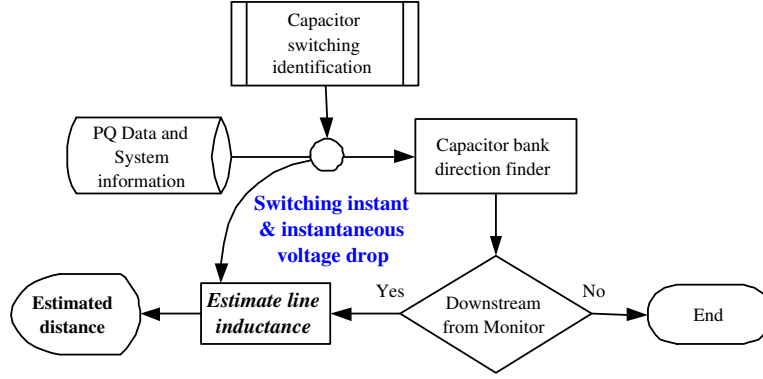
Figure 7.2: Data flow and process diagram of an energized capacitor bank distance estimation.

capacitor switching transient data (three phase voltage and current waveforms) is identified, transient portions of voltage waveforms are extracted. Wavelet transform techniques can be used effectively to determine the exact switching instant. The relative location of the bank is determined using a method described in [64]. If the capacitor bank is downstream from the power quality monitor, the distance to the capacitor bank is then estimated using Eqs. (7.6) and (7.7). The efficacy of the proposed algorithm will be demonstrated in the following section. For practical applications, it is recommended that the distance estimation be performed using waveforms from all three phases and the resulting distance estimates be investigated. One simple way to determine the final distance estimate is to take an arithmetic average or median of the distance estimates. However, care should be taken since the magnitude of the initial voltage change Δ_{v_s,t_s} is a function of the switching instant as illustrated in Fig. 7.3 below. For example, if the switching instant occurs at the peak voltage, the initial voltage change Δ_{v_s,t_s} will be large. On the other hand, if the

157
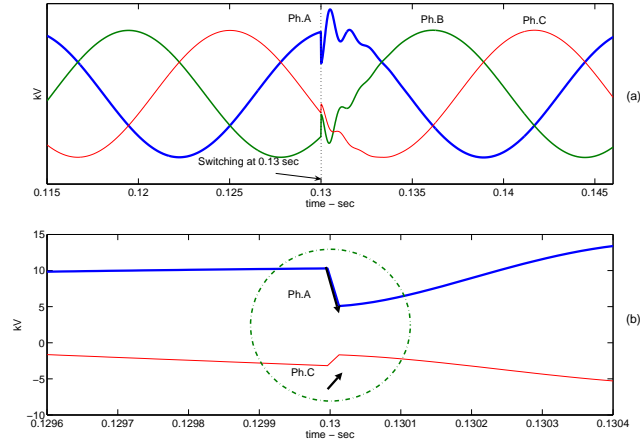
Figure 7.3: Voltage waveforms measured by PQM 1for a moderately loaded system (a) and zoomed-in phase A and C voltage waveforms around switching instant(b): The Δ_{v_s,t_s} of phase C voltage is much smaller than those of phase A and B voltages.

switching instant is close to the zero voltage, Δ_{v_s,t_s} will be small. Therefore, a simple arithmetic averaging does not always produce an overall good estimate. A more accurate result can be accomplished by taking an arithmetic average of only estimates that are close to one another. This approach is applied in Section 7.5.

7.5 Validation and Applications

This section demonstrates the application of the distance estimation method using the IEEE power distribution test feeder [44,61] as illustrated in Figure 7.4. The test system is a 12.47 kV radial distribution system served by a 12 MVA 115/12.47 kV delta-Yg transformer. The Thevenin equiva-

158

lent impedance is essentially due to the transformer leakage impedance, i.e., $Z(\%) = 1 + j10$ on a 12 MVA base. Thus, the equivalent source inductance L_s would be 3.4372 mH. The evaluation of distance estimates is carried out with unbalanced $[Z_{012}]_{UB}$ (Ω/mi) and balanced $[Z_{012}]_B$ (Ω/mi) feeder conditions. Their sequence impedance matrices in ohms per mile [61] are as follows:

$$[Z_{012}]_{UB} = \begin{bmatrix} 0.7737 + \text{j}1.9078 & 0.0072 - \text{j}0.0100 & -0.0123 - \text{j}0.0012 \\ -0.0123 - \text{j}0.0012 & 0.3061 + \text{j}0.6334 & -0.0488 + \text{j}0.0281 \\ 0.0072 - \text{j}0.0100 & 0.0487 + \text{j}0.0283 & 0.3061 + \text{j}0.6334 \end{bmatrix},$$

$$[Z_{012}]_B = \begin{bmatrix} 0.7737 + \text{j}1.9078 & 0 & 0 \\ 0 & 0.3061 + \text{j}0.6333 & 0 \\ 0 & 0 & 0.3061 + \text{j}0.6334 \end{bmatrix}$$

and

$$[C]\,(\mu F/\text{mi.}) = \begin{bmatrix} 0.0145 & -0.0037 & -0.0037 \\ -0.0037 & 0.0156 & -0.0018 \\ -0.0037 & -0.0018 & 0.0145 \end{bmatrix}$$

In many cases, shunt admittances of overhead lines are neglected in modeling and analyzing a power distribution system, since the distribution lines are relatively short [5]. Thus, this shunt admittance was not be considered in the following application studies. However, we will discuss the impact of line charging capacitance on the estimation accuracy of the proposed method based on our numerous simulation results while evaluating the overall performance of the proposed method.

The positive sequence line inductance per mile, L_u, for both balanced and unbalanced feeders is 1.6801 mH/mi. Distributed loads are modeled as a combination of fixed impedance and complex constant power loads. They are connected at the 12.47 kV as well as at the 0.48 kV level through a 1
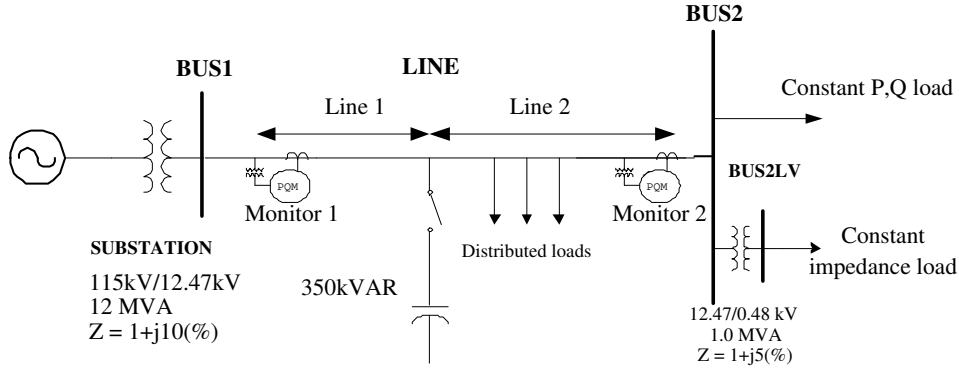
Figure 7.4: IEEE distribution system test case with modification and additional capacitor bank.

MVA service transformer ($Z(\%) = 1 + j5$). A 350 kVar switched three phase capacitor bank is located d_1 miles on the feeder. Two PQ monitors are installed both at the BUS 1 (substation) and BUS 2. The efficacy of the proposed technique is evaluated under the following conditions: (A) ignore loads and circuits downstream from the switched capacitor bank, (B) include loads and circuits downstream from the bank and vary the loading conditions when all loads and lines are assumed balanced, (C) evaluate the same system as in (B), however, loads and lines are unbalanced.

7.5.1 Evaluation Cases with Downstream Loads and Circuits Excluded

In this section, loads and circuits downstream from the capacitor bank are excluded from the simulation model. The distance estimation technique is evaluated for both a balanced and unbalanced feeder. The estimated distances are compared and summarized in Table 7.1 (for $d_1 = 2$ miles) and Table 7.2

160

Table 7.1: Estimation results for a case with d_1=2 mi. for various sampling rates.

		256 samples/cycle	512 samples/cycle	1024 samples/cycle
$v_{abc}(t_s^-)$	B	10.17, -4.61, -5.55	10.16, -4.49, -5.66	10.16, -4.47, -5.68
(kV)	U	10.17, -4.61, -5.55	10.16, -4.50, -5.66	10.16, -4.50, -5.66
$v_{abc}(t_s^+)$	B	5.41, -2.35, -3.07	5.13, -2.22,-2.91	5.05,-2.20,-2.85
(kV)	U	5.88, -2.46, -3.44	5.33, -2.18,-3.18	5.18,-2.13,-3.08
κ	B	1.09	1.00	0.98
(ratio)	U	1.25	1.11	1.04
d_1	B	2.23	2.04	2.00
(mile)	U	2.68	2.26	2.13

(for $d_1 = 3$ miles). Note that B and UB denote balanced and unbalanced lines, respectively. Tables 7.1 and 7.2 present the following:

- voltage measurements immediately before and after the switching instants for all phases, i.e., $v_{abc}(t_s^-)$ and $v_{abc}(t_s^+)$ in peak voltage, respectively,

- average κ value from Eq. (7.6), and distance estimate for varying sampling rates of 256, 512, and 1024 samples/cycle.

Note that capacitor switching occurs at the peak of phase A voltage.

The above results show the proposed technique provide reasonably accurate estimates of distance to the capacitor bank even when the sampling rate is only 256 samples/cycle for both balanced and unbalanced lines. However, as expected, the results of the unbalanced lines are not as good as those of

161

Table 7.2: Estimation results for a case with d_1=3 mi. for various sampling rates.

		256 samples/cycle	512 samples/cycle	1024 samples/cycle
$v_{abc}(t_s^-)$	B	10.17, -4.61, -5.55	10.16, -4.50,-5.66	10.16, -4.47, -5.68
(kV)	U	10.17, -4.61, -5.55	10.16, -4.50, -5.66	10.16, -4.50, -5.66
$v_{abc}(t_s^+)$	B	6.30,-2.73, -3.57	6.30,-2.73, -3.57	6.06,-2.64,-3.42
(kV)	U	6.63, -2.78, -3.88	6.27, -2.59,-3.71	6.18,-2.57,-3.63
κ	B	1.54	1.46	1.46
(ratio)	U	1.69	1.63	1.56
d_1	B	3.15	3.00	3.00
(mile)	U	3.62	3.31	3.18

the balanced lines since the proposed method basically neglects the unbalance mutual coupling between sequence components. It is also clear that the accuracy of the distance estimates is influenced by the sampling rate. A higher sampling rate provides a more precise voltage measurement immediately after the switching, thus yielding a more accurate distance estimate. Doubling or quadrupling the sampling rate significantly improves the distance estimation. Note the perfect estimation results for balanced 2 and 3-mile lines when the sampling rate is increased to 1024 samples/cycle. However, in practise, careful measures should be also taken to remove the high frequency noisy signals mainly arising from the shunt capacitance of the feeder lines. The higher the sampling rate, the more complicated this filtering. This will be a drawback of increasing the sampling rate.

It is worthwhile to note that a precise estimation of the line inductance is critical for an accurate estimation of the distance to the switched capacitor bank. By using Eq. (7.6), the estimated total line inductances are 3.40 and 5.08 mH, respectively. These values are very close to the theoretical values. The actual line inductance per mile, L_u is equal to 1.6801 mH. Thus, $L_1(= L_u \cdot d_1)$ values should be 3.360 mH for $d_1 = 2$ miles and 5.04 mH for $d_1 = 3$ miles. The resulting κ values, i.e. L_1/L_s are found to be 0.98 and 1.46, respectively, and are identical to the estimated values as well. The line inductance estimates can also be verified by computing the inductance from the measured capacitor switching frequency, f_n of Eq. (7.3). Obviously, the capacitance of the bank must be known to verify the value of L_1.

The above results also demonstrate that our hypothesis stated in Section 7.2.3, that the initial change of voltage during the switching can be used to estimate the distance between the monitoring and the capacitor location, is true.

7.5.2   Evaluation Cases for Balanced lines and Balanced loads

In this section, loads and circuits downstream from the capacitor bank are included in the simulation and they are balanced. The proposed technique is applied to estimates distance d_1 under moderate and peak loading conditions. Note that capacitor switching is not modeled to occur exactly at the voltage peak of phase A, i.e. several milliseconds prior to the exact switching time in order to investigate more generic situations. The tap changers for both

163

transformers are set to 1.05 to resolve voltage regulation problem in these case studies. Also, note that phase C voltage is eventually disregarded in finding the distance as it results in the smallest Δ_{v_s,t_s} in Cases 7.5.2 and 7.5.3.

7.5.2.1 Moderate load condition: 3 MVA, power factor: 0.93

The system loading condition is modeled such that the apparent power measured by PQM 1 is about 3 MVA with lagging 0.93 pf. Analysis using data measured by PQM 1 around the capacitor switching leads to estimation results presented in the following Tables 7.3 through 7.6. Although the estimates with a sampling rate of 256 samples/cycle are not as accurate as those of Section 7.5.1, they converge to the theoretical values as the sampling rate increases. Damping from the loads and capacitor switching at non-peak voltage value may account for these numerical errors, especially when the sampling rate is not sufficient to pinpoint the instantaneous voltage change. Similar results are obtained for 2-mile and 3-mile cases. It is observed that the d_2 can affect the estimation results by changing the degree of system damping. Note that the κ values are almost identical to actual values, which confirms our previous assertion that κ in Eq. (7.6) is independent of loads and circuits downstream from the capacitor bank.

7.5.2.2 Peak load condition: 8 MVA, power factor: 0.89

The system loading condition is modeled such that the apparent power measured by PQM 1 is about 8MVA with a lagging 0.89 pf. One can observe

164

Table 7.3: Estimation results under a moderate load condition with $d_1 = 2$ mi.and $d_2 = 4$ mi. for various sampling rates.

	256 samples/cycle	512 samples/cycle	1024 samples/cycle
$v_{abc}(t_s^-)$(kV)	10.25, -7.29, -2.96	10.28, -7.19, -3.08	10.30, -7.12, -3.18
$v_{abc}(t_s^+)$(kV)	6.22, -4.24, -1.98	5.35, -3.61, -1.74	5.08, -3.41, -1.67
κ(ratio)	1.47	1.04	1.00
d_1(mile)	3.01	2.14	2.05

Table 7.4: Estimation results under a moderate load condition with $d_1 = 2$ mi. and $d_2 = 2$ mi. for various sampling rates.

	256 samples/cycle	512 samples/cycle	1024 samples/cycle
$v_{abc}(t_s^-)$(kV)	10.25, -7.29, -2.96	10.28, -7.19, -3.08	10.30, -7.12, -3.18
$v_{abc}(t_s^+)$(kV)	6.43, -4.39, -2.04	5.45,-3.68,-1.77	5.12, -3.43, -1.69
κ(ratio)	1.59	1.09	0.96
d_1(mile)	3.25	2.23	1.96

Table 7.5: Estimation results under a moderate load condition with $d_1 = 3$ mi. and $d_2 = 4$ mi. for various sampling rates.

	256 samples/cycle	512 samples/cycle	1024 samples/cycle
$v_{abc}(t_s^-)$(kV)	10.24, -7.28, -2.96	10.27, -7.19,-3.08	10.29, -7.12, -3.17
$v_{abc}(t_s^+)$(kV)	6.95,-4.72, -2.23	6.31,-4.26,-2.05	6.12,-4.10,-2.02
κ(ratio)	1.97	1.52	1.43
d_1(mile)	4.01	3.12	2.91

Table 7.6: Estimation results under a moderate load condition with $d_1 = 3$ mi. and $d_2 = 2$ mi. for various sampling rates.

	256 samples/cycle	512 samples/cycle	1024 samples/cycle
$v_{abc}(t_s^-)$(kV)	10.25, -7.29, -2.96	10.28, -7.19,-3.09	10.30, -7.12, -3.18
$v_{abc}(t_s^+)$(kV)	7.12,-4.84, -2.28	6.40,-4.32,-2.08	6.15,-4.12,-2.03
κ(ratio)	2.12	1.56	1.43
d_1(mile)	4.30	3.22	2.92

Table 7.7: Estimation results under a peak load condition with $d_1 = 2$ mi. and $d_2 = 4$ mi. for various sampling rates.

	512 samples/cycle	1024 samples/cycle	2048 samples/cycle
$v_{abc}(t_s^-)$(kV)	9.87, -7.25,-2.63	9.90, -7.18, -2.72	9.90, -7.18, -2.72
$v_{abc}(t_s^+)$(kV)	5.57, -3.68, -1.77	5.19, -3.54, -1.65	5.08, -3.47, -1.61
κ(ratio)	1.21	1.04	0.99
d_1(mile)	2.48	2.13	2.03

that the estimation results presented in Tables 7.7 and 7.8 converge to actual values. However, estimates under moderate loading conditions are more satisfactory because we need approximately twice the sampling rate to obtain the results comparable to those of moderate loading condition. This is because initial voltage change is so instantaneous due to the higher damping influence of the heavy loads that PQM 1 cannot pinpoint exact voltage values at the very switching instant. Nevertheless, the estimates eventually converge to the actual distance of 2 miles as the sampling rate increases. This is also confirmed by the resulting κ values, which are close to the actual values. It

166

Table 7.8: Estimation results under a peak load condition with $d_1 = 2$ mi. and $d_2 = 2$ mi. for various sampling rates.

	512 samples/cycle	1024 samples/cycle	2048 samples/cycle
$v_{abc}(t_s^-)$(kV)	9.90, -7.27, -2.64	9.93, -7.20, -2.73	9.93, -7.20, -2.73
$v_{abc}(t_s^+)$(kV)	5.86, -4.06, -1.80	5.33, -3.64, -1.69	5.13, -3.50, -1.63
κ	1.36	1.09	1.01
d_1(mile)	2.78	2.23	2.07

is also found that changing size and configuration of the capacitor bank does not significantly affect the overall estimation results via numerous simulation studies. Capacitor banks of 500kVar and 750kVar are tested and lead to very similar estimation results. The configuration of the capacitor bank is changed from Yg to delta. Although the delta configuration for the same kVar size causes faster transients than the Yg configuration, which may affect the data reading, the resulting trend for various sampling rates is still the same as that of the Yg configuration and provides good estimated distances. As discussed in Section 7.3.2, adding a secondary capacitor bank (irrespective of its size) in parallel with the loads does affect the overall result, either based on our investigation.

7.5.3 Evaluation Cases for Unbalanced lines and Unbalanced loads

In this case study, the original phase impedance matrix is used and all of the constant PQ loads are modified to be unbalanced. Both moderate and peak loading conditions are investigated. Line lengths are also adjusted to

Table 7.9: Estimation results under a moderate load condition with $d_1 = 2$ mi. and $d_2 = 4$ mi. for various sampling rates.

	256 samples/cycle	512 samples/cycle	1024 samples/cycle
$v_{abc}(t_s^-)$(kV)	10.21, -7.27, -2.91	10.24, -7.17,-3.04	10.26, -7.10, -3.13
$v_{abc}(t_s^+)$(kV)	6.24,-4.13, -2.11	5.39,-3.47,-1.94	5.13,-3.26,-1.90
κ(ratio)	1.44	1.02	0.93
d_1(mile)	3.08	2.19	1.97

Table 7.10: Estimation results under a moderate load condition with $d_1 = 2$ mi. and $d_2 = 2$ mi. for various sampling rates.

	256 samples/cycle	512 samples/cycle	1024 samples/cycle
$v_{abc}(t_s^-)$(kV)	10.22, -7.27, -2.92	10.25, -7.17,-3.05	10.27, -7.10, -3.14
$v_{abc}(t_s^+)$(kV)	6.43,-4.25, -2.18	5.49,-3.54,-1.96	5.16,-3.28,-1.91
κ(ratio)	1.55	1.06	0.94
d_1(mile)	3.54	2.27	2.00

study the impact of line impedance on the results. The degree of unbalance is described by the NEMA definition of voltage unbalance, given as follows [5]:

$$V_{unbalance} = \frac{|Maximum\ deviation\ from\ the\ average|}{|V_{average}|} \cdot 100(\%)$$

7.5.3.1   Moderate load condition: 3MVA, power factor: 0.92

Under moderate loading conditions, the system load is about 3MVA with 0.92 lagging pf and $V_{unbalance}$ is approximately 0.5%.

Tables 7.9 through 7.11 describe the estimation results when the PQM1

Table 7.11: Estimation results under a moderate load condition with $d_1 = 3$ mi. and $d_2 = 2$ mi. for various sampling rates.

	256 samples/cycle	512 samples/cycle	1024 samples/cycle
$v_{abc}(t_s^-)$(kV)	10.22, -7.27, -2.92	10.25, -7.17,-3.04	10.27, -7.10, -3.13
$v_{abc}(t_s^+)$(kV)	7.13,-4.70, -2.42	6.43,-4.17,-2.27	6.20,-3.97,-2.24
κ(ratio)	2.07	1.54	1.39
d_1(mile)	4.43	3.29	2.98

Table 7.12: Estimation results under a peak load condition with $d_1 = 2$ mi. and $d_2 = 2$ mi. for various sampling rates.

	512 samples/cycle	1024 samples/cycle	2048 samples/cycle
$v_{abc}(t_s^-)$(kV)	9.87, -7.28,-2.56	9.92, -7.21, -2.65	9.92, -7.21, -2.65
$v_{abc}(t_s^+)$(kV)	5.89, -3.94, -1.95	5.37, -3.49, -1.89	5.19, -3.34, -1.85
κ(ratio)	1.21	1.06	0.99
d_1(mile)	2.83	2.26	2.09

is 2 and 3 miles away. As the sampling rate increases, the estimated distances move toward the actual distances. However, as expected, numerical discrepancies from the actual distance at each sampling rate are bigger than those of the balanced cases. Note that calculated κ values deviate slightly from those of previous cases due to the increased voltage unbalance (%) of the unbalanced feeder lines.

Table 7.13: Estimation results under a peak load condition with $d_1 = 3$ mi. and $d_2 = 2$ mi. for various sampling rates.

	512 samples/cycle	1024 samples/cycle	2048 samples/cycle
$v_{abc}(t_s^-)$(kV)	9.89, -7.21,-2.63	9.92, -7.21, -2.65	9.89, -7.20, -2.64
$v_{abc}(t_s^+)$(kV)	6.38, -4.17, -2.20	6.24, -4.06, -2.17	6.19, -4.02, -2.16
κ(ratio)	1.64	1.50	1.47
d_1(mile)	3.41	3.20	3.14

7.5.3.2   Peak loading condition: 8.2 MVA, power factor: 0.87

Under peak loading conditions, the load of about 8.2 MVA, 0.87 lagging power factor is served and $V_{unbalance}$ is calculated to be about 1.5%. As in the case study B, the sampling rate must be doubled to obtain the comparable results to those of moderate loading condition. Thus, the sampling rate starts at 512 samples/cycle in Tables 7.12 and 7.13. However, the distances become close to the theoretical values eventually as the sampling rate is doubled.

Overall performance of the proposed algorithm is quite satisfactory for all of case studies as the estimated distances are very close to the actual values. However, the numerical errors are noticeable when the test system consists of unbalanced three phase lines and is operating under heavy loading conditions. It is also observed that the switching instant can affect the estimation results. Capacitor switching at a peak voltage has a lower chance of producing an outlier from the good estimates that may mislead our final evaluation since the other two phases would theoretically be very close to each other at the

switching instant and would provide consistent analysis results.

The gentle curvature of the sinusoidal voltage wave around its peak also supports the accurate sampling of the data, which was confirmed during our study as better performance was achieved by approximately 10 to 30% for cases studies with the sampling rate of 256 samples/cycle.

Numerous simulation studies were conducted to investigate the impact of line charging capacitance on the estimation accuracy. The simulation studies show that the influence of line-charging capacitance is negligible since the discrepancies between the estimated and actual distance is less than 5%. Therefore, in real-world applications, line-charging capacitance can be omitted without appreciable errors.

When a capacitor bank is energized through three single-phase mechanical oil switches, there will be three distinct transients corresponding to each individual pole closing. Typically all phases close within 5 cycles [65]. The first pole closing pushes the system into the most unbalanced state during the capacitor energizing since the other two poles are not closed yet. However, the system is reasonably balanced during the last pole closing since the other two poles are already in. The transient resulting from the last pole closing is used to estimate the distance between the capacitor bank and the monitoring instrument. Table 7.14 illustrates the distance estimates during three independent pole closing for balanced and unbalanced lines. The sampling rate of the transient waveform is 512 samples/cycle. The estimates are compared to those of three-phase pole closing with balanced and unbalanced lines shown in

171

Table 7.14: Estimation results under a moderate load condition with $d_1 = 3$ mi. and $d_2 = 2$ mi. with the sampling rate of 512 samples/cycle

	Balanced lines	Unbalanced lines
$v_{abc}(t_s^-)$(kV)	10.28, 10.54, **10.48**	10.25, 10.57, **10.43**
$v_{abc}(t_s^+)$(kV)	7.32, 7.19, **6.97**	7.33, 7.07, **7.04**
d_1(mile)	5.10, 4.73, **3.73**	5.10, 4.44, **3.69**

Tables 7.6 and 7.11, respectively. The comparison results are given as follows (independent pole closing vs. three-phase pole closing), (3.73 mi. vs. 3.22 mi.) and (3.69 mi. and 3.29 mi.) for balanced and unbalanced lines, respectively. It is clear that independent pole closing causes errors in the distance estimates. However, they are worse off by about 12% and 15%. The estimate error can be reduced by using a higher sampling rate.

7.6 Conclusion and Summary

In this chapter, an efficient and accurate methodology is presented for estimating the exact distance of a downstream energized capacitor bank from a monitoring location. This is the first analytical study of the initial voltage change due to an energized capacitor bank associated with locating an energized capacitor bank. The efficacy of the method is validated using an IEEE test model under various operation scenarios by changing the line distances, loading conditions, capacitor bank size, and configuration. It is demonstrated that the distance estimates are identical or almost identical to theoretical distances for all of the case studies. The accuracy of the proposed method depends

on the sampling rate of the waveform. In general, the higher sampling rate, the more accurate results the algorithm will be able to provide. The proposed method can be applied to existing power quality monitor with a sampling rate of 256 samples/cycle. On-going advances in power quality monitoring technology with improved data acquisition capability will allow very precise distance estimation.

Chapter 8

Conclusion

This dissertation is devoted to the development of new, practical methodologies for characterizing power system response and for locating the switched capacitor banks. In keeping with a realistic approach, conventional power quality data, either real-time or stored in databases, are the only required input for these algorithms. In this chapter, the main ideas and contributions of the developed methodologies are summarized in terms of approaches, benefits, and future research opportunities.

8.1 Summary

Other than the benefits to increase the value of collected data, the proposed algorithms are shown to provide the novel contributions to the area of system harmonic assessment with regard to the following technical aspects:

8.1.1 Algorithm for Estimating Parallel Resonant Frequencies

This dissertation proposed a practical algorithm for estimating system parallel resonant frequencies using only capacitor switching transient data. Expanded from the previous research, the proposed method can suppress the

misleading influence of harmonic currents from nonlinear loads and present accurate resonant frequency estimates, even when the data are not taken at the capacitor bank locations. By utilizing only the effective transient voltage and current segments due to capacitor bank energizing (zero-input or free response of the capacitor bank energizing), the techniques provide a fundamentally sound alternative to monitor the existence of harmful resonance conditions. Unlike the impedance scan method, this empirical method does not require any system short-circuit data. A profile of system parallel resonant frequencies is obtained by applying the proposed methods to a series of capacitor switching transient events captured during a given monitoring period.

8.1.2   Algorithms for Estimating System Damping Information

This dissertation presented two algorithms for estimating the system damping parameters. Combined with the estimated resonant frequencies, the system damping data provides the essential knowledge about the system response needed for performing preventive maintenance or taking mitigation measures. The proposed algorithms take advantage of the notion of an asymptotic or weakly-modulated signal, for which the signal phase varies much more rapidly than the amplitude. The zero-input (free) voltage response of the capacitor bank energizing can be categorized into this asymptotic signal and can be assigned unique time varying amplitude. This amplitude provides the system damping information in terms of damping ratio. Two practical algorithms have been developed to estimate this damping ratio based on the Hilbert trans-

form and analytic wavelet transform. The damping information can be also interpreted as an effective X/R ratio, a common index in the power industry, using system order reduction theory.

8.1.3 Algorithm for Determining the Relative Direction of Energized Capacitor Banks

This dissertation defined two fundamental signatures of shunt capacitor bank energizing and proved that these two signatures can be utilized to accurately determine the relative location of an energized capacitor bank whether it is upstream or downstream from the monitoring location. Mathematical analysis of a capacitor bank energizing proves that: (1) the energized capacitor bank affects only the upstream reactive power flow, (2) at the energizing instant, the gradients of voltage and current waveforms measured upstream from the capacitor location will have opposite signs, and (3) at the energizing instant gradients of voltage and current waveforms measured downstream from the same capacitor location will have equal signs. Thus, one can precisely determine the relative location of the switched capacitor bank by simply evaluating power factor changes and the signs of voltage and current waveform gradients at the switching instant. This method is very practical in that one can determine the relative location of a switched capacitor bank simply by observing the conventional capacitor switching data. It is also academically significant since the method is solely built upon the physics of capacitor bank energizing making sophisticated signal processing based techniques unnecessary.

8.1.4 Algorithm for Estimating the Distance of an Energized Capacitor Bank

This dissertation presented an efficient and accurate methodology for estimating the exact distance of a downstream energized capacitor bank from a monitoring location. This is the first analytical study of the initial voltage change due to an energized capacitor bank associated with locating an energized capacitor bank. The method also proves that the initial voltage change should be the same irrespective of the load conditions, although the damping from the load can cause erroneous results due to limited sampling rates. Thus, the accuracy of the proposed method depends on the sampling rate of the waveform. In general, the higher sampling rate, the more accurate results of the algorithm. However, the proposed method can be applied to an existing power quality monitor with a sampling rate of 256 samples/cycle and produce rather accurate results. On-going advances in power quality monitoring technology with improved data acquisition capability will allow very precise distance estimation.

8.2 Future Work

The outcomes of this research raise several interesting research problems that could aid in further improvements in the quality of power distribution.

1. Further investigation is needed on the erroneous effect of nonlinear loads on the current impedance estimation techniques. Given the lack of de-

tailed information normally available on the characteristics of harmonics sources, they have been often represented as approximate harmonic current injections or six-phase rectifiers injecting the 5th and 7th harmonic currents. Thus, it is desirable to develop more accurate models of the load components and efficiently integrate them into the whole power system model, which will surely enhance the modeling and simulation inaccuracy.

2. More investigation is also required for multiple resonant modes due to interactions of numerous capacitor banks installed in the whole power system, along with interharmonic problems due to prevalent power electronic loads in the system. In particular, more effort should be made to clearly identify modal components that are very close to each other. This research is mainly related to reduce the end effects of the wavelet transform in an efficient and systematic way.

3. The developed methodologies are limited to radial feeders. This is especially the restriction of the method for estimating the exact location of a switched capacitor bank. Thus, more realistic mathematical models should be developed to improve the methodologies used for complicated distributed systems.

4. More study is also needed for developing a methodology to analyze the overall system response of the distribution system to which multiple feeders are connected because it is well understood that it is very important

to investigate all of the feeders connected to the point of interest, such as the substation bus when evaluating the overall system response. This will require the more technical consideration of the unbalanced nature of power distribution systems.

5. Further research opportunity finds the impact of dynamic load on system damping since the power system itself is being reconfigured and loads are always changing. Thus, a real-time tracing of the varying system damping is needed. This research can be related with future algorithms for estimating multiple resonant and interharmonic frequency components.

6. Research can also focus on renewable energy issues, such as the impact of wind energy generation on the interconnected power system from a synergistic viewpoint on reliable and economic operations. This will involve several challenging tasks: (1) The integration of the large-scale nature of power systems and the sophisticated nonlinear characteristics of the modern power electronic devices into a single framework, (2) Simulating and modeling the dynamic system operations, and (3) Providing reliable operational strategies, as well as control methods to meet desirable PQ levels [66]. However, the enormous benefits to be gained from these investigations should motivate further research when one considers the proliferation of switching power electronic devices. Additionally, the significant technical and economic wind energy impact on the existing power grid should not be overlooked.

In conclusion, the proposed methodologies provide enormous benefits for improving power system quality. First, when forewarned of an imminent harmonic resonance, the utility has time to repair the system before catastrophic failures occur. Second, preventive maintenance saves money by informing the utility of suspicious equipment (capacitor banks) before they actually cause significant harmonic problems. Often those capacitor banks may be converted into harmonic filters or relocated to avoid harmonic issues. Third, this system gives the utility greater knowledge of system conditions occurring on the grid. This in itself is useful because harmonic resonance is still one of the most significant power quality problems. The proposed intelligent algorithms in principle turn raw measurement data into knowledge and subsequently into control actions by eliminating potentially damaging resonance source if necessary.

Appendices

Appendix A

Continuous Wavelet Transform of an Asymptotic Signal

A.1 Derivation of Equation (5.9)

As discussed in Chapters 4 and 5, a sinusoidal signal, $x(t)$ can be represented as a real part of an analytic signal $\mathrm{Re}(x_a(t))$ where $x_a(t) = a(t)e^{j\theta(t)}$. Thus, the CWT (Continuous Wavelet Transform) of a signal, $x(t)$ can be represented by the CWT of an analytic signal, $x_a(t)$: $Wx(u,s) = \frac{1}{2}Wx_a(u,s)$. Specifically, the Gabor wavelet of a real signal can be expanded as follows [51, 52]:

$$Wx(u,s) = \frac{1}{2}\int_{-\infty}^{\infty} a(t)e^{j\theta(t)}\frac{1}{\sqrt{s}}\frac{1}{(\sigma^2\pi)^{1/4}}e^{-((t-u)/s)^2/2\sigma^2}e^{-j\eta(t-u)/s}dt \quad (A.1)$$

In order to integrate this equation, substitute the time $t = t + u$ by abusing a variable name, and then use the Taylor series around u. For the amplitude of order 0, $a(t+u) = a(u)$, and for the phase of order 1, $\theta(t+u) = \theta(u) + \theta'(u)(t-u)$. Consequently, the following expression is obtained:

$$Wx(u,s) = \frac{1}{2}a(u)\,\hat{\psi}_{u,s}\left(\theta'(u)(u),\sigma,\eta\right)e^{j\theta(u)} + \varepsilon\left(a'(t),\theta''(u)\right) \quad (A.2)$$

The last term is an approximation error and can be neglected if the derivative of the phase is greater than the bandwidth $\Delta\omega$ [52].

A.2 Bandwidth, $\Delta\omega$

The bandwidth $\Delta\omega(= 2\pi f)$ of the translated and scaled Gabor wavelet function can be derived as follows [52]: Consider a ratio of the $\hat{g}(s\omega, \sigma)$ to $\hat{g}(0, \sigma)$. Since this is an exponential function, we can set up the following relationship for this:

$$e^{z_1} = \frac{|\hat{g}(s\omega, \sigma)|}{|\hat{g}(0, \sigma)|} \ll 1 \tag{A.3}$$

where $|s\omega| \geq \Delta\omega$ and $\hat{g}$ is the Gaussian window as shown below:

$$\hat{g}(\omega, \sigma) = \frac{1}{(4\sigma^2\pi)^{1/4}} \exp\left(\frac{-\sigma^2\omega^2}{2}\right) \tag{A.4}$$

It follows that the bandwidth of the wavelet function is:

$$\Delta\omega(s) = \sqrt{\frac{-2z_1}{\sigma^2 s^2}}$$

Thus, the parameter z_1 can determine the bandwidth, $\Delta\omega(s)$. If z_1 is chosen to be -8, then the e^{-z_1} becomes $33.5 \cdot 10^{-6}$, which means that the value of the wavelet at the bandwidth is only $33.5 \cdot 10^{-6}$ of the maximum value.

Appendix B

Prony Analysis

Given accurate system parameters, eigenvalues from linear matrices arising from the dynamic model of a system may provide analytical modal parameters. However, the actual system may be too complex to model or may have time-varying parameters. In these cases, it may be practical to substitute an estimated linear model for the actual dynamic model. The estimated model can be derived from the system output waveform. One of viable approaches to estimate the system parameters is Prony analysis [28, 56].

The Prony analysis is basically designed to fit the parameters of a sum of damped sinusoidal functions to an observed measurement.

$$\hat{v}(t) = \sum_{i=1}^{n} a_i e^{-\zeta_i \omega_{ni} t} \cos\left(\omega_{di} t + \phi_i\right) = \sum_{i=1}^{n} \alpha_i e^{\lambda_i t} \tag{B.1}$$

where $v(t)$ consist of N samples, i.e. $v(t_k) = v(k), k = 0, 1, \ldots, N-1$ that are evenly sampled by Δt. In practice, the measurement may be corrupted by by high-frequency noise or offset by a dc value, and thus one may need to preprocess the measurement before applying the Prony method. In general, the following basic procedures are required for Prony analysis.

B.1 Linear Prediction Model

The first step is to construct a linear prediction model[1] in z-domain from the measurement set. In z-domain, (B.1) can be represented as follows: $\hat{v}(k) = \sum_{i=1}^{n} \alpha_i z_i^k$ where $z_i = e^{\lambda_i \Delta t}$ and λ_i's are system eigenvalues.

B.2 Roots of the Characteristic Equation

The second step is to find the roots of the characteristic polynomial equation of the model:

$$z^n - \left(a_1 z^{n-1} + a_2 z^{n-2} + \ldots + a_n z^0\right) = 0 \tag{B.2}$$

where the a_i's are unknown parameters and should be estimated based on the following relationship (B.3):

$$\begin{bmatrix} v(n-1) & v(n-2) & \cdots & v(0) \\ v(n-2) & v(n-1) & \cdots & v(1) \\ \vdots & \vdots & \vdots & \vdots \\ v(N-2) & v(n-3) & \cdots & v(N-n-1) \end{bmatrix} \begin{bmatrix} a_1 \\ a_2 \\ \vdots \\ a_n \end{bmatrix} = \begin{bmatrix} v(n) \\ v(n+1) \\ \vdots \\ v(N-1) \end{bmatrix} \tag{B.3}$$

It should be noted that N is generally larger than the selected system order of n. Therefore, the least squares method should be applied to determine unknown a_i's. Given a_i's, one can find z_i's from (B.2). Using z_i's and $\hat{v}(k) = v(k)$,

---

[1]This model is considered to be Pole-Zero (ARMA) System Model [40]. The prony function in MATLAB implements the Prony analysis for time-domain design of IIR filters. It models a signal using a specified number of poles and zeros [67].

185

one can further determine the α_i's in (B.1) from the following relationship:

$$
\begin{bmatrix}
z_1^0 & z_2^0 & \cdots & z_n^0 \\
z_1^0 & z_2^0 & \cdots & z_n^0 \\
\vdots & \vdots & \vdots & \vdots \\
z_1^{N-1} & z_2^{N-1} & \cdots & z_n^{N-1}
\end{bmatrix}
\begin{bmatrix}
\alpha_1 \\
\alpha_2 \\
\vdots \\
\alpha_n
\end{bmatrix}
=
\begin{bmatrix}
v(n) \\
v(n+1) \\
\vdots \\
v(N-1)
\end{bmatrix}
\qquad (B.4)
$$

which can be represented by $Z\mathrm{A} = \mathrm{V}$. Since the matrix Z is $N \times n$, the least squares method should be applied again to solve the vector A. The estimating waveform $\hat{v}(t)$ is then obtained from (B.1). An appropriate measure for the goodness of this fit is a signal-to-noise ratio (SNR) given by:

$$
SNR = 20 \log \frac{\|\hat{v} - v\|}{\|v\|} \quad (dB)
$$

B.3   Complex Modal Frequencies for the Signal

The final step is to determine the amplitude and phase for each mode based on $z_i = e^{\lambda_i \Delta t}$ and $\lambda_i = \frac{\ln(z_i)}{\Delta t}$.

Bibliography

[1] J. J. Burke, *Power Distribution Engineering: Fundamentals and Applications.* NY: M. Dekker, 1994.

[2] R. D. Dugan, M. F. McGranaghan, S. Santoso, and W. H. Beaty, *Electrical Power Systems Quality.* NY: McGraw-Hill, 2003.

[3] EPRI, "Electricity technology roadmap: 2003 summary and synthesis power delivery and markets," EPRI, Tech. Rep. 1009321, Nov. 2003.

[4] E. Acha, C. R. Fuerte-Esquivel, H. Ambriz-Pérez, and C. Angeles-Camacho, *FACTS: Modelling and Simulation in Power Networks.* John Wiley & Sons, LTD., 2004.

[5] W. H. Kersting, *Distribution System Modeling and Analysis.* CRC Press, 2002.

[6] H. L. Willis, *Power Distribution Planning Reference Book.* Marcel Dekker, INC., 1997.

[7] Power System Damping Ad Hoc Task Force, "Damping representation for power system stability studies," *IEEE Transactions on Power Systems*, vol. 4, pp. 151–157, Feb. 1999.

[8] K. Hur, "Methodology for evaluating and predicting power systems resonance," Tech. Rep., 2004, research Proposal for Ph.D Qualifying Examination.

[9] S. Santoso, S. McCormick, and K. Hur, "Automated evaluation system for capacitor switching transient concerns," Tech. Rep., 2004.

[10] K. Hur and S. Santoso, "An improved method to estimate empirical system parallel resonant frequencies using capacitor switching transient data," *IEEE Transactions on Power Delivery*, vol. 21, pp. 1751–1753, July 2006.

[11] J. Arrillaga and N. Watson, *Power System Harmonics.* Wiley, 2003.

[12] K. Hur, S. Santoso, and I. Y. H. Gu, "On the empirical estimation of utility distribution damping parameters using power quality waveform data," *EURASIP (European Association for Signal Speech and Image Processing) Journal on Advances in Signal Processing*, vol. 2007, 2007, Article ID:95328.

[13] K. Hur and S. Santoso, "Estimation of system modal parameters using analytic wavelet transform," *IEEE Transactions on Power Delivery*, 2007, in preparation.

[14] ——, "On two fundamental signatures for determining the relative location of switched capacitor banks," *IEEE Transactions on Power Delivery*, under review.

[15] ——, "Distance estimation of switched capacitor banks in utility distribution feeders," *IEEE Transactions on Power Delivery*, to appear.

[16] *Dictionary of the English Language*, 4th ed. The American Heritage.

[17] ARUP, *Millennium Bridge*, http://www.arup.com/MillenniumBridge/.

[18] F. Tisseur and K. Meerbergen, "The quadratic eigenvalue problem," *SIAM review*, vol. 43, no. 2.

[19] E. Kreyszig, *Advanced engineering mathematics*, 6th ed. New York: Wiley, 1988.

[20] D. E. Johnson, J. L. Hilburn, and J. R. Johnson, *Basic electric circuit analysis*, 4th ed. Englewood Cliffs, N.J.: Prentice Hall, 1990.

[21] P. Kundur, *Power System Stability and Control.* EPRI, 1994.

[22] F. C. De La Rosa, *Harmonics and Power Systems.* FL: CRC Press, 2006.

[23] K. Hur and S. Santoso, "Analysis and modeling of dynamic overvoltage phenomena due to transformer energizing," in *IEEE Power Engineering Society General Meeting*, vol. 2, 2005, pp. 1126–1130.

[24] M. Klein, G. J. Rogers, and P. Kundur, "A fundamental study of inter-area oscillations in power systems," *IEEE Transactions on Power Systems*, vol. 6, pp. 914–921, Aug. 1991.

[25] B. Pal and B. Chaudhuri, *Robust Control in Power Systems.* Springer, 2005.

[26] A. Greenwood, *Electrical Transients in Power Systems*, 2nd ed. John Wiley & Sons, 1991.

[27] M. Banejad and G. Ledwich, "Quantification of damping contribution from loads," *IEE Proceedings Generation, Transmission & Distribution*, vol. 152, pp. 429–434, May 2005.

[28] J. F. Hauer, "Application of prony analysis to the determination of modal content and equivalent models for measured power system response," *IEEE Transactions on Power Delivery*, vol. 6, pp. 1062–1068, Aug. 1991.

[29] H. Okamoto, A. Kurita, J. J. Sanchez-Gasca, K. Clark, N. W. Miller, and J. H. Chow, "Identification of equivalent linear power system models from electromagnetic transient time domain simulations using prony's method," in *The 35th IEEE Decision and Control*, vol. 4, Dec. 1996, pp. 3857–3863.

[30] D. I. Trudnowski, "Order reduction of large-scale linear oscillatory system models," *IEEE Transactions on Power Systems*, vol. 9, pp. 451–458, Feb. 1994.

[31] J. Arrillaga, N. Watson, and S. Chen, *Power System Quality Assessment*. Wiley, 2000.

[32] S. Santoso, E. Powers, W. M. Grady, and P. Hoffman, "Power quality and the security of electricity supply," *Proceedings of the IEEE*, vol. 89, pp. 1830–1836, Dec. 2001.

190

[33] S. Santoso and A. Maitra, "Empirical estimation of system parallel resonant frequencies using capacitor switching transient data," *IEEE Transactions on Power Delivery*, vol. 20, pp. 1151–1156, Apr. 2005.

[34] D. Tong, V. G. Nikolaenko, N. Ginbey, and I. Lau, "Harmonic propagation in transmission system with multiple capacitor installations," in *PowerCon 2000 International Conference on Power System Technology*, vol. 2, 2000, pp. 1007–1023.

[35] J. R. Harries and J. L. Randall, "Harmonic resonance on parallel high voltage transmission lines," *IEEE Transactions on Power Delivery*, pp. 477–482, January 1997.

[36] E. J. Currence, J. E. Plizga, and H. N. Nelson, "Harmonic resonance at medium-sized industrial plant," *IEEE Transactions on Industrial Applications*, vol. 31, no. 4, pp. 682–690, July 1995.

[37] S. Santoso, J. D. Lamoree, and R. P. Bingham, "Answermodule: autonomous expert systems for turning raw pq measurements into answers," in *International Conference on Harmonics and Quality of Power*, vol. 2, 2000, pp. 499–503.

[38] S. Santoso, E. J. Powers, W. M. Grady, and P. Hoffman, "Power quality assessment via wavelet transform analysis," *IEEE Transactions on Power Delivery*, vol. 11, pp. 924–930, July 1996.

191

[39] S. Santoso, E. Powers, W. M. Grady, and P. Hoffman, "Power quality assessment via wavelet transform analysis," *IEEE Transactions on Power Delivery*, vol. 11, pp. 924–930, Apr. 1996.

[40] L. L. Scharf, *Statistical Signal Processing: Detection, Estimation and Time-Series Analysis.* NY: Addison Wesley, 1991.

[41] T. E. Grebe, "Application of distribution system capacitor banks and their impact on power quality," *IEEE Transactions on Power Delivery*, vol. 64, pp. 1623–1628, Oct. 1991.

[42] M. H. Bollen, E. Styvaktakis, and I. Y. Gu, "Categorization and analysis of power system transients," *IEEE Transactions on Power Delivery*, vol. 20, pp. 2298–2306, July 2005.

[43] I. Y. Gu and E. Styvaktakis, "Bridge the gap: signal processing for power quality applications," *Electric Power Systems Research*, vol. 66, pp. 83–96, 2003.

[44] PES Distribution Systems Analysis Subcommittee, *Radial Test Feeders*, IEEE, http://ewh.ieee.org/soc/pes/dsacom/testfeeders.html.

[45] *PSCAD/EMTDC version 4.2*, Manitoba HVDC Research Centre, Winnipeg, Canada.

[46] J. S. Bendat and A. G. Piersol, *Random Data: Analysis and Measurement Procedures.* Wiley & Sons, 1986.

192

[47] B. C. Kuo and F. Golnaraghi, *Automatic Control Systems*, eigth ed. John Wiley & Sons, 2003.

[48] A. C. Antoulas, *Approximation of Large-Scale Dynamical Systems*. Philadelphia: SIAM, 2005.

[49] T. Kijewski and A. Kareem, "Wavelet transforms for system identification in civil engineering," *Computer-Aided Civil and Infrastructure Engineering*, vol. 18, pp. 339–355, Sep. 2003.

[50] S. Santoso, "Wavelet-based signal analysis techniques with applications to nonstationary plasma fluctuations and electric power quality disturbances," Ph.D. dissertation, The University of Texas at Austin, 1996.

[51] W. J. Staszewski, "Identification of damping in mdof systems using time-scale decomposition," *Journal of Sound and Vibration*, vol. 203, pp. 283–305, 1997.

[52] S. Mallat, *A wavelet tour of signal processing*, 2nd ed. Academic Press, 1999.

[53] A. V. Oppenheim and R. W. Schafer, *Discrete-time signal processing*, 2nd ed. New Jersey: Prentice Hall, INC., 1999.

[54] N. Delprat, B. Escudié, P. Guillemain, R. Kronland-Martinet, P. Tchamitchian, and B. Torrésani, "Asymptotic wavelet and gabor analysis: extraction of instantaneousfrequencies," *IEEE Transactions on Information Theory*, vol. 38, pp. 644–664, Mar. 1992.

[55] J. Slavič, I. Simonovski, and M. Boltežar, "Damping identification using a continuous wavelet transform: application to real data," *Journal of Sound and Vibration*, vol. 262, pp. 291–307, Apr. 2003.

[56] M. Crow, *Computational Methods for Electric Power Systems.* FL: CRC Press, 2003.

[57] IEEE Std 1036-1992, *IEEE Guide for application of shunt power capacitors*, New York, NY 10017, 1992.

[58] A. C. Parsons, W. M. Grady, E. J. Powers, and J. C. Soward, "A direction finder for power quality disturbances based upon disturbance power and energy," *IEEE Transactions on Power Delivery*, vol. 15, pp. 1081–1085, July 2000.

[59] J. S. Kim, W. M. Grady, A. Arapostathis, J. C. Soward, and S. C. Bhatt, "A time domain procedure for locating switched capacitors in power distribution systems," *IEEE Transactions on Power Delivery*, vol. 17, pp. 1044–1049, Oct. 2002.

[60] G. W. Chang, M. H. Shih, S. Y. Chu, and R. Thallam, "An efficient approach for tracking transients generated by utility shunt capacitor switching," *IEEE Transactions on Power Delivery*, vol. 21, pp. 510–512, Jan. 2006.

[61] S. Santoso, K. Hur, and Z. Zhou, "Induction machine modeling for distribution system analysis - a time domain solution," in *IEEE Power En-*

gineering Society Transmission and Distribution Conf., 2005/2006, pp. 583–587.

[62] S. R. McCormick, K. Hur, S. Santoso, A. Mitra, and A. Sundaram, "Capacitor bank predictive maintenance and problem identification using conventional power quality monitoring systems," in *IEEE PES General Meeting*, 2004, pp. 1846–1850.

[63] D. Sochuliakova, D. Niebur, C. Nwankpa, R. Fischl, and D. Richardson, "Identification of capacitor position in a radial system," *IEEE Transactions on Power Delivery*, vol. 14, pp. 1368–1373, Oct. 1999.

[64] S. Santoso, J. D. Lamoree, and M. F. McGranaghan, "Signature analysis to track capacitor switching performance," in *IEEE Power Engineering Society Transmission and Distribution Conf.*, 2001, pp. 259–263.

[65] D. L. Brooks and D. D. Sabin, "An assessment of distribution system power quality: Volume 3: The library of distribution system power quality monitoring case studies, TR-106294-V3," Tech. Rep., May 1996.

[66] E. F. Fuchs, D. J. Roesler, and M. A. S. Masoum, "Are harmonic recommendations according to ieee and iec too restrictive?" *IEEE Transactions on Power Delivery*, vol. 19, pp. 1775–1786, Oct. 2004.

[67] *MATLAB Signal Processing Toolbox, Version 7.04*, The MathWorks, Inc., Natick, MA USA.

Vita

Kyeon Hur was born in Seoul, Korea on 12 September 1973, the son of Don Hur and Hyangsik Kim. After graduating from Dankuk High School, Seoul, Korea in 1992, he attended Yonsei University, Seoul, Korea, receiving the Bachelor of Science degree and the Master of Science degree in Electrical Engineering in February, 1996 and 1998, respectively. He was with Samsung Electronics as an R&D engineer from 1998 through 2003, where he developed advanced motor control algorithms and designed user interface for AC drives.

He started doctoral studies in the Department of Electrical and Computer Engineering under supervision of Professor Surya Santoso at The University of Texas at Austin in August 2003. His main research interests are at the intersection of control, signal processing, power systems engineering and power electronics, and especially include power quality, condition-based system monitoring, time-domain modeling of electromagnetic transient phenomena in electric power systems, FACTs and wind energy systems. During his time as a doctoral student, he held positions as a graduate research assistant and a teaching assistant, and authored or co-authored four journal and four conference papers. He is a recipient of KOSEF (Korea Science and Engineering Foundation) graduate scholarship.

Permanent address: Olympic Family Town 219-1502, Munjung Dong,
Songpa Gu, Seoul, Republic of Korea, 138-768

196

This dissertation was typeset with LaTeX[†] by the author.

197